Velocity Enhancement Models for Polymer Flooding in Reservoir Simulations

by

E. Guarnerio

In partial fulfillment of the requirements for the degree of

Master of Science
in
Applied Mathematics

at the Delft University of Technology,
to be defended publicly on Tuesday August 28, 2018 at 09:30 AM.

Student number:	4747259	
Thesis Commette:	Dr. ir. J.E. Romate,	TU Delft & Shell Global Solutions International (supervisor)
	Prof.dr.ir. C. Vuik ,	TU Delft
	Dr.ir. W.T. van Horssen,	TU Delft

TU Delft Delft University of Technology

Abstract

In the past decades, several EOR (Enhanced Oil Recovery) techniques have been developed to increase the amount of oil recoverable from a reservoir. Among these techniques, polymer flooding consists in the injection of a solution of water and polymer into the reservoir, and it is performed in order to lower the mobility of injected water. A peculiarity of a water-polymer flow through a porous medium is the velocity enhancement, or hydrodynamic acceleration, that affects the polymer molecules. Experimentally, polymers are observed to travel faster than inert chemical species. Therefore, when simulating numerically a polymer flooding, a velocity enhancement effect has to be incorporated into the governing equations to accurately predict oil recovery. The simple model that introduces a constant enhancement factor, usually implemented in commercial simulators, leads to an ill-posed problem, causing stability issues in the simulations, which further leads to a monotonicity loss in the solution: the polymer is predicted to pile-up at the water-oil interface. While accumulation of polymer at the water front is not necessarily unphysical, it should not be the result of a mathematical ill-posed problem. Hence, an alternative model, employing a saturation dependent factor, has been proposed in the work of Bartelds et al. [4], and has been extended by Hilden et al. [21] to overcome some physical restrictions. In this thesis, these models are re-examined through a thorough analytical study in the one-dimensional case. An analytical solution, resulting in an acceleration of the polymer front, is computed for the well-posed model proposed by Bartelds, while the extended enhancement factor derived in [21] is shown to lead again to an ill-posed problem. A study of the monotonicity of the numerical schemes reveals that accumulation of polymer at the water front is strictly related to ill-posedness.

Obtaining accurate numerical solutions is not an easy task. Commercial simulators adopt fully implicit schemes to solve the multi-phase flow, and transport of chemical agents is solved through the development and coupling of separate modules. In this case, the use of high-resolution methods for the transport of polymer is not compatible with the first order solver for the underlying flow.

To investigate the interaction of the enhancement model proposed by Bartelds with other physical phenomena, adsorption of polymer onto the reservoir rock is added to the governing equations. The problem maintains the well-posedness property, but because of a raise in equations complexity, only numerical results are presented. The model is then extended to the two-dimensional case and, relying on numerical solutions, similar conclusions as in the one-dimensional case are derived.

Acknowledgements

This thesis has been written within the joint programme *Computer Simulations for Science and Engineering (COSSE)* at TU Delft and TU Berlin. The supervisor of this project has been Dr.ir. J.E. Romate, of Shell Global Solutions International and member of the Numerical Analysis group at the Delft Institute of Applied Mathematics. The research has been conducted during an internship at the Chemical Enhanced Oil Recovery Technology team of Shell Global Solution International.

During the past two years, I had the chance to study at the Technical University of Berlin, Germany, and at the Technical University of Delft, Netherlands. Beside the highly stimulating scientific environments, the COSSE programme gave me the opportunity to meet and work with people from all over the world, sharing academic interests and building solid friendships that allowed me to spend this time away from home in the most delightful way. Therefore, I want to thank Reinhard Nabben (TU Berlin) and Kees Vuik (TU Delft) as the coordinators of the programme in their respective institutes, and all the people involved in the COSSE organization that made this experience possible.

A special thanks goes to my daily supervisor, Johan Romate, for giving me the chance to work on and write my thesis during an internship at Shell, and for his guidance and advices throughout the duration of this project. I would also like to thank my colleagues for the precious feedbacks that contributed to this research and for the pleasant working environment.

Last but not least, I want to thank my family, whose encouragement and support have been invaluable during these two years.

E. Guarnerio
Delft, August 2018

Contents

1 Introduction

It is needless to state the importance of oil in the world economy, as it is one of the primary sources of energy worldwide. Many different techniques are applied to maximize the amount of oil that can be extracted from a reservoir. During the producing life of a reservoir, three phases are usually distinguished: primary, secondary and tertiary recovery. Primary recovery is driven by natural mechanisms, such as fluid expansion due to pressure decline, and no injection process is involved. The absence of water injection in the production makes this phase the most profitable one of the reservoir's life. Once the pressure drops below a certain limit, usually water or gas is injected to maintain a higher pressure and to sweep out oil through a displacement process. This is known as the secondary recovery. However, oil is left behind after a waterflood, either because it is trapped by capillary forces, or because it is bypassed by the water, which has a higher mobility and may find a path through the reservoir. At this point, at the production well, water is also produced and the method becomes inefficient and uneconomical. All the other techniques used after waterflooding are tertiary recovery. The nature of the recovery is now based on displacement of the oil. These techniques includes thermal, solvent and chemical methods. In general, Enhanced Oil Recovery (EOR) are all the techniques for oil recovery that involve the injection of materials not normally present in the reservoir. This definition does not restrict EOR to a particular phase of oil recovery. The purpose of EOR is to displace the amount of oil which is unrecoverable through conventional methods.

In this work, the focus will be on polymer flooding, that is, polymer is added to the injected water in order to increase its viscosity, resulting in a more favourable mobility ratio M, defined as

$$M = \frac{\lambda_w}{\lambda_o} = \frac{k_{r,w}\mu_o}{k_{r,o}\mu_w},$$

where λ, μ and k_r are the mobility, viscosity and relative permeability respectively, and the subscripts $\{o, w\}$ refer to oil and water phase. A lower mobility ratio means that water flow will behave more similarly to oil. Thus, the displacement of oil will be more uniform and the overall recovery will improve [9]. In order to study polymer flooding from a theoretical point of view, a mathematical model for the flow of a fluid in a reservoir (a porous medium) is needed. The complexity of these models raises rather quickly as more physical and chemical factors are considered, thus it is essential to state reasonable assumptions to simplify the models, allowing for analytical study and numerical simulations of the flow.

The report will be structured as follows: in chapter 2, general theory for hyperbolic equations is discussed. The governing equations of the presented models are mainly in hyperbolic form, so a detailed understanding of the main features of the solution of these equations, such as rarefaction and shock waves, is necessary. In Chapter 3, first a glossary of petroleum terms is given, so that the reader will become familiar with the chemical and physical properties of a reservoir. Then, the

basic theory and equations of fluid flow in porous media are discussed, including the fractional flow formulation, which is used in a wide range of models and simulators. This chapter is concluded by an overview of numerical methods, based on a finite volume discretization with upwind schemes for the fluxes, that will be used to simulate the flow through the reservoir. Chapter 4 will focus on the discussion of more advanced one-dimensional models of specific use for polymer flooding. Here, the inaccessible pore volume (IPV) effect, which is the main object of study of this research, will be discussed: since the polymer molecules are larger, they will not enter all the pores available for water, so that the polymer may travel faster than inert chemical species. As a consequence, velocity enhancement models are considered. These models must be treated with caution since, as it will be shown, they may lead to ill-posed problems, causing an uncontrolled pile-up of polymer at the water front in the numerical simulations. A (monotone) analytical solution for the velocity enhancement model proposed in [4] is computed. In chapter 5, the monotonicity of the numerical schemes employed is investigated for the different models proposed in chapter 4. Finally, in chapter 6 the models are extended to the two-dimensional case, and the effects of other phenomena, such as adsorption, are added to the governing equations. Conclusions and recommendations for future work are given in chapter 7.

2

Hyperbolic Conservation Laws

Hyperbolic laws arise in many different applications. They have a central role also in EOR, especially in water and polymer flooding, where even basic models for fluid flow present typical features related to its hyperbolic nature. Thus, a complete understanding of the peculiarities of the solutions that are generated, such as rarefaction waves and discontinuities (often referred to as shocks), is essential. In this chapter, the main ingredients needed to build a (unique) solution to scalar and systems of conservation laws are recalled. Since it is not feasible to present here a thorough discussion on the theory of conservation laws, we concentrate on the key aspects of the solutions to such equations that will be useful to analyze the well-posedness of the models introduced in later chapters. For an introduction to conservation laws, the reader is referred to Salsa [19]. For a formal and detailed study, one should consult the work of Leveque [17] and Holden-Risebro [5].

2.1. Introduction to Conservation Laws

The general form of a scalar conservation law is

$$u_t + f(u)_x = 0, \quad x \in \mathbb{R}, t > 0, \tag{2.1}$$

where $f \in C^1$ is usually referred to as the flux function and u represents some physical property such as concentration. Equation (2.1) and the initial condition

$$u(x,0) = u_0(x), \quad x \in \mathbb{R}, \tag{2.2}$$

together form an initial value (or Cauchy) problem.

The characteristic theory is used to build the solution of this kind of problems: it is possible to find curves on the $(x,t)-$plane for which u is constant. That is, curves of the form $x = \xi(t;x_0)$ such that

$$\frac{d}{dt} u(\xi(t;x_0),t) = 0.$$

Let us consider the Cauchy problem in the case of a linear equation

$$\begin{cases} u_t + a u_x = 0 & x \in \mathbb{R}, t > 0 \\ u(x,0) = u_0(x) \end{cases} \tag{2.3}$$

where $a > 0$ is a given constant. For this simple case, the characteristics are of the form $\xi(t;x_0) = at + x_0$. Indeed,

$$\frac{d}{dt} u(\xi(t;x_0),t) = \frac{d}{dt} u(x(t),t) = u_t + a u_x = 0.$$

The initial data $u_0(x)$ is then transported along the characteristics, where $u(x,t)$ is constant. Formally,

$$u(\xi(t;x_0),t) = u(\xi(0;x_0),0) = u(x_0,0) = u_0(x_0),$$

meaning, more explicitly,

$$u(at+x_0,t) = u_0(x_0).$$

Rewriting $x = at+x_0$ and $x_0 = x-at$ gives the solution to problem (2.3):

$$u(x,t) = u_0(x-at).$$

In the linear scalar case studied above, the characteristics do not intersect and the solution is well defined in every point (x,t). In the more general case (2.1), the characteristic theory is still applied, but a more precise analysis would show that, even with regular initial data, singularities may arise within the solution.

The equation for the characteristics reads

$$x(t) = f'(u_0(x_0))\,t + x_0, \quad f' = \frac{df}{du}.$$

To compute $u(x,t)$, consider the characteristic through (x,t) and follow it backward in time to determine the point $(x_0,0)$. One then has $u(x,t) = u_0(x_0)$. Substituting the equation for the characteristic in the latter gives

$$u(x,t) = u_0(x - f'(u_0(x_0))\,t),$$

which can be rewritten as

$$u = u_0(x - f'(u)\,t).$$

Note that the last expression determines u implicitly.

The slope of the characteristics depends on the initial data u_0 and on $f'(u)$. It is clear then that existence and uniqueness of the solution in every point is not ensured, since the characteristics may intersect or be absent from a part of the (x,t)-plane. To deal with these situations, it is necessary to introduce a more flexible definition of solution which allows for discontinuities.

Definition 2.1. *A function u, bounded in $\mathbb{R}\times[0,\infty)$, is called a weak solution to problem (2.1)-(2.2) if, for every test function $\varphi \in C_0^\infty(\mathbb{R}\times[0,\infty))$ it holds*

$$\int_0^\infty \int_{\mathbb{R}} (u\varphi_t + f(u)\varphi_x)\,dx\,dt + \int_{\mathbb{R}} u_0\varphi(x,0)\,dx = 0.$$

The subscript in C_0^∞ stands for compact support of the test function $\varphi(x,t)$. A classical solution is also a weak solution. Definition (2.1) seems quite flexible, since it allows for discontinuous solutions. It is though necessary to understand the behaviour of a weak solution around such discontinuity.

A discontinuity, referred to as shock, arises when multiple characteristics meet in a point, as depicted in figure 2.1. The locus of points determined by the intersection of the characteristics defines the shock curve $s(t)$. The well-known Rankine-Hugoniot condition is used to compute the derivative $\dot{s}(t)$ of the shock wave (i.e. the velocity of the wave):

$$\dot{s}(t) = \frac{f(u_r(s,t)) - f(u_l(s,t))}{u_r(s,t) - u_l(s,t)}. \tag{2.4}$$

Here, u_r and u_l stand for the solution u immediately right and immediately left of the shock, respectively. The velocity of the shock given by (2.4) is usually the quantity one is interested in. However, along with an appropriate initial condition (in the case depicted in Figure 2.1 it would be $s(0) = 0$),

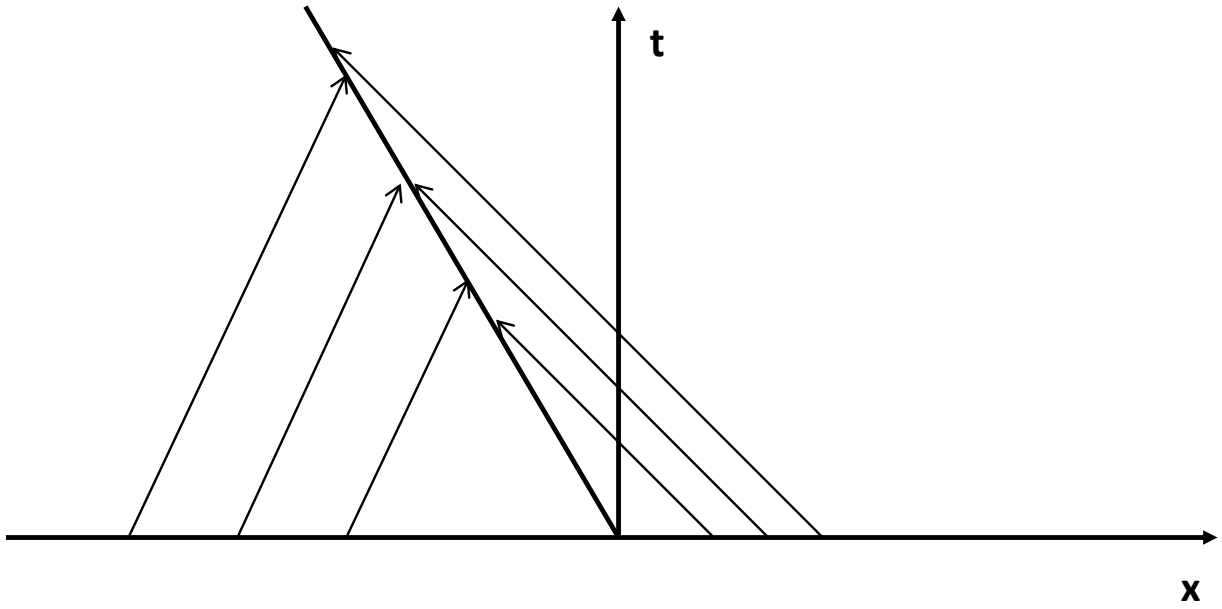

Figure 2.1: Characteristics collide: generation of a shock wave.

(2.4) can be solved to determine also the equation of the shock wave $s(t)$. The solution u across the shock jumps from u_l to u_r.

Consider now a case where the characteristics are absent from a region of the (x,t)-plane, as depicted in figure 2.2. No characteristics enter the central region: an alternative way must be found to define a solution in such region. In this case, the solution is found through rarefaction waves: lines spread out from a point and fill the empty region. The fan of characteristics is depicted in Figure 2.3. One can show that, if f' is monotone, the following formula gives the solution in a region where rarefaction waves (centered at $x=0$) occur:

$$u(x,t) = r\left(\frac{x}{t}\right), \quad r = (f')^{-1}. \tag{2.5}$$

Rarefaction and shock waves seem to ensure existence of a solution in the different configurations that may occur. What about uniqueness?

There are cases where both rarefaction and shock waves can be built to define a (weak) solution, so one may wonder if further conditions can be derived to ensure uniqueness. To this purpose, it is convenient to think of a physical interpretation of the solution. These solutions are referred to as entropy solutions, related to the study of gas dynamic. There are various ways to formulate an entropy condition. One of the most common is the viscous regularization: equation (2.1) is replaced by

$$u_t + f(u)_x = \epsilon u_{xx}. \tag{2.6}$$

Note that (2.6) is a parabolic equation, thus, even if ϵ is small, the equation has a much more regular behaviour. The idea is that, physically, a model is more realistic if some diffusion is taken into account, and a conservation law represents a limit model when diffusion goes to zero. A unique solution for (2.1) is selected as the limit of the solution of (2.6) for $\epsilon \to 0$.

One can show that, for sufficiently regular solutions, this entropy condition is equivalent to the *Kružkov* entropy condition. A solution satisfies a *Kružkov* entropy condition if

$$\iint (\eta(u)\phi_t + q(u)\phi_x)\,dx\,dt \geq 0 \tag{2.7}$$

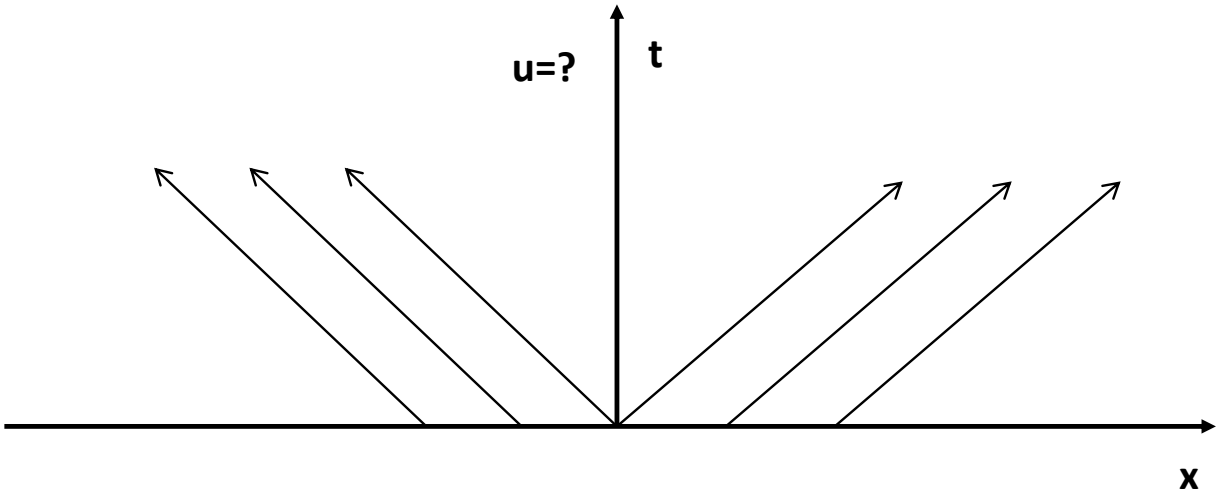

Figure 2.2: No information in the central region: generation of a rarefaction wave.

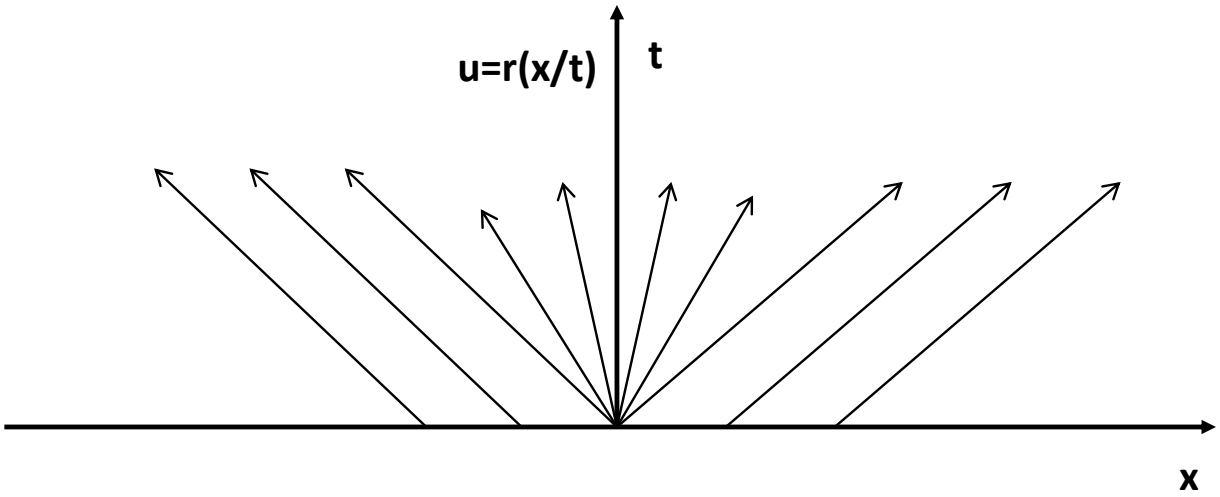

Figure 2.3: Rarefaction wave centered in the origin.

holds for all convex functions η and all nonnegative test functions $\phi \in C_0^\infty(\mathbb{R} \times (0,\infty))$, where $q(u)$ is such that $q'(u) = f'(u)\eta'(u)$. It is often more convenient to work with this condition to show that solutions satisfy entropy conditions.

2.2. The Riemann Problem

Studying a particular initial value problem, the Riemann problem, gives useful insights on the behaviour of problems with more complicated initial value.

The Riemann problem is the initial value problem

$$u_t + f(u)_x = 0, \qquad u(x,0) = \begin{cases} u_l & \text{for } x < 0, \\ u_r & \text{for } x \geq 0, \end{cases} \tag{2.8}$$

where both u_l and u_r are constant. Since both the equation and initial data are invariant under the transformation $x \mapsto kx$ and $t \mapsto kt$, it makes sense to look for a similarity solution of the form $u(x,t) = w(x/t)$. Assuming for a moment that $f \in C^2$ and substituting the similarity solution into the equation yields

$$-\frac{x}{t^2}w' + \frac{1}{t}f'(w)w' = 0. \tag{2.9}$$

Equation (2.9) has either the simple solution $w'(x/t) = 0$ or, rewriting the equation as

$$x/t = f'(w(x/t)), \tag{2.10}$$

the solution $w = (f')^{-1}(x/t)$ if f' is strictly monotone, recovering (2.5). Of course, in general the monotonicity of f' cannot be guaranteed. In the case of a non-convex or non-concave flux function f, the solution to the Riemann problem (2.8) will consist of a sequence of shock and rarefaction waves. The typical approach that provides a way to build the solution in this general case, consists in replacing f' by a monotone function on the interval between u_l and u_r (see for instance [5],[17]). Depending whether $u_l < u_r$ or $u_l > u_r$, f is replaced, respectively, by its lower convex envelope $f_\smile$ or by its upper concave envelope $f_\frown$.

Consider the case $u_l < u_r$. Then, permitting jump discontinuities where $f'_\smile$ is constant, so that its inverse can be defined, one can show that a solution to (2.8) satisfying a Kružkov entropy condition is given by

$$u(x,t) = \begin{cases} u_l & \text{for } x \le f'_\smile(u_l)\,t, \\ (f'_\smile)^{-1}(x/t) & \text{for } f'_\smile(u_l)\,t \le x \le f'_\smile(u_r)\,t, \\ u_r & \text{for } x \ge f'_\smile(u_r)\,t. \end{cases} \tag{2.11}$$

The intervals where $(f'_\smile)^{-1}$ is continuous correspond to the rarefaction waves, while the discontinuities correspond to the shocks.

Analogously, the solution in the case $u_l > u_r$ is found by taking the concave upper envelope of f':

$$u(x,t) = \begin{cases} u_l & \text{for } x \le f'_\frown(u_l)\,t, \\ (f'_\frown)^{-1}(x/t) & \text{for } f'_\frown(u_l)\,t \le x \le f'_\frown(u_r)\,t, \\ u_r & \text{for } x \ge f'_\frown(u_r)\,t. \end{cases} \tag{2.12}$$

These results can be summarized in the following theorem [5]:

Theorem 2.2. *The initial value problem (2.8) with a flux function f(u) such that $f_{\smile,\frown} \neq f$ on finitely many intervals, alternating with intervals where they coincide, has a weak solution given by (2.11) if $u_l < u_r$, or by (2.12) if $u_r < u_l$. This solution satisfies the Kružkov entropy condition.*

2.3. Systems of Conservation Laws

The governing equations that describe water and polymer flooding consist of a system of two conservation laws. Therefore, it is essential to present here the main results regarding the study of systems of conservation laws. The typical features arising from scalar laws will be extended to the case of systems. In this section, mainly the work of Leveque [17] and Holden-Risebro [5] will be followed, and we refer to these texts for a thorough discussion.

2.3.1. Linear Systems of Conservation Laws

A linear system of hyperbolic equations has the form

$$u_t + Au_x = 0, \quad x \in \mathbb{R},\ t > 0, \tag{2.13}$$

where $A \in \mathbb{R}^{m\times m}$, $u : \mathbb{R} \times [0,\infty) \mapsto \mathbb{R}^m$. A system is *hyperbolic* if the matrix A is diagonalizable with real eigenvalues. If, in addition, the eigenvalues are distinct, the system is *strictly hyperbolic*. For a hyperbolic linear conservation law, one can obtain a system of m decoupled equations by writing

$$A = R\Lambda R^{-1},$$

where R is the matrix of the right eigenvectors. Introducing the new variables

$$v = R^{-1}u,$$

equation (2.13) is rewritten as

$$v_t + \Lambda v_x = 0. \tag{2.14}$$

Analogously to the scalar case, when the initial data

$$u(x,0) = u_0(x), \quad x \in \mathbb{R},$$

is given, the solution to (2.14) can be found through the m characteristic curves $\xi(t;x_0) = x_0 + \lambda^p t$, $p = 1, \cdots, m$. In particular, the pth equation will have the solution

$$v^p(x,t) = v_0^p(x - \lambda^p t),$$

where $v_0(x) = R^{-1}u_0(x)$. The solution for u, given by $u(x,t) = Rv(x,t)$, can then be seen as a superposition of waves with velocities λ^p. For this reason, the eigenvalues λ^p are sometimes referred to as characteristic velocities, and their respective characteristic curves $\xi(t;x_0) = x_0 + \lambda^p t$ as *p-characteristics*. These manipulations are valid as long as the matrix A is constant. In general, for a non-linear system, the equations cannot be decoupled, and it will be much harder to find an analytical solution.

At this point, it is convenient to look at the solution of the Riemann problem for equation (2.13). The piecewise constant initial data is given by

$$u(x,0) = \begin{cases} u_l & \text{for } x < 0, \\ u_r & \text{for } x \geq 0. \end{cases} \tag{2.15}$$

To build the solution to the Riemann problem, decompose the initial data in the basis formed by the eigenvectors r^p:

$$u_l = \sum_{p=1}^{m} v_l^p r^p, \qquad u_r = \sum_{p=1}^{m} v_r^p r^p. \tag{2.16}$$

The pth uncoupled equation has initial data

$$v^p(x,0) = \begin{cases} v_l^p & \text{for } x < 0, \\ v_r^p & \text{for } x \geq 0, \end{cases} \tag{2.17}$$

so that the solution is given by the propagation of the initial discontinuity:

$$v^p(x,t) = \begin{cases} v_l^p & \text{for } x - \lambda^p t < 0, \\ v_r^p & \text{for } x - \lambda^p t \geq 0. \end{cases} \tag{2.18}$$

The solution for the system of equations is then

$$u(x,t) = \sum_{p:\lambda^p < x/t} v_r^p r^p + \sum_{p:\lambda^p > x/t} v_l^p r^p. \tag{2.19}$$

Thus, when the pth characteristic is crossed, the respective v^p jumps from the left to the right state. Consequently, the solution consists of m discontinuities separating $m+1$ wedges where $u(x,t)$ is constant.

It is important to note that the jump in the solution across the pth characteristic is an eigenvector of A:

$$(v_r^p - v_l^p) r^p \equiv \beta^p r^p.$$

This fact can be generalized in the context of nonlinear systems, and the more general Rankine-Hugoniot condition for shock solutions is consequently derived, see [17].

2.3.2. Nonlinear Systems of Conservation Laws

In this section, we will present the basic concepts for shock and rarefaction waves for nonlinear systems. We will state the main results of the theory, which will be used in later chapters to build analytical solutions of the physical models.

A nonlinear conservation law takes the form

$$u_t + f(u)_x = 0, \quad x \in \mathbb{R},\ t > 0. \tag{2.20}$$

For smooth solutions, equation (2.20) can be rewritten in the quasi-linear form

$$u_t + f'(u)u_x = 0, \tag{2.21}$$

where $f'(u)$ is the Jacobian of the flux function. A nonlinear conservation law (2.20) is *hyperbolic* if the Jacobian $f'(u)$ is diagonalizable with real eigenvalues for each physically relevant value of u; it is *strictly hyperbolic* if it is hyperbolic and the eigenvalues are distinct. Although the quasi-linear form is often useful for analytical purposes, the conservation form (2.20) is the correct one to use when computing shock solutions and deriving numerical methods. In fact, discretizations based on the quasi-linear form (2.21) may lead to unphysical results [17].

Analytical solutions to systems of conservation laws are generally hard to find, since the equations cannot be decoupled and the waves continuously interact with each other. However, it turns out that, under some requirements, existence and uniqueness of the solution to the Riemann problem can be ensured.

First, we will see how shock and rarefaction waves are computed in the case of a nonlinear system of hyperbolic equations. The Rankine-Hugoniot condition (2.4) can be extended to systems without restrictions:

$$\dot{s}(t) = \frac{f(u_r(s,t)) - f(u_l(s,t))}{u_r(s,t) - u_l(s,t)}, \tag{2.22}$$

where $\dot{s}(t)$ is the velocity of the shock. The concept of entropy is though much more difficult, but we will not focus on it in this thesis.

To find an expression for a rarefaction wave, let us consider the Riemann problem

$$u_t + f(u)_x = 0, \qquad u(x,0) = \begin{cases} u_l & \text{for } x < 0, \\ u_r & \text{for } x > 0. \end{cases} \tag{2.23}$$

As in the scalar case, looking for similarity solutions of the form $u(x,t) = w(x/t) = w(\eta)$ leads to the system of ODEs

$$f'(w(\eta))\,w'(\eta) = \eta\, w'(\eta). \tag{2.24}$$

Since we are considering a system of hyperbolic equations, the term $w'(\eta)$ is no longer a scalar and cannot be cancelled from (2.24). Note that (2.24) requires $w'(\eta)$ to be an eigenvector of the Jacobian $f'(w(\eta))$ for each value of η. Since the Jacobian has the m eigenvectors r^p, $p = 1, \cdots, m$, it must hold

$$w'(\eta) = r^p(w(\eta)), \quad \lambda^p(w(\eta)) = \eta \tag{2.25}$$

for a certain value of p. The differential equation in (2.25) must be completed with an initial condition. Since the left edge of the rarefaction wave should be the ray $\eta = \lambda^p(u_l)$ and the right edge should be the ray $\eta = \lambda^p(u_r)$, the following conditions hold:

$$w(\lambda^p(u_l)) = u_l, \quad w(\lambda^p(u_r)) = u_r. \tag{2.26}$$

Relation (2.25) defines also the normalization of the eigenvectors, since differentiating $\lambda^p(w(\eta)) = \eta$ gives

$$\nabla\lambda^p(w(\eta)) \cdot r^p(w(\eta)) = 1. \tag{2.27}$$

Thus, the system of ODEs can be rewritten in the form

$$w'(\eta) = \frac{r^p(w(\eta))}{\nabla\lambda^p(w(\eta)) \cdot r^p(w(\eta))}. \tag{2.28}$$

The ODEs (2.28) make sense provided that the denominator is nonzero. If this is the case and, moreover, $\lambda^p(u_l) < \lambda^p(u_r)$, then the centered rarefaction wave for the initial value problem (2.20) has the form

$$u(x,t) = \begin{cases} u_l & \text{if } x/t \le \lambda^p(u_l), \\ w(x/t) & \text{if } \lambda^p(u_l) \le x/t \le \lambda^p(u_r), \\ u_r & \text{if } x/t \ge \lambda^p(u_r). \end{cases} \tag{2.29}$$

A pth field for which $\nabla\lambda^p(u) \cdot r^p(u) \neq 0$ for all u is called genuinely nonlinear. There might be systems for which $\nabla\lambda^p(u) \cdot r^p(u) \equiv 0$ for all u. In this case, the field is said to be *linearly degenerate*. A trivial example of when this situation occurs is the constant coefficient linear hyperbolic system, where λ^p is constant and hence $\nabla\lambda^p \equiv 0$. For this kind of fields, if the initial data is a discontinuity, then this discontinuity will propagate at constant speed given by the respective eigenvalues. This discontinuity is not properly a shock, because the characteristic velocities on each side agree with the velocity of the wave. The solutions of linearly degenerate fields are often referred to as contact discontinuities, because they arise when considering passive tracers in a general flow equation. The tracer will not influence the flow because its equation is decoupled from the governing equations, and it will simply be advected by the velocity of the flow.

A theorem that guarantees the existence and uniqueness of a (local) solution, satisfying entropy conditions, of the Riemann problem (2.23) can be found in [5].

3

Introduction to Reservoir Simulation

In this chapter, the main aspects of the physics of a reservoir, along with numerical methods used to simulate the flow of a fluid through it, are introduced.

First, the terminology and the physical quantities that describe reservoir properties are presented. The traditional models employed for these quantities, together with typical assumptions made to simplify the expression of the governing flow equations, are also briefly discussed. The purpose of this research is to clarify a specific phenomenon (the velocity enhancement) that occurs when a solution of water and polymer is injected in the reservoir, therefore we will avoid the use of more complicated models that would distract us from our goal.

A section dedicated to study the multi-phase flow equations that govern the flow will then follow. These equations will be tailored in order to model two main scenarios: the (simpler) case when pure water is injected into the reservoir, and the case where polymer is added to the injected water. The analytical solution of the two cases will be discussed in detail, so that, when the model will be refined to incorporate also the velocity enhancement effects, it will be easier to make conjectures on the behaviour of the solution.

Last, the finite volume method, adopted to solve the equations numerically, is presented. While the equation for water conservation is solved through a fully implicit solver, a separate module is developed to simulate the transport of chemical agents dissolved in water. In particular, different discretizations are introduced and compared. First order upwind schemes and high resolution methods are discussed for the discretization in space, while for the discretization in time, implicit and semi-implicit schemes are introduced.

3.1. Introduction to Petroleum Terms

Before starting to develop mathematical models for fluid flow in porous media, it is essential to be familiar with the physical and chemical properties that characterize both the rock and the fluid. These properties will influence the flow of the fluid through the rock. The main rock properties of interest are porosity and permeability, while for the fluid density, compressibility and viscosity will have relevant importance. In addition, the rock-fluid interaction properties will play an important role in the modeling. Material is taken from Chen [23].

3.1.1. Reservoir Rock Properties

The tiny empty passages in a reservoir rock are called *pores*. Typically, their size varies between 1 and 200μm, depending on the rock layer. The *porosity*, indicated by ϕ, is the fraction of volume of rock which is pore space. One may further distinguish between total porosity and effective porosity: the latter includes only the pores which are interconnected, hence the ones responsible for fluid

flow, while the total porosity includes also isolated pores. We shall consider effective porosity in the rest of the discussion. Porosity often varies in space, since in a reservoir different layers of rock may be present, but in many models will be considered constant for simplicity.

Permeability, denoted by k, measures the capacity of the rock to conduct fluids through its interconnected pores. This quantity is also known as *absolute permeability*, to distinguish it from the *relative permeability* that will be introduced later. A common unit for permeability is the *millidarcy* (*md*) (1 *darcy* $\simeq 10^{-12} m^2$). Permeability usually varies on location and flow direction, but, in 3 dimensions, it is possible to assume it is a diagonal tensor (i.e. the porous medium is isotropic). However, most of the models considered later are one-dimensional, so that the permeability k will be a scalar, and for simplicity we may assume it constant.

Often, porosity and permeability are positively correlated: this result should not be surprising, since larger pores are most likely going to allow for more fluid to flow through the porous medium.

3.1.2. Reservoir Fluid Properties

The main properties of fluids in a reservoir are now introduced.

A fundamental notion to be familiar with is the compressibility of a fluid: a fluid is classified as incompressible if its density is independent of pressure, otherwise it is said to be compressible. At reservoir condition the fluids may have a slightly compressible behaviour, but often the assumption of incompressibility will be used to derive mathematical models.

The *viscosity* of a fluid, denoted by μ, is a measure of the energy dissipated when it is in motion resisting an applied shearing force. It has the dimension of force/area and the most commonly used unit in field is *centipoise* (*cp*). Viscosity is basically a consequence of the friction between the molecules of the fluid. In a gas, for example, where molecules are very far apart, viscosity will be low and the fluid will have a low resistance to flow.

3.1.3. Reservoir Rock/Fluid Properties

The interaction between the rock and the fluid is fundamental to derive realistic and appropriate models.

The first definition to be considered is *wettability*: the wettability of the rock measures the preference of the rock surface to be wetted by a particular phase. A formation which has a preference to be wetted by water is called *water wet*; an *oil wet* formation has a preference to be wetted by oil. The wettability influences other physical quantities, such as relative permeability and capillary pressure. This definition leads to the following characterization of a fluid displacement process:

- *Imbibition*: a displacement process where the wetting phase increases. In a water wet system, water flood will be an imbibition process: water will imbibe into a core containing mobile oil and occupy the smaller pores, thus displacing the oil.
- *Drainage*: a displacement process where the nonwetting phase increases.

Other properties, like capillary pressure and relative permeability, depend on the nature of the fluid displacement process.

A quantity widely used in the governing equations for fluid flow in porous media is the fluid phase *saturation* S_σ, where the subscript σ denotes the fluid phase (typically, $\sigma = \{w, o, g\}$, indicating water, oil and gas). The saturation is the fraction of the pore space that a fluid phase occupies. For a two phase flow with oil and water, it holds

$$S_o + S_w = 1.$$

The *residual saturation* of a phase is the amount of that phase which is trapped and cannot be displaced, i.e. the fluid is immobile. For oil, this saturation is usually indicated as S_{or} (residual oil

saturation), while for water the threshold value is called irreducible water saturation, S_{wir}. In the literature sometimes this saturation value is also referred to as connate water saturation S_{wc}, but there is a subtle yet important difference between the two terms: connate water saturation is more precisely defined as the fraction of water that remains trapped within sedimentary rocks during the process of sedimentation. This definition does not imply that connate water is immobile, although this will be the case in most of the reservoirs and many authors consider the connate water immobile.

Capillary pressure refers to the discontinuity between the pressure of the nonwetting phase, say oil, and the wetting phase, say water, thus taking the form

$$p_c = p_o - p_w. \tag{3.1}$$

Capillary pressure appears in a two-phase flow as a consequence of interfacial tension at the interface between the two immiscible fluids, such as oil and water. Throughout this thesis, the capillary pressure will be assumed to be zero, so that we have $p_w = p_o = p$.

The *relative permeability* is a dimensionless quantity (a fraction) that measures the effective permeability of a phase in the case of multiphase flow. In a two phase flow, one would expect the permeability to either fluid to be lower than that for the single fluid since it occupies only part of the pore space. Relative permeabilities are usually modeled as functions of saturation. A popular model for an analytic expression of relative permeabilities was proposed by Corey [11]:

$$k_{r,w} = k^0_{r,w} \begin{cases} 0 & S_w \le S_{wir}, \\ \left(\dfrac{S_w - S_{wir}}{1 - S_{wir} - S_{or}}\right)^{n_w} & S_{wir} < S_w < 1 - S_{or}, \\ 1 & S_w \ge 1 - S_{or}, \end{cases} \tag{3.2}$$

$$k_{r,o} = k^0_{r,o} \begin{cases} 0 & S_w \le S_{wir}, \\ \left(\dfrac{1 - S_w - S_{or}}{1 - S_{wir} - S_{or}}\right)^{n_o} & S_{wir} < S_w < 1 - S_{or}, \\ 1 & S_w \ge 1 - S_{or}, \end{cases} \tag{3.3}$$

where n_w, n_o are the Corey coefficients and $k^0_{r,w}$, $k^0_{r,o}$ the endpoints of the relative permeabilities curves. The values of these coefficients can be chosen to capture the physical properties of the reservoir. Typical curves for the relative permeabilities are shown in figure 3.1.
Relative permeability models for three phase flows are rather complicated and will not be discussed here, as the focus throughout the report will be on two phase systems.

Next, it is useful to define the *mobility* λ_σ and the fractional flow f_σ of a phase σ. The mobility is the ratio between relative permeability and viscosity of a certain phase:

$$\lambda_w = \frac{k_{r,w}}{\mu_w}, \qquad \lambda_o = \frac{k_{r,o}}{\mu_o}. \tag{3.4}$$

The mobility ratio M is the ratio between the mobility of the displacing fluid and the mobility of the displaced fluid. For waterflooding:

$$M = \frac{\lambda_w}{\lambda_o}. \tag{3.5}$$

Typically, $M > 1$ because water is more mobile than oil. This is the quantity that a polymer flood targets: polymer will increase water viscosity μ_w, resulting in a smaller (and more favourable) mobility ratio.

The interstitial velocity of the flowing phase is denoted by v_σ. In the derivation of the model for the flow through the porous medium, it is common to work with the superficial (or Darcy) velocities

n_w	n_o	$k^0_{r,w}$	$k^0_{r,o}$	μ_w	μ_o	S_{wir}	S_{or}
2	3	0.6	0.9	1cP	5cP	0.15	0.2

Table 3.1: Reference case for the reservoir parameters.

$u_\sigma = \phi S_\sigma v_\sigma$. The reason is that an empirical law for u_σ has been discovered by the French engineer Henry Darcy in 1856. Such law will be illustrated in the next section. Note that it holds $u_\sigma \leq v_\sigma$.

The fractional flow is a quantity that determines the (fractional) volumetric flow rate of a phase in the presence of another phase. The fractional flow of a phase is expressed as the ratio between the Darcy velocity of that phase and the total Darcy velocity $u = u_o + u_w$:

$$f_w = \frac{u_w}{u}, \qquad f_o = \frac{u_o}{u}. \tag{3.6}$$

Note that $f_w + f_o = 1$. The fractional flow is a really useful quantity, as many models used in waterflooding and polymer flooding adopt a fractional flow formulation, which allows for the construction of analytical solutions. It depends strongly on the saturation of the associated phase. The fractional flow curve has a typical s-shaped form, as it is shown in figure 3.2. We establish in table 3.1 a reference case for the reservoir parameters that will be used to compute both analytical and numerical solutions, unless specified otherwise.

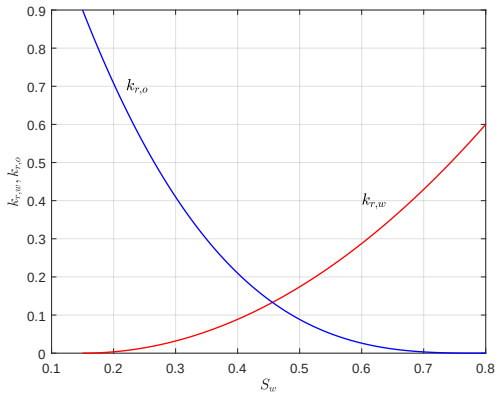

Figure 3.1: Corey's relative permeabilities with $k^0_{r,w} = 0.6$, $k^0_{r,w} = 0.9$, $n_w = 2$, $n_o = 3$, $S_{wir} = 0.15$, $S_{or} = 0.2$.

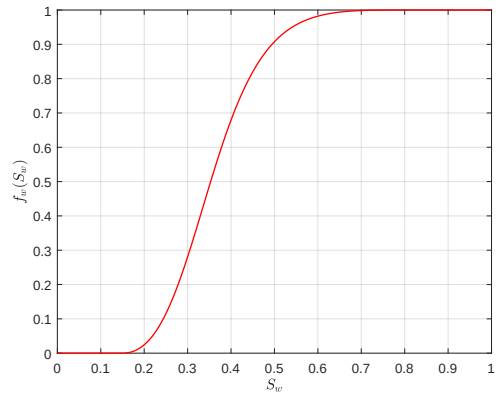

Figure 3.2: Typical fractional flow curve $f_w(S_w)$.

3.2. Multi-Phase Flow in Porous Media

Before deriving models for the velocity enhancement effect, it is necessary to present the general and basic equations for fluid flow in porous media. These equations arise from the usual fundamental law of conservation of mass, and they are completed employing the empirical Darcy's law as a constitutive relation. Typically, the assumption of incompressibility is made, which is an appropriate approximation far away from the well, where velocities are low. First, the case of a waterflooding (injection of pure water) is studied. In order to find an analytical solution, the equations are reformulated within the fractional flow theory, resulting in a hyperbolic system of equations. This formulation is also known as the Buckley-Leverett formulation.

3.2.1. Mass Conservation

Consider a control volume V with outward normal $\mathbf{n}$ and a general scalar property φ of a one-phase fluid flowing with velocity $\mathbf{v}$ through V. The law of mass balance for the control volume states:

rate of inflow-rate of outflow=change in mass.

This statement is formulated as

$$\int_{\partial V} -\varphi \mathbf{v}\cdot\mathbf{n}\, d\partial V = \int_V \frac{\partial \varphi}{\partial t} dV. \tag{3.7}$$

In the framework that will be considered, the source term is usually incorporated in the boundary conditions (injection of water-polymer at $x = 0$), therefore it is absent in (3.7). Using the divergence theorem, (3.7) is rewritten as

$$\int_V \left(\frac{\partial \varphi}{\partial t} + \nabla\cdot(\varphi \mathbf{v}) \right) dV = 0. \tag{3.8}$$

Since the control volume V is arbitrary, the integrand must be equal to zero, namely

$$\frac{\partial \varphi}{\partial t} + \nabla\cdot(\varphi \mathbf{v}) = 0. \tag{3.9}$$

Note that equation (3.9) is a general relation for a conservation of a fluid's property when the source term is absent. For a porous medium, we take $\varphi = \phi\rho$, with ϕ the porosity of the rock and ρ the density of the fluid, and $\mathbf{v}$ is the interstitial velocity. Using the superficial (or Darcy) velocity $\mathbf{u} = \phi\mathbf{v}$, equation (3.9) reads

$$\frac{\partial(\phi\rho)}{\partial t} + \nabla\cdot(\rho\mathbf{u}) = 0. \tag{3.10}$$

For multi-phase flow, the concept of saturation is used. In this case, $\varphi = \phi S_\sigma \rho_\sigma$ and $\mathbf{u}_\sigma = \phi S_\sigma \mathbf{v}_\sigma$, where $\sigma \in \{o, w\}$ denotes the phase considered (oil or water). The equation then reads

$$\frac{\partial(\phi\rho_\sigma S_\sigma)}{\partial t} + \nabla\cdot(\rho_\sigma \mathbf{u}_\sigma) = 0. \tag{3.11}$$

At this point, it is necessary to have an expression for the Darcy's velocities $\mathbf{u}_w$, $\mathbf{u}_o$. Darcy's law is an empirical law discovered by Henri Darcy. The differential form of this relation in the case of a single-phase flow, disregarding gravitational effects, is

$$\mathbf{u} = -\frac{k}{\mu}\nabla p, \tag{3.12}$$

where k is the absolute permeability and μ the viscosity. The minus sign is needed because the fluid flows from high pressure to low pressure.

In the case of multi-phase flow, the definition of Darcy's velocity is slightly modified by introducing the relative permeabilities:

$$\mathbf{u}_\sigma = -\frac{k k_{r,\sigma}}{\mu_\sigma}\nabla p_\sigma. \tag{3.13}$$

Darcy's velocity (3.13) can be used in the governing equation (3.11) to obtain

$$\frac{\partial(\phi\rho_\sigma S_\sigma)}{\partial t} - \nabla\cdot\left(\rho_\sigma \frac{k k_{r,\sigma}}{\mu_\sigma}\nabla p_\sigma \right) = 0, \qquad \sigma \in \{w, o\}. \tag{3.14}$$

The system of equations (3.14) has four unknowns, so further relations for the saturations and pressures are needed in order to close the model. From chapter 3, we can use the definitions of saturation and capillary pressure to obtain the following equations:

$$S_w + S_o = 1, \tag{3.15}$$

$$p_c = p_o - p_w. \tag{3.16}$$

The system of differential-algebraic equations (3.14), (3.15) and (3.16) describes the flow of water and oil through a porous medium. As stated previously, capillary pressure effects will be disregarded, so that (3.16) gives $p_w = p_o = p$ and hence the pressure in (3.14) will not depend on the phase σ.

3.2.2. Fractional Flow Formulation

Classical fractional flow theory was firstly developed by Buckley-Leverett [9, 20] to describe waterflooding. This formulation allows to find an analytical profile for the water saturation. The major assumptions of the model are:

1. Fluids are incompressible.
2. The flow is horizontal and one dimensional.
3. Two phases are flowing.
4. Dispersion is negligible
5. Gravity and capillary forces are negligible.
6. Darcy's law is valid
7. The reservoir is homogeneous.
8. A constant composition is continuously injected, starting at time zero.

Since the flow is one-dimensional, Darcy's velocities have now the form

$$u_\alpha = \frac{k k_{r,\alpha}}{\mu_\alpha} \frac{\partial p}{\partial x}. \tag{3.17}$$

Due to the incompressibility assumption, the density ρ_σ is canceled from (3.14), and equations for the saturation of oil and water read

$$\phi \frac{\partial S_w}{\partial t} + \frac{\partial u_w}{\partial x} = 0, \tag{3.18}$$

$$\phi \frac{\partial S_o}{\partial t} + \frac{\partial u_o}{\partial x} = 0. \tag{3.19}$$

Summation of the above equations, along with condition (3.15), yields

$$\frac{\partial u}{\partial x} = 0, \tag{3.20}$$

where $u = u_w + u_o$ is the total (constant) velocity. Using the fractional flow functions defined in (3.6), equations (3.18)-(3.19) become

$$\phi \frac{\partial S_w}{\partial t} + u \frac{\partial f_w}{\partial x} = 0, \tag{3.21}$$

$$\phi \frac{\partial S_o}{\partial t} + u \frac{\partial f_o}{\partial x} = 0. \tag{3.22}$$

Note that using the expression (3.17) for the Darcy velocities, the fractional flow functions can be rewritten as

$$f_w = \frac{\lambda_w}{\lambda_w + \lambda_o}, \quad f_o = \frac{\lambda_o}{\lambda_w + \lambda_o}. \tag{3.23}$$

Since the mobilities λ_σ, defined in (3.4), depend on the relative permeabilities which, in turn, depend on the saturation, it is evident that $f_w = f_w(S_w)$ and $f_o = f_o(S_w)$ (recall that $S_o = 1 - S_w$). For the relative permeabilities, Corey's model is employed. Note that if the velocity u is known, then it is sufficient to solve equation (3.21) for water saturation, since the saturation of oil will follow from (3.15).

Initial and boundary conditions for a one-dimensional reservoir where the fluid is injected at $x = 0$ and water is initially at the irreducible saturation, can be modeled setting the Riemann problem

$$S_w(x,0) = \begin{cases} S_{w,inj} & x < 0, \\ S_{wir} & x \geq 0, \end{cases} \tag{3.24}$$

where $S_{w,inj}$ indicates the saturation of water at the injection point. Unless diversely specified, we will set $S_{w,inj} = 1 - S_{or}$. Note that water will flow from left to the right, hence $u > 0$.

Consider now the equation for water conservation (3.21). Since the fractional flow function is neither convex or concave, we expect the formation of both a rarefaction and a shock wave. Rewriting it in quasi-linear form gives the classical Buckley-Leverett formulation, namely

$$\frac{\partial S_w}{\partial t} + \frac{u}{\phi}\frac{df_w}{dS_w}\frac{\partial S_w}{\partial x} = 0. \tag{3.25}$$

This is a hyperbolic equation for S_w, with characteristic velocity given by

$$\lambda_w = \left(\frac{dx}{dt}\right)_{S_w} = \frac{u}{\phi}\frac{df_w}{dS_w}. \tag{3.26}$$

On a front propagating with such velocity, the saturation is constant [14]. However, because of the s-shaped graph of $f(S_w)$, the derivative df/dS_w is not monotone: after a first increasing phase, it starts decreasing in correspondence of the inflection point of $f(S_w)$. Thus, the characteristic lines intersect and, as discussed in chapter 2, a shock forms. Since $1 - S_{or} > S_{wir}$, a solution is formally given by (2.12), i.e. taking the concave upper envelope of f_w. The rarefaction wave starting from $x = 0$ is given by

$$\hat{S}_w(x/t) = \left(\frac{u}{\phi}\frac{df_w}{dS_w}\right)^{-1}(x/t), \qquad \lambda_w(1 - S_{or}) < x/t < \lambda_w(S^*), \tag{3.27}$$

where S^* is the value of saturation on the left of the shock. Note that $\lambda_w(1 - S_{or}) = 0$. The velocity of the shock σ_w can be found through the usual Rankine-Hugoniot condition. For the point ahead of the shock, $S_w = S_{wir}$. The condition then gives

$$\sigma_w = \frac{u}{\phi}\frac{f_w(S^*) - f_w(S_{wir})}{S^* - S_{wir}}. \tag{3.28}$$

Since the velocities given by (3.26) and (3.28) must be equal at the contact between the shock and the continuous saturation distribution, it holds

$$\frac{f_w(S^*) - f_w(S_{wir})}{S^* - S_{wir}} = \frac{df_w}{dS_w}(S^*). \tag{3.29}$$

Thus, S^* can be obtained from (3.29). The value of S^* can also be obtained graphically, by building the upper concave envelope of $f_w(S_w)$, see figure 3.3. From this figure, we see that the two methods are indeed equivalent, since (3.29) defines a straight line with slope df_w/dS_w and intercept $(S_{wir}, 0)$. The straight line in figure 3.3 corresponds to the shock, while the smooth part for $S_w > S^*$ corresponds to the rarefaction wave. The solution to the Riemann problem defined by (3.21)-(3.24) is

$$S_w(x,t) = \begin{cases} 1 - S_{or} & \text{for} \quad x/t < 0, \\ \hat{S}_w(x/t) & \text{for} \quad 0 < x/t < \lambda_w(S^*), \\ S_{wir} & \text{for} \quad x/t > \lambda_w(S^*). \end{cases} \tag{3.30}$$

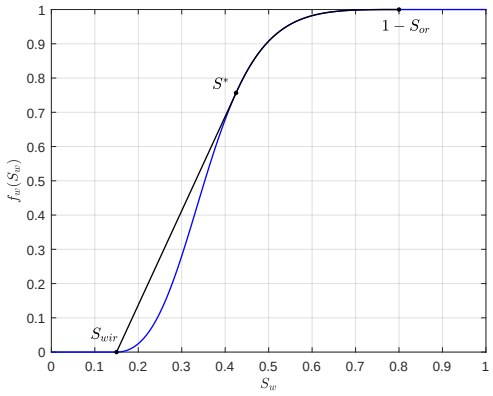

Figure 3.3: Construction of the Buckley-Leverett solution for water flooding. $S_{wir} = 0.15$, $S_{or} = 0.2$.

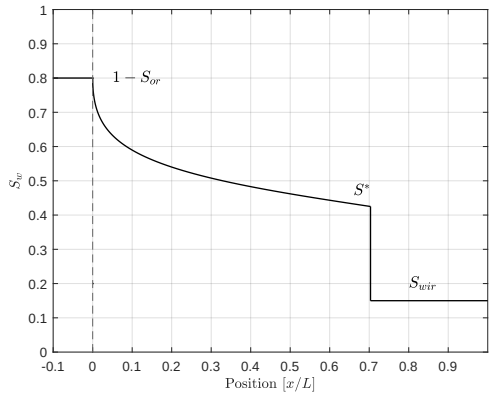

Figure 3.4: Buckley-Leverett solution for water flooding and a fixed $t > 0$. $S_{wir} = 0.15$, $S_{or} = 0.2$.

3.3. Polymer Flood

To improve oil recovery, polymer is added to the injected water in order to increase its viscosity, resulting in a more favourable mobility ratio M. The mobility ratio here is defined by

$$M = \frac{\lambda_w}{\lambda_o} = \frac{\mu_o k_{r,w}}{\mu_w k_{r,o}}. \tag{3.31}$$

For a water flood, typically $M > 1$. Adding polymer to the injected water will usually lower the mobility ratio to values close to 1. A thorough discussion on polymer flooding can be found in [9, 11].

Since the polymer does not change the residual oil saturation, both waterflooding and polymer flooding will theoretically produce all of the moveable oil over a very long time scale. This time scale, however, is usually many times the practical reservoir development period. The polymer will essentially speed up the recovery, see figure 3.5. The figure shows also an approximated economic limit for both water and polymer flood. Polymer flooding will be particularly useful in those reservoirs where waterflooding is or is predicted to be inefficient. In order to evaluate projects, it is important to predict recovery profiles for waterflood and polymer flood employing different chemical agents. One way of obtaining these data is to perform different simulations of the proposed projects. This motivates the development and analysis of mathematical models for polymer flood. Although there are many physical and chemical effects that influence the flow of the polymer-water solution through the reservoir, simulations of these models are a good and efficient mean to evaluate proposed projects. Under reasonable assumptions, models for the flow through the reservoir are derived, giving the chance to simulate saturation and polymer concentration profiles for injected water and polymer.

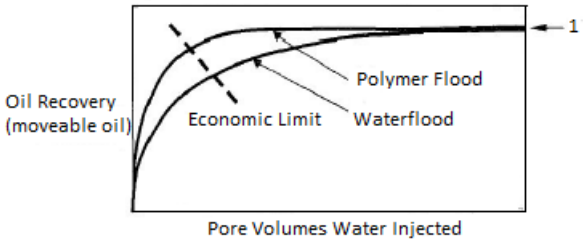

Figure 3.5: Comparison of production profiles for a water flood and a polymer flood. From [9].

3.3.1. Thick Water Model

A first simple approach is to apply classical Buckley-Leverett theory to polymer flooding [2]. This means that the polymer flood is treated as a water flood, only with a different value for viscosity. This model is called the thick water model. Thus, this model is mathematically equivalent to the Buckley-Leverett waterflooding and no new features must be discussed. Figure 3.6 shows two saturation profiles for different water viscosity: $\mu_w = 1cP$ corresponds to a waterflooding; $\mu_w = 5cP$ corresponds to a polymer flooding. Figure 3.7 shows the recovery for the two cases. As it can be seen, the polymer delays the breakthrough of the water front. As a consequence, even if the ultimate recovery will be the same for both cases, a higher oil recovery will be reached earlier when employing a polymer flooding instead of a waterflooding.

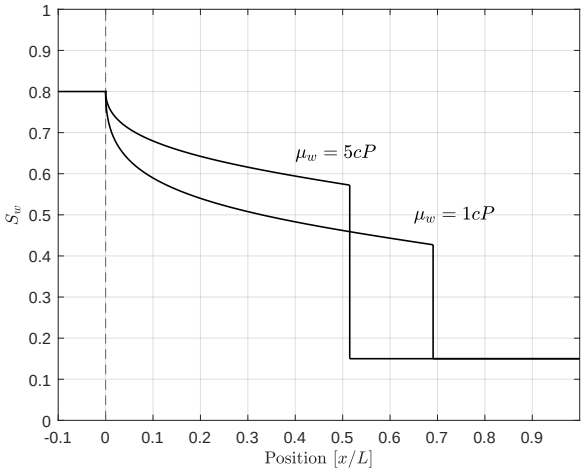

Figure 3.6: Floods for different values of water viscosity. Compared to the waterflooding ($\mu_w = 1cP$), the front of the polymer-water solution ($\mu_w = 5cP$) is delayed.

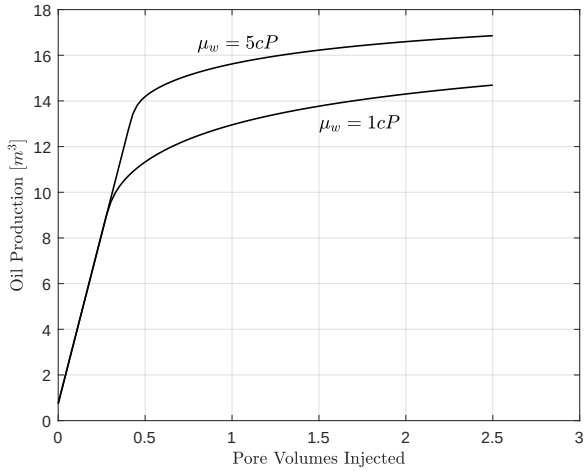

Figure 3.7: Oil production for values of water viscosity in figure 3.6, on a longer time scale. The polymer delays the breakthrough of water, so that the recovery is improved.

3.3.2. Extended Fractional Flow Theory

To have a more accurate model, classical Buckley-Leverett fractional flow theory can be extended [9, 14], deriving a continuity equation also for the polymer concentration c. On top of the assumptions

stated above for the fractional flow theory for waterflooding, further assumptions for the polymer are

1. The polymer solution has a Newtonian flow behaviour.
2. Polymer dispersion, gravity, capillary forces and adsorption to rock are negligible.
3. The polymer is present only in the aqueous phase.

The purpose of this section is to derive a qualitative profile for the water saturation and polymer concentration, therefore we disregard effects that would lead to unnecessary complexities.

Since the polymer influences the water viscosity, and thus the mobility, the fractional flow function depends not only on the water saturation, but also on the polymer concentration. The dependence of water viscosity on polymer concentration can be modelled by the Flory-Huggins equation [11]:

$$\mu_w(c) = \mu_w^0\left(1+\alpha_1 c+\alpha_2 c^2+\alpha_3 c^3\right) = \mu_w^0 \mu_{mult}(c), \tag{3.32}$$

where μ_w^0 is the water viscosity without polymer, μ_{mult} the viscosity multiplier function ans α_i some constants. A typical curve for the viscosity multiplier μ_{mult} is shown in figure 3.8. When adding polymer to water, the fractional flow curve shifts toward the right, as shown in figure 3.9.

According to Pope [14], continuity equations for water and polymer in fractional flow formulation are

$$\phi\frac{\partial S_w}{\partial t}+u\frac{\partial(f_w(S_w,c))}{\partial x}=0, \tag{3.33}$$

$$\phi\frac{\partial(S_w c)}{\partial t}+u\frac{\partial(c f_w(S_w,c))}{\partial x}=0. \tag{3.34}$$

To complete equations (3.33) and (3.34), a Riemann initial condition is assigned for both water and polymer:

$$S_w(x,0)=\begin{cases}1-S_{or} & x<0,\\ S_{wir} & x>0,\end{cases} \tag{3.35}$$

$$c(x,0)=\begin{cases}\bar{c} & x<0,\\ 0 & x>0.\end{cases} \tag{3.36}$$

During a polymer flood, generally two shocks arise [14]: one at the polymer front, where polymer contacts connate water, and one as the water saturation increases from its initial value (as in the

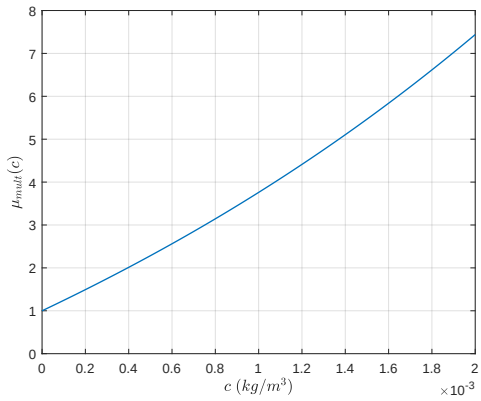

Figure 3.8: Viscosity multiplier $\mu_{mult}(c)$, with $\alpha_1 = 24$, $\alpha_2 = 31$, $\alpha_3 = 50$.

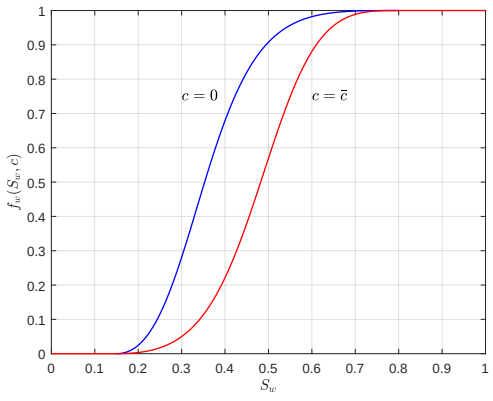

Figure 3.9: Fractional flow curves for different values of polymer concentration.

waterflood). The procedure to build an analytical solution commonly followed in the literature is rather intuitive and guided from physical concepts, but lacks of a more formal and detailed discussion. Therefore, we will investigate the behaviour of the solution using the ingredients introduced in chapter 2.

Expanding equation (3.34) and using (3.33), the equation for polymer concentration is rewritten as

$$\phi S_w \frac{\partial c}{\partial t} + u f_w \frac{\partial c}{\partial x} = 0, \tag{3.37}$$

so that the system of hyperbolic equations (3.33)-(3.34) in quasi-linear form is

$$\frac{\partial}{\partial t}\begin{pmatrix} S_w \\ c \end{pmatrix} + A\frac{\partial}{\partial x}\begin{pmatrix} S_w \\ c \end{pmatrix} = \begin{pmatrix} 0 \\ 0 \end{pmatrix}, \tag{3.38}$$

where

$$A = \frac{u}{\phi}\begin{pmatrix} \frac{\partial f_w}{\partial S_w} & \frac{\partial f_w}{\partial c} \\ 0 & \frac{f_w}{S_w} \end{pmatrix}. \tag{3.39}$$

Note $S_w \in [S_{wir}, 1 - S_{or}]$, so division by zero in (3.39) does not occur. The eigenvalues of the system for the water and polymer waves are, respectively,

$$\lambda_w = \frac{u}{\phi}\frac{\partial f_w}{\partial S_w}, \qquad \lambda_p = \frac{u}{\phi}\frac{f_w}{S_w}. \tag{3.40}$$

The respective eigenvectors are

$$r_w = \begin{bmatrix} 1 \\ 0 \end{bmatrix}, \qquad r_p = \begin{bmatrix} \frac{\partial f_w}{\partial c} \\ \frac{f_w}{S_w} - \frac{\partial f_w}{\partial S_w} \end{bmatrix}. \tag{3.41}$$

We compute now the gradients of the eigenvalues (3.40) to check if the water and polymer fields are genuinely nonlinear or linearly degenerate. The gradients are

$$\nabla\lambda_w = \frac{u}{\phi}\begin{bmatrix} \frac{\partial^2 f_w}{\partial S_w^2} \\ \frac{\partial^2 f_w}{\partial S_w \partial c} \end{bmatrix}, \qquad \nabla\lambda_p = \frac{u}{\phi}\begin{bmatrix} \frac{1}{S_w}\frac{\partial f_w}{\partial S_w} - \frac{f_w}{S_w^2} \\ \frac{1}{S_w}\frac{\partial f_w}{\partial c} \end{bmatrix}. \tag{3.42}$$

Computing the inner products between these gradients and the eigenvectors gives

$$\nabla\lambda_p \cdot r_p = 0,$$
$$\nabla\lambda_w \cdot r_w = \frac{u}{\phi}\frac{\partial^2 f_w}{\partial S_w^2}.$$

Hence, the polymer field is linearly degenerate and will behave as a contact discontinuity. The water field, instead, is genuinely nonlinear as long as the second derivative of the fractional flow function is nonzero. We have seen that $f_w(S_w)$ has an inflection point, so the water field is not genuinely nonlinear for all the values of S_w in its interval of definition. However, we will see that this inflection point is not reached by the solution.

The water field defines the system of ODEs (2.28), as discussed in chapter 2, which theoretically give raise to a rarefaction wave for both water and polymer. In this case, though, the second component of r_w is zero, meaning that the ODE for polymer concentration has the constant solution

$$c(x,t) = \bar{c}, \qquad \lambda_w(1 - S_{or}, \bar{c}) < x/t < \lambda_w(S_l, \bar{c}),$$

where S_l is the value of saturation on the left of the shock, see figure 3.11. The rarefaction wave for $S_w(x,t) = \tilde{S}_w(x/t)$ is given by solving the ODE

$$\tilde{S}_w'(x/t) = \left(\frac{u}{\phi}\frac{\partial^2 f_w}{\partial S_w^2}\right)^{-1}(x/t), \qquad \lambda_w(1-S_{or},\bar{c}) < x/t < \lambda_w(S_l,\bar{c}).$$

Note that $\partial^2 f_w/\partial^2 S_w$ at $S_w = 1-S_{or}$ is zero, hence the rarefaction wave at $x = 0$ will start with a vertical slope. Since the front where the polymer concentration jumps to zero corresponds to a contact discontinuity, the value of S_l is the one for which the characteristic velocities (i.e. the eigenvalues (3.40)) are equal. Thus, S_l is found by solving

$$\frac{f_w(S_l,\bar{c})}{S_l} = \frac{df_w}{dS_w}(S_l,\bar{c}). \tag{3.43}$$

Note that if the eigenvalues are equal, the system is no more strictly hyperbolic. The consequences of the loss of strict hyperbolicity are still poorly understood. However, the fact that the polymer wave is linearly degenerate ensures that no mathematical difficulties arise [17].

In figure 3.10 we depict the fractional flow curves for the concentration values $c = 0$, $c = \bar{c}$ and the Buckley-Leverett construction of the solution. From this picture, it is clear that relation (3.43) excludes the possibility of crossing the inflection point of the fractional flow curve, since it defines a straight line through the origin and tangent to $f_w(S_w,\bar{c})$.

Since at the contact discontinuity the fractional flow function jumps from $f_w(S_w,\bar{c})$ to $f_w(S_w,0)$, we expect a shock in the water saturation. To compute the value of S_w on the right of the polymer front, which we will denote by S_r, we can impose, as in the waterflood case, that the characteristic velocity of water equals the shock velocity. Using the Rankine-Hugoniot relation, the shock velocity takes the form

$$\sigma_2 = \frac{u}{\phi}\frac{f_w(S_l,\bar{c}) - f_w(S_r,0)}{S_l - S_r}. \tag{3.44}$$

The value of S_r is then computed through the relation

$$\frac{df_w}{dS_w}(S_l,\bar{c}) = \frac{f_w(S_l,\bar{c}) - f_w(S_r,0)}{S_l - S_r}. \tag{3.45}$$

In front of this shock, $c = 0$ and we are in the standard case of a waterflooding. In most of the cases, the value S_r will be smaller than the saturation value S^* for which the concave envelope of $f_w(S_w,0)$ becomes a straight line (i.e. the value of saturation at the front in a waterflooding). However, we consider the general case where it may happen that $S_r > S^*$. Ahead of the polymer front, there is a constant saturation plateau where $S_w = S_r$. If $S_r > S^*$, ahead of the constant plateau another rarefaction wave forms, defined, as for waterflooding, by

$$\hat{S}_w(x/t) = \left(\frac{u}{\phi}\frac{df_w}{dS_w}\right)^{-1}(x/t), \qquad \lambda_w(S_r,0) < x/t < \lambda_w(S^*,0). \tag{3.46}$$

Finally, the water saturation jumps to the irreducible saturation, with velocity given by the Rankine-Hugoniot relation

$$\sigma_1 = \frac{u}{\phi}\frac{f_w(S^*,0) - f_w(S_{wir},0)}{S^* - S_{wir}}. \tag{3.47}$$

S^* is found by the relation $\sigma_1 = \lambda_w(S^*,0)$. If $S_r < S^*$, no rarefaction wave occurs, and S^* must be substituted by S_r in (3.47). This scenario is the one depicted in figures 3.10-3.11. The solution to the

Riemann problem for polymer flooding is

$$S_w(x,t) = \begin{cases} 1 - S_{or} & \text{for} \quad x/t < 0, \\ \tilde{S}_w(x/t) & \text{for} \quad 0 < x/t < \lambda_w(S_l, c_l), \\ S_r & \text{for} \quad \lambda_w(S_l, c_l) < x/t < \lambda_w(S_r, 0) \quad \text{and} \quad S_r > S^*, \\ \hat{S}_w(x/t) & \text{for} \quad \lambda_w(S_r, 0) < x/t < \sigma_1 \quad \text{and} \quad S_r > S^*, \\ S_r & \text{for} \quad \lambda_w(S_l, c_l) < x/t < \sigma_1 \quad \text{and} \quad S_r < S^*, \\ S_{wir} & \text{for} \quad x/t > \sigma_1, \end{cases} \tag{3.48}$$

$$c(x,t) = \begin{cases} \bar{c} & \text{for} \quad x/t < \lambda_w(S_l, \bar{c}), \\ 0 & \text{for} \quad x/t > \lambda_w(S_l, \bar{c}). \end{cases} \tag{3.49}$$

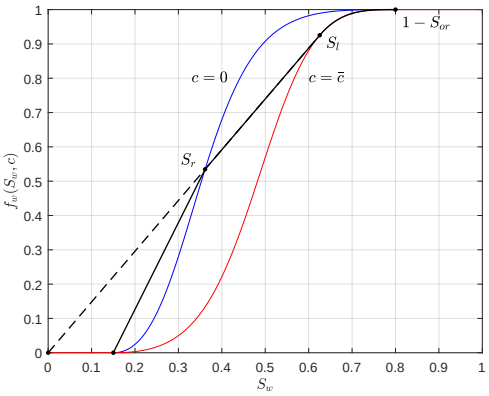

Figure 3.10: Construction of the Buckley-Leverett solution for polymer flooding.

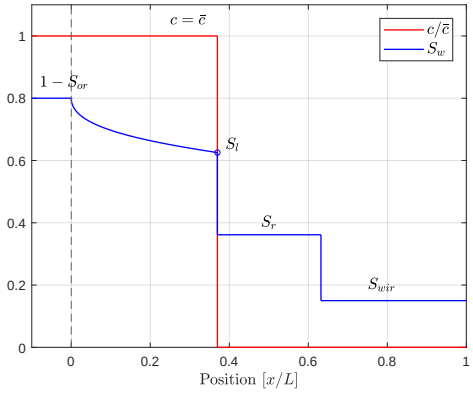

Figure 3.11: Buckley-Leverett solution for polymer flooding and a fixed $t > 0$.

3.4. Overview of Numerical Methods

Except for very simple cases, analytical solutions for water saturation and polymer concentration profiles are not available and therefore numerical methods are needed. Sintef provides a Matlab simulation toolbox (MRST, Matlab Reservoir Simulation Toolbox [8]) in order to simulate the flow both in the case of a waterflood or polymer flood. This toolbox uses a finite volume discretization in space with first order upwind schemes for the fluxes and an implicit discretization in time in order to avoid stability issues. Equations are rewritten in conservation form and then discretized. In this chapter, the numerical scheme used by the MRST toolbox is presented first for the waterflood case. The method is then extended to the polymer flood, where the water and polymer equations are coupled and solved simultaneously using a fully implicit first order upwind method. Although this approach yields an unconditionally stable method, it introduces a strong numerical diffusion and, moreover, it is computationally expensive since equations are non-linear and must be solved using the Newton method. Thus, an alternative approach was proposed in [10]. Focusing first on the transport of an inert tracer (so that the transport equation is decoupled from the flow equations), implicit and semi-implicit methods are studied and higher-resolution methods are employed to improve the accuracy of the solution. These methods are then extended to polymer flooding, solving the equations sequentially: flow equations are solved with the old concentration value, while the polymer continuity equation is solved using the current value of water saturation. Information presented in the following sections are mainly taken from [10].

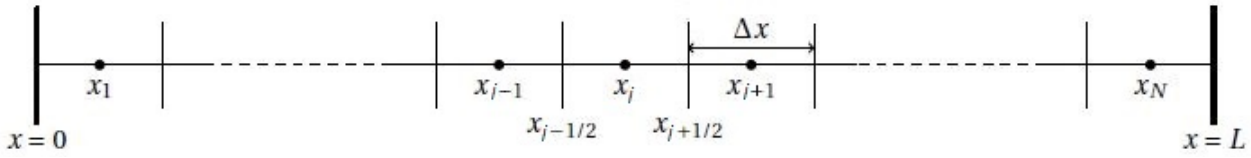

Figure 3.12: Cell-centered grid.

3.4.1. Numerical Methods for Waterflooding

The one-dimensional domain $[0, L]$ is discretized into N equal sized control volumes V_j, $j = 1, \cdots, N$, $|V_j| = \Delta x$, using a cell-centered discretization. Cell centers are denoted by x_j (see figure 3.12). Equations for water and oil in conservation form and with incompressibility assumption are recalled to be

$$\frac{\partial}{\partial t}(\phi S_\sigma) + \frac{\partial}{\partial x}(u_\sigma) = 0, \qquad \sigma \in \{o, w\}. \tag{3.50}$$

Disregarding capillary pressures, integration of the spatial derivative (3.50) over a control volume gives

$$\int_V \frac{\partial}{\partial x}(u_\sigma)\,dx = -\int_V \frac{\partial}{\partial x}\left(\lambda_\sigma \frac{\partial p}{\partial x}\right) = -\left[\lambda_\sigma \frac{\partial p}{\partial x}\right]_{x_{j-1/2}}^{x_{j+1/2}} = -(F_{\sigma,j+1/2} - F_{\sigma,j-1/2}), \tag{3.51}$$

where $F_{\sigma,j+1/2}$ and $F_{\sigma,j-1/2}$ represent the fluxes through the right and left boundaries, respectively. The pressure derivative is discretized using a central difference scheme

$$\left.\frac{\partial p}{\partial x}\right|_{x_{j+1/2}} \approx \frac{p_{j+1} - p_j}{\Delta x},$$

while the mobility $\lambda_\sigma(S_\sigma)$ is discretized through a first order upwind scheme. Since water is injected at $x = 0$, the flow is from left to right and the upwind approximation reads

$$\lambda_{\sigma,j+1/2} = \lambda_\sigma(S_{\sigma,j+1/2}) \approx \lambda_\sigma(S_{\sigma,j}) = \frac{k k_{r,\sigma}(S_{\sigma,j})}{\mu_\sigma}.$$

For the time derivative of (3.50), a first order backward scheme with time step Δt gives

$$\frac{\partial}{\partial t}(\phi S_\sigma) \approx \phi \frac{S_\sigma^{n+1} - S_\sigma^n}{\Delta t}.$$

Integration over a control volume V_j and mean value theorem lead to the fully implicit discretized form of equation (3.50)

$$\phi \Delta x \frac{S_{\sigma,j}^{n+1} - S_{\sigma,j}^n}{\Delta t} = \left(\lambda_{\sigma,j}^{n+1} \frac{p_{j+1}^{n+1} - p_j^{n+1}}{\Delta x} - \lambda_{\sigma,j-1}^{n+1} \frac{p_j^{n+1} - p_{j-1}^{n+1}}{\Delta x}\right). \tag{3.52}$$

Since the mobilities are non-linear functions of the saturation, Newton method is used to solve the discrete system. Rewriting (3.52) in the residual form

$$R_{\sigma,j} = \phi \Delta x \frac{S_{\sigma,j}^{n+1} - S_{\sigma,j}^n}{\Delta t} - \left(\lambda_{\sigma,j}^{n+1} \frac{p_{j+1}^{n+1} - p_j^{n+1}}{\Delta x} - \lambda_{\sigma,j-1}^{n+1} \frac{p_j^{n+1} - p_{j-1}^{n+1}}{\Delta x}\right) = 0,$$

the system of discretized equations that must be solved is

$$\mathbf{R}(\mathbf{x}^{n+1}, \mathbf{x}^n) = 0,$$

where $\mathbf{x}$ is the vector containing the unknowns. The Newton scheme solves the following system at each iteration:

$$\frac{d\mathbf{R}}{d\mathbf{x}}\delta\mathbf{x}^{k+1} = -\mathbf{R}(\mathbf{x}^k), \quad k = 0, 1, \cdots,$$

updating at each step $\mathbf{x}^{k+1} = \delta\mathbf{x}^{k+1} + \mathbf{x}^k$. The iterations continue until $||\mathbf{R}(\mathbf{x}^k)||_\infty < \epsilon$, where ϵ is some given tolerance. The analytical expression of the Jacobian $\frac{d\mathbf{R}}{d\mathbf{x}}$ may be extremely expensive to compute. The MRST simulator uses automatic differentiation to prevent this problem: all operations applied to the variables are also applied to their derivatives in differential form [18].

The implicit scheme used by the MRST simulator is unconditionally stable, but this comes at the expenses of accuracy. The water front might be severely smeared out at the discontinuity. Furthermore, Taylor series expansion cannot be carried out at the discontinuity since it requires the function to be smooth, so at the shock the order of accuracy is even less than one [10]. For these reasons, both implicit and semi-implicit schemes will be discussed when discretizing the polymer continuity equation. A semi-implicit scheme is usually less computationally intensive than an implicit one, but restrictions on the time step are needed in order to ensure stability. To improve accuracy, higher order fluxes will also be considered. Figure 3.13 shows how the implicit solver fails to capture the discontinuity accurately and smears out the water saturation profile.

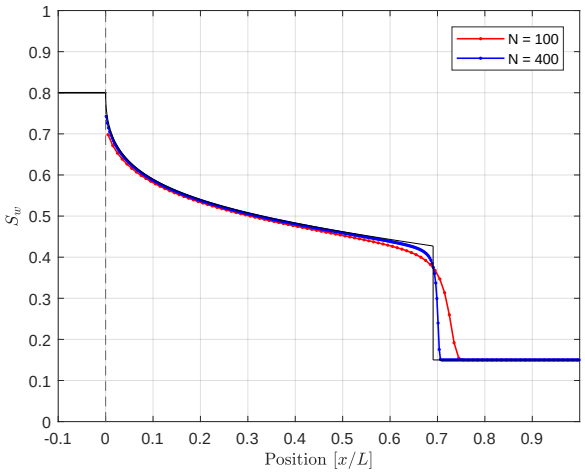

Figure 3.13: Water saturation profile for a water flood. The black line represents the analytical solution, N is the number of cells and time steps.

3.4.2. Numerical Methods for Inert Tracer

Before dealing with numerical schemes for polymer flooding, it may be useful to investigate the case of transport of an inert tracer in order to gain insights on the behaviour of semi-implicit and implicit schemes, as well as higher-resolution methods, when applied to an uncoupled transport equation. Water properties are not affected by the presence of the tracer, so that the fractional flow function depends only on water saturation. The transport equation for the tracer concentration c is

$$\frac{\partial}{\partial t}(\phi c S_w) + \frac{\partial}{\partial x}(c u_w) = 0. \tag{3.53}$$

The tracer front is simply advected at velocity

$$v_t = \frac{u f_w(\bar{S})}{\phi \bar{S}},$$

where $\bar{S}$ is the value for which the characteristic velocities of water and tracer are equal, see [10].

First, the flow is solved with the fully implicit method. Then, the obtained discrete values of u_w and S_w are used to solve the transport equation. Similarly to the previous section, a finite volume discretization combined with a first order backward time scheme results in

$$\phi \Delta x \frac{(cS_w)_j^{n+1} - (cS_w)_j^n}{\Delta t} = -(F_{j+1/2} - F_{j-1/2}), \tag{3.54}$$

where the fluxes $F_{j\pm1/2}$ are again approximated by a first order upwind scheme. Two approaches, that will be extended to the polymer flooding, are compared:

- Semi-implicit
$$F_{j+1/2} = c_j^n u_{w,j}^{n+1}, \tag{3.55}$$
- Implicit
$$F_{j+1/2} = F_{j+1/2}^{n+1} = c_j^{n+1} u_{w,j}^{n+1}. \tag{3.56}$$

In [10], a pure explicit discretization $F_{j+1/2} = F_{j+1/2}^n = c_j^n u_{w,j}^n$, is discussed as well, but it will not be adopted in the polymer flooding case because the polymer transport equation is not uncoupled from the flow equation. Therefore, we do not discuss it here. Equation (3.54) is solved for the unknown $(cS_w)_j^{n+1}$ and the concentration is found as $c_j^{n+1} = \frac{(cS_w)_j^{n+1}}{S_{w,j}^{n+1}}$. If $S_{w,j}^{n+1}$ is close to zero, this term is replaced by a value ϵ in order to avoid numerical issues which can lead to unphysical solutions.

Numerical solutions for the two choices of fluxes are shown in figure 3.14. The semi-implicit method reduces numerical diffusion, but the front is still severely smeared out. Monotonicity of the concentration profile for the semi-implicit scheme can be guaranteed by imposing restriction on the time step, which may though be stricter than the CFL condition for small values of S_w. No restrictions on the time step are needed for the implicit scheme. For a thorough analysis of the monotonicity, refer to [10].

To reduce the numerical diffusion, high-resolution methods are introduced. The idea of these methods is to use a higher order scheme for the fluxes, switching to a first order scheme near the discontinuity. This approach is well suited for advection problems since first order upwind smears out the solution, while higher order schemes result in oscillations close to the jump. The high resolution methods considered here are the total variation diminishing (TVD) flux-limiter methods, i.e.

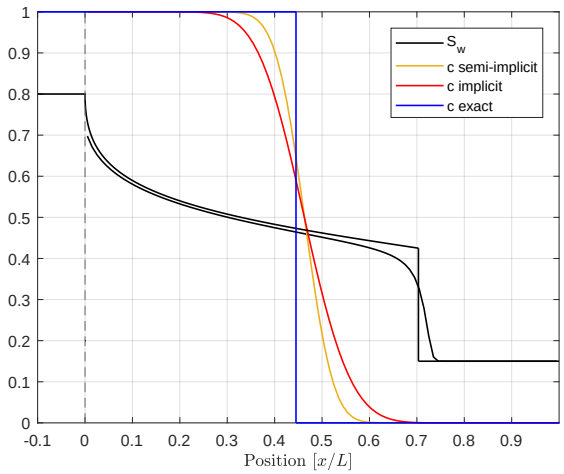

Figure 3.14: Saturation and concentration profiles for exact and numerical solutions, with 100 cells and 100 time steps.

methods for which the total variation (of the concentration)

$$TV(c) = \sum_{j=1}^{N} |c_j - c_{j-1}|$$

does not grow over time, meaning that $TV(c^{n+1}) \leq TV(c^n)$. Such methods guarantee that no unphysical oscillations will arise in the solution [10].

The expression of the flux will then take the form

$$F_{j+1/2} = F_{L,j+1/2} + \Phi_{j+1/2}(F_{H,j+1/2} - F_{L,j+1/2}), \tag{3.57}$$

where F_L is the low order flux given by the upwind scheme discussed previously, F_H the higher order flux given by the second order scheme

$$F_{H,j+1/2} = \frac{1}{2}u_{w,j}(c_j + c_{j+1}) - \frac{1}{2}(u_{w,j})^2\frac{\Delta t}{\Delta x}(c_{j+1} - c_j),$$

and $\Phi = \Phi(\theta_{j+1/2})$ the flux limiter function, where

$$\theta_{j+1/2} = \frac{c_j - c_{j-1}}{c_{j+1} - c_j}.$$

Flux limiter functions Φ are chosen such that, far away from the discontinuity, $\theta_{j+1/2} \approx 1$ and $\Phi(1) = 1$, while close the discontinuity $\theta_{j+1/2} \approx 0$ and $\Phi(0) = 0$. TVD flux limiters must be used in order to have a TVD scheme. Among the most common TVD limiters are the van Leer one, defined by

$$\Phi(\theta) = \frac{\theta + |\theta|}{1 + |\theta|}, \tag{3.58}$$

and the superbee, defined by

$$\Phi(\theta) = \max(0, \min(1, 2\theta), \min(2, \theta)). \tag{3.59}$$

Again, the two cases with semi-implicit and implicit schemes are compared. The resulting fluxes are:

- Semi-implicit

$$F_{j+1/2} = c_j^n u_{w,j}^{n+1} + \Phi(\theta_{j+1/2}^n)\frac{1}{2}u_{w,j}^{n+1}\left(1 - \frac{\Delta t}{\Delta x}u_{w,j}^{n+1}\right)(c_{j+1}^n - c_j^n), \tag{3.60}$$

- Implicit

$$F_{j+1/2} = F_{j+1/2}^{n+1} = c_j^{n+1} u_{w,j}^{n+1} + \Phi(\theta_{j+1/2}^{n+1})\frac{1}{2}u_{w,j}^{n+1}\left(1 - \frac{\Delta t}{\Delta x}u_{w,j}^{n+1}\right)(c_{j+1}^{n+1} - c_j^{n+1}). \tag{3.61}$$

While the semi-implicit method is linear in c_j^{n+1}, the implicit method results in a non-linear scheme in c_j^{n+1}, so that Newton's method has to be used to solve the non-linear system.

Simulation results using a van Leer limiter are shown in figures 3.15-3.16. The semi-implicit high-resolution scheme performs best, strongly reducing the numerical diffusion. As mentioned before, when using a non-fully implicit flux, restrictions on the time step are needed in order to preserve monotonicity. The implicit scheme has the advantage of being unconditionally stable and monotone, but the numerical diffusion smears out the solution even with higher order fluxes. Moreover, due to the non-linearity, this scheme is more expensive. Overall, given the efficiency in term of accuracy and computation time, the semi-implicit high resolution scheme should be preferred over

the implicit one. The method is TVD, so it is stable provided that the CFL condition holds. Using the method of frozen coefficients and Von Neumann analysis [10], a local stability criterion for the transport equation in the form of CFL condition is found to be

$$C_T = \frac{\Delta t}{\Delta x}|v_{max}| = \max_{S_w}\left|\frac{\Delta t}{\phi \Delta x}\frac{u_w(S_w)}{S_w}\right| \leq 1, \tag{3.62}$$

where v_{max} is the maximum wave speed encountered and C_T is the Courant number. If the restriction on the time step becomes too strict, it is safer to switch to the implicit scheme.

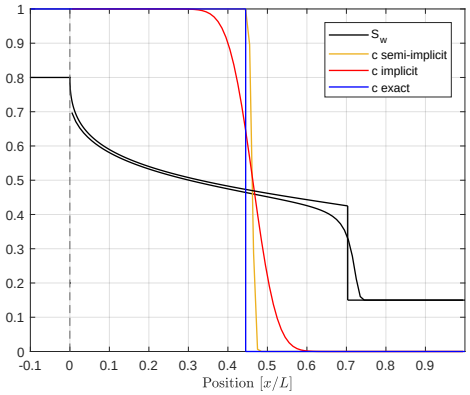

Figure 3.15: Saturation and concentration profiles for exact and numerical solutions, with 100 cells and 100 time steps and high resolution methods.

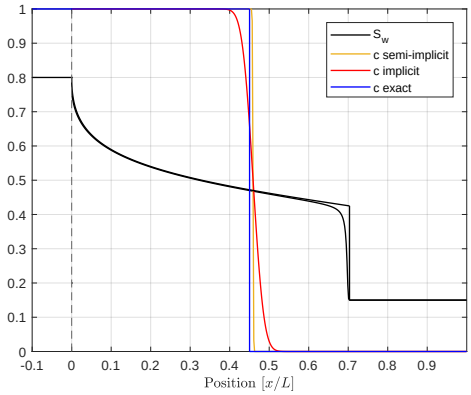

Figure 3.16: Saturation and concentration profiles for exact and numerical solutions, with 500 cells and 500 time steps and high resolution methods.

3.4.3. Numerical Methods for Polymer Flooding

Adding polymer to the injected water will influence chemical and physical properties of the fluid. In this case, continuity equation for water saturation and polymer concentration are coupled. The MRST simulator solves the equations simultaneously with a fully implicit first order upwind method. This approach result in the following scheme

$$\begin{cases} S_{o,j}^{n+1} & = S_{o,j}^{n} - \frac{\Delta t}{\phi \Delta x}\left(u_o(S_{o,j}^{n+1}, c_j^{n+1}) - u_o(S_{o,j-1}^{n+1}, c_{j-1}^{n+1})\right), \\ S_{w,j}^{n+1} & = S_{w,j}^{n} - \frac{\Delta t}{\phi \Delta x}\left(u_w(S_{w,j}^{n+1}, c_j^{n+1}) - u_w(S_{w,j-1}^{n+1}, c_{j-1}^{n+1})\right), \\ (cS_w)_j^{n+1} & = (cS_w)_j^{n} - \frac{\Delta t}{\phi \Delta x}\left(c_j^{n+1}u_w(S_{w,j}^{n+1}, c_j^{n+1}) - c_{j-1}^{n+1}u_w(S_{w,j-1}^{n+1}, c_{j-1}^{n+1})\right). \end{cases}$$

Although it has the advantage to be a more stable scheme, accuracy is low due to the first order upwind fluxes, and the non linearities in both S_w and c makes it computationally expensive. For this reason, an alternative sequential approach has been proposed [10]: the flow equations are solved implicitly using the value of concentration at time level n and subsequently the polymer continuity equation is solved using the updated value of S_w. The scheme reads:

1. Compute S_w^{n+1} using c^n and the fully implicit solver:

$$\begin{cases} S_{o,j}^{n+1} = S_{o,j}^{n} - \frac{\Delta t}{\phi \Delta x}\left(u_o(S_{o,j}^{n+1}, c_j^{n}) - u_o(S_{o,j-1}^{n+1}, c_{j-1}^{n})\right) \\ S_{w,j}^{n+1} = S_{w,j}^{n} - \frac{\Delta t}{\phi \Delta x}\left(u_w(S_{w,j}^{n+1}, c_j^{n}) - u_w(S_{w,j-1}^{n+1}, c_{j-1}^{n})\right). \end{cases}$$

2. Compute c^{n+1} using S_w^{n+1}

$$(cS_w)_j^{n+1} = (cS_w)_j^{n} - \frac{\Delta t}{\phi \Delta x}\left(F_{j+1/2}(S_w^{n+1}, c^n, c^{n+1}) - F_{j-1/2}(S_w^{n+1}, c^n, c^{n+1})\right).$$

In order to complete the scheme, an expression for the fluxes $F_{j\pm1/2}$ must be selected. Given the discussion of the previous section, the two first order upwind (3.55)-(3.56) and the two high-resolution methods (3.60)-(3.61) are compared. Note that in this case the water velocity is evaluated as $u_{w,j}^{n+1} = u_w(S_{w,j}^{n+1}, c_j^n)$, so technically the implicit scheme is not fully implicit.

Results are shown in figures 3.17 and 3.18. Again, the semi-implicit scheme seems to perform best in term of accuracy, while the implicit scheme smears the water saturation profile at the polymer front and the concentration profile.

A stability criterion for the semi-implicit scheme can be found via Von Neumann analysis [10], giving the necessary condition

$$C_p = \max_{S_w,c} \left| \frac{\Delta t}{\phi \Delta x} \frac{u_w(S_w,c)}{S_w} \right| = \max_{S_w,c} \left| \frac{\Delta t}{\Delta x} \frac{u_T}{\phi} \frac{f_w(S_w,c)}{S_w} \right| \leq 1. \tag{3.63}$$

Since the fractional flow curve shifts to the right when polymer is added to water, the above maximum is attained at $c = 0$, so that condition (3.63) is equivalent to (3.62).

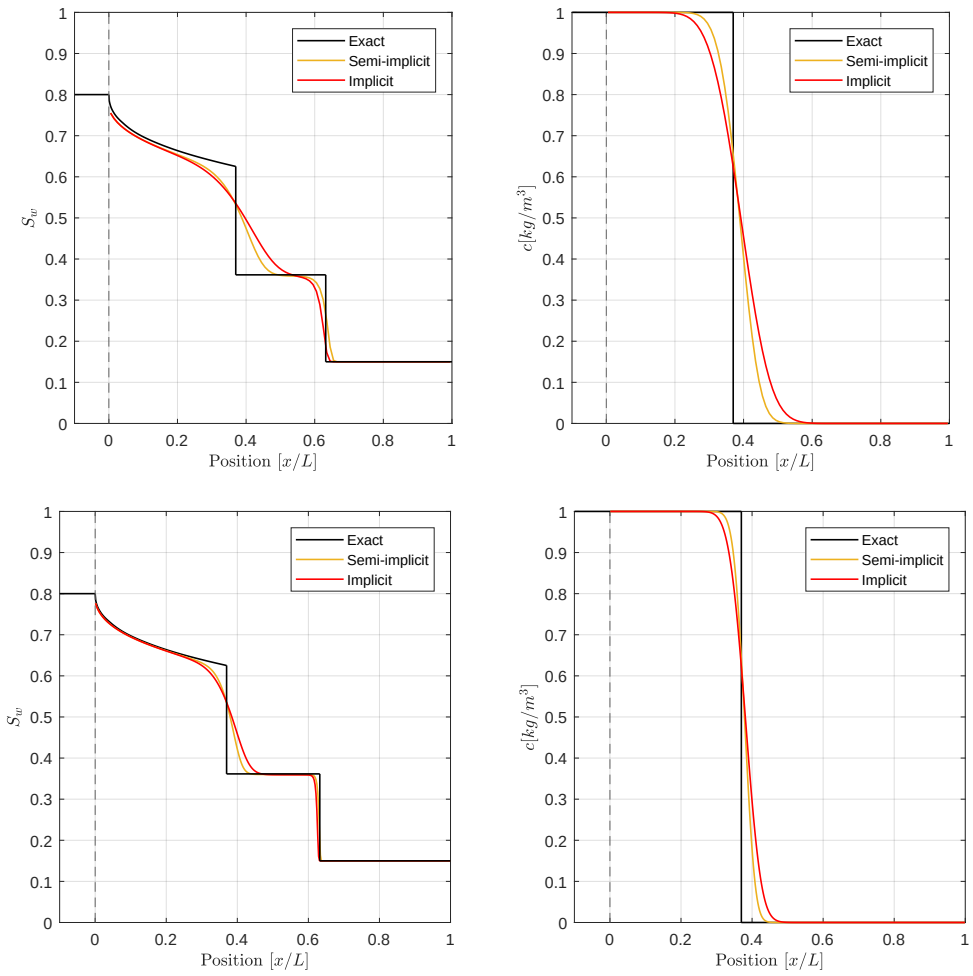

Figure 3.17: Saturation and concentration profiles for exact and numerical solutions, with first order upwind methods and 100 cells, 100 time steps (above) and 400 cells, 400 time steps (bottom).

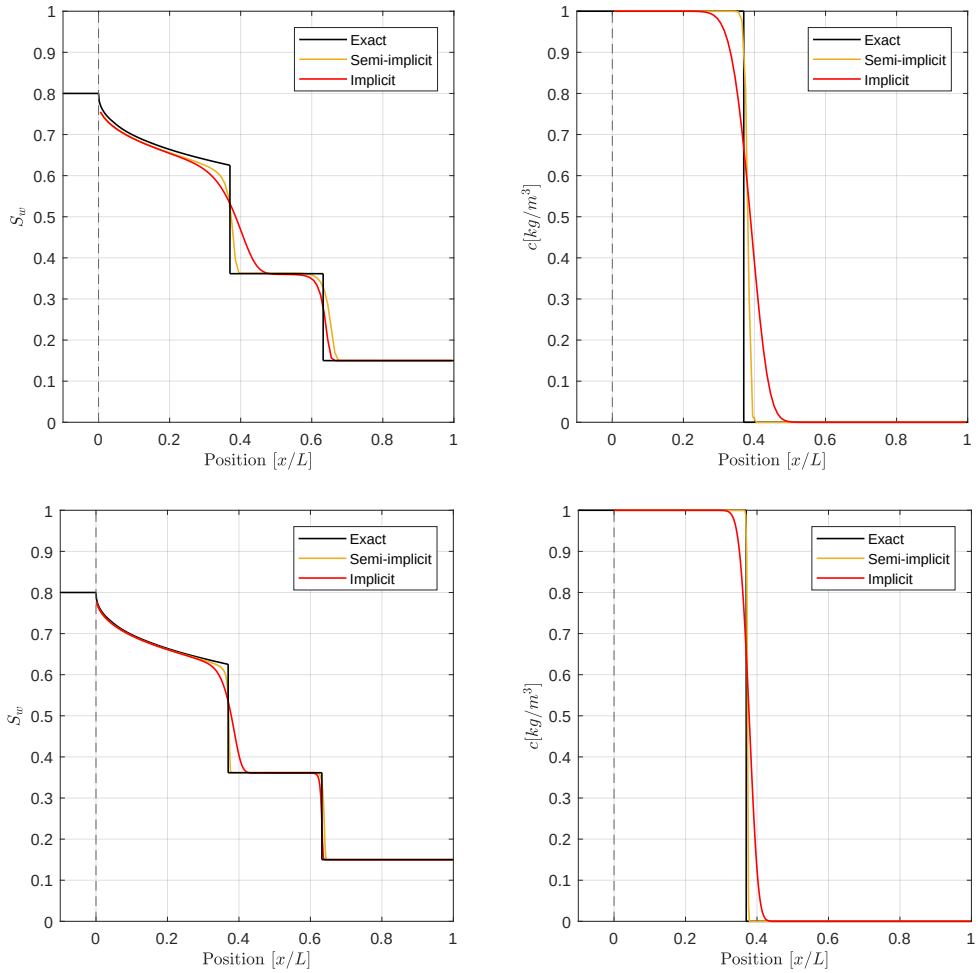

Figure 3.18: Saturation and concentration profiles for exact and numerical solutions, with high-resolution methods and 100 cells, 100 time steps (above) and 400 cells, 400 time steps (bottom).

4

Velocity Enhancement in Polymer Flooding

The models introduced in chapter 4 for polymer flooding are rather qualitative and disregard many physical and chemical properties of rock, fluid and their interaction. Although they are useful to gain insights on the behaviour of the floods, these models should be refined to achieve more realistic simulations. Modeling further physical phenomena may quickly lead to complexities in the analytical model, requiring numerical methods to be very accurate and computationally efficient. According to Dawson et al. [15], adsorption of polymer molecules onto the rock plays an important role in polymer flooding, causing a delay of the polymer effluent profile. The resulting water bank will be gradually denuded of polymer, depending on the nature of the polymer and reservoir rock. Therefore, adsorption should be included in any realistic mathematical model. However, the effect that will be investigated in this chapter, studied previously for instance in [15], [9], [2], is the velocity enhancement effect (also referred to as hydrodynamic acceleration) due to inaccessible and excluded pore volume (IPV and EPV, respectively). Since the polymer's molecules have a larger size, they may not access the smallest pores of the rock (IPV) and they may be excluded from the layer close to the wall of the pore channels (EPV), where velocities are lower. These combined effects result in a macroscopic velocity enhancement of the polymer's molecules. In some experiments, the polymer is observed to travel faster than the water in which it is dissolved [22], meaning that IPV and EPV effects overwhelm adsorption and other polymer retention mechanisms. One may wonder if the velocity enhancement will cause an accumulation of polymer at the water/oil interface, especially when the flood is performed in secondary mode (i.e. when water in the reservoir is at the irreducible saturation). Experimentally, a pile-up effect at the front has not been investigated exhaustively and there is no clear evidence of a raise in polymer concentration. Mathematically, the classic approach adopted in the literature to model enhancement effects leads to a peak in the polymer concentration at the water front [4], [21], [10]. A formal analysis of the analytical model carried out by Bartelds et al. [4] reveals that the resulting system of PDEs is not strictly hyperbolic, but contains elliptic regions that cause instabilities in the numerical simulations. Therefore, alternative models are proposed in [4] and by Hilden et al. [21]. Although the numerical simulations presented in these papers show more stable results and no accumulation effects, it is not clear if this will always be the case, and no analytical solutions have been computed. Hence, in the current research we focus on a detailed study of the velocity enhancement models and the respective analytical solutions. The goal is to discuss thoroughly and fully understand the consequences that an enhancement term will produce on the water saturation and polymer concentration profiles, so that the model can be adjusted suitably to catch the properties of a certain reservoir.

4.1. Inaccessible and Excluded Pore Volume

It was first observed experimentally by Dawson et al. [15] that polymer molecules are transported through the porous media faster than those of an inert tracer. They explained this by introducing the Inaccessible Pore Volume theory. The physical interpretation was that the polymer's molecules, due to their larger size, cannot enter the smallest pores of the rock (the ones whose size is smaller than polymer's molecules). Since the polymer flows through larger pores, it tends to move ahead, resulting in an acceleration effect. The result of the original experiments demonstrating the IPV effect is shown in figure 4.1, where polyacrylamide is employed in a Berea sandstone. The polymer's effluent concentration profile anticipates the one of salt. Dawson and Lantz worked then on several experiments where they managed to combine adsorption and IPV effects, to see how the concentration profile would look depending on which factor is dominating the polymer's flow. Results are illustrated in figure 4.2. We see that in absence of adsorption, the acceleration effect becomes more evident. They concluded that IPV has a beneficial effect on field performance as it contrasts adsorption, so that polymer response will be seen sooner than expected at the production well. In addition, they stated that mathematical models and fields predictions developed without including IPV and adsorption effects will be in error. They did not mention any accumulation effect of the polymer at the front.

An alternative physical interpretation of the velocity enhancement effect, known as Excluded Pore Volume, has been given later (see [9], [2] and literature referenced there). Polymer molecules, once more due to their larger size, are excluded from a layer close to the pore wall. The polymer tends then to travel at the center of the pore throats. Since the streamlines away from the wall are associated with higher velocities, the polymer winds up travelling faster than an inert tracer. The overall velocity enhancement effect is due to a combination of IPV and EPV. At low permeabilities ($\leq 100\ md$), hydrodynamic acceleration is mainly due to IPV, while at higher permeabilities ($\geq 500\ md$) the effect is primarily caused by EPV.

Although it is well established that polymer will flow faster than an inert tracer, there is more uncertainty concerning whether it will accumulate at the water/oil interface. Experimental results

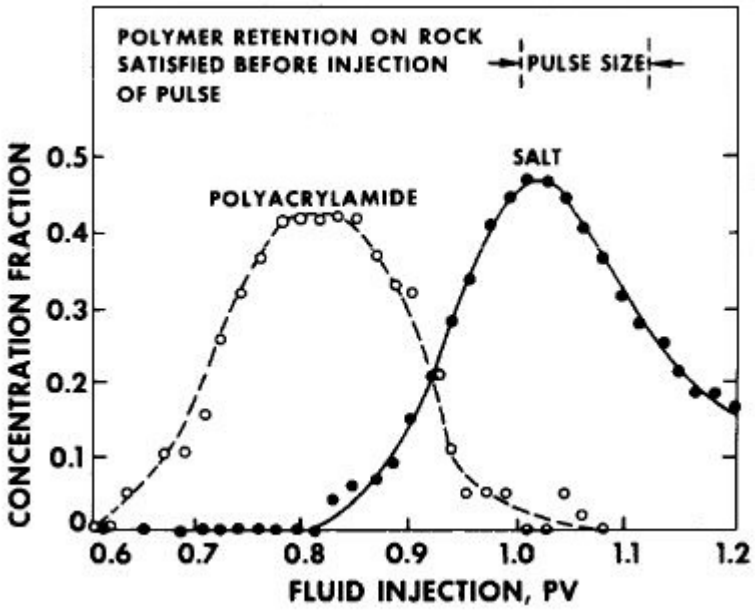

Figure 4.1: Experimental concentration profiles for polymer (polyacrylamide) and salt. The amount of fluid injected is measured in pore volume (PV), with $PV = 1$ being the total pore volume of the rock sample. From [15].

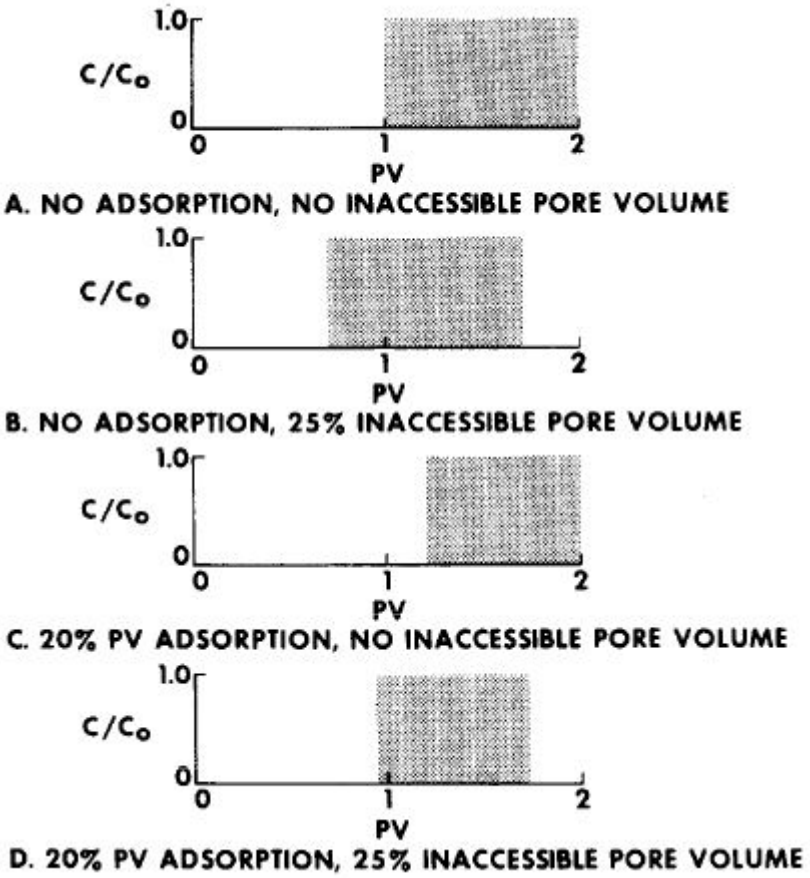

Figure 4.2: Breakout curves for various combination of IPV and adsorption. From [15].

from the literature do not clearly catch a pile-up of polymer, but these experiments are not specifically designed to measure this phenomenon. The typical experimental setup consists of a core (i.e. a rock sample) that has been previously flushed with water before injecting the polymer solution. In this case, the oil is approximately at the residual oil saturation and there is a significant amount of water ahead of the polymer front. The polymer will thus be able to invade this bulk of water, so that no accumulation is measured. We are instead more interested in a core filled with oil, where water is at the connate (or irreducible) water saturation. In this situation, there will be less water to invade for the polymer, so there might be a chance to observe an accumulation of polymer at the front. Experiments carried out in these conditions are though more focused on measuring oil recovery rather than the propagation of polymer concentration within the core. In the PhD thesis of Bartelds [2], they aim to measure a peak in polymer concentration at the front, but results are not entirely reliable: concentration is measured to be up to 8-10 times initial concentration (in some cases even more), while there is no measure of a local increase in viscosity[1]. Moreover, the methods they use to measure concentration (UV measurement) may not be appropriate, leading to considerable experimental errors. When they employ a different method (TOC), the peak in polymer concentration is much lower. For these reasons, we do not consider these results to constitute a sufficient experimental evidence to state that polymer will accumulate at the water/oil interface.

The reason why polymer may not accumulate even when the flooding is performed in secondary mode, is that a non negligible amount of water free of polymer is commonly seen to precede the

[1]Viscosity is an increasing function of polymer concentration, meaning that a significant difference in viscosity values should be observed as well.

polymer solution. The water bank free of polymer originates because polymer dilutes into connate water. This water bank is also predicted by the extended fractional flow theory (in the case of no adsorption and no hydrodynamic acceleration), see previous chapter. This is a crucial fact to consider when studying the velocity enhancement effect: it suggests that polymer does not accumulate at the front, but rather invades the available water ahead. As a consequence, the water that has been invaded by the polymer will suffer from an alteration of its flow properties (i.e. mobility), so that the overall result is that the velocity of the water-polymer front becomes higher than the case without hydrodynamic acceleration.

The chemical nature of the polymer is also playing a role: molecule interactions are an important factor that could influence the hydrodynamic acceleration and, especially, the accumulation effect. The structure of a synthetic polymer such HPAM is most likely not going to allow for an accumulation: polymer molecules form a chain, so that a local raise in the concentration is not expected. Bio-polymer structure would be more keen to allow for polymer accumulation, but the pile-up should be restricted to a slight increase of injected concentration [11].

The above considerations show the many difficulties and uncertainties related to the velocity enhancement effect. Deriving an accurate model is thus a complex task and many commercial simulators insert simply a constant factor in the governing equations to take into account the hydrodynamic acceleration. Typically, the magnitude of the velocity enhancement factor is such that the polymer travels at velocities up to about 20% faster than inert tracer species. When velocity enhancement effects are observed, they may be caused by a combination of IPV and EPV. More experimental results on the velocity enhancement and its relation to other reservoir properties can be found in [22].

If the velocity enhancement effect is simply modeled mathematically by a constant factor α, essentially both IPV and EPV effects discussed above are included. A constant velocity enhancement factor may though lead to an unphysical peak of polymer concentration at the water front. Bartelds [4] showed that using a constant α results in an ill-posed problem. Refined model for the factor α are then necessary to get rid of unphysical behaviours. At this point, IPV and EPV may be modeled differently, since they have distinct physical interpretations. Typically, the EPV effect is preponderant over IPV, but it is also more difficult to model. Bartelds proposed a model for the IPV effect using a percolation approach; the same approach is used also in [2] to model EPV. Hilden et al. [21] extended then the IPV model of Bartelds. These models will be presented and discussed in this chapter.

4.2. Models for the Velocity Enhancement Factor

Given the influence of IPV and EPV effects on the polymer flood, models for the velocity enhancement factor α are needed in order to perform more realistic simulations. Following the approach of Bartelds [4], the velocity enhancement factor is defined as the ratio between the average interstitial velocities of polymer and water, namely

$$\alpha = \frac{\langle v_p \rangle}{\langle v_w \rangle}. \tag{4.1}$$

4.2.1. Constant Velocity Enhancement Factor

In first approximation, one may employ a constant value for α. Introducing the effective porosity ϕ_p for the polymer and using Darcy's velocities, (4.1) takes the form

$$\alpha = \frac{v_p}{v_w} = \frac{u_w/\phi_p}{u_w/\phi} = \frac{\phi}{\phi_p} > 1. \tag{4.2}$$

In this section results from Bartelds [4], showing that this choice for α leads to an ill-posed problem when dispersive effects are ignored, will be presented. We will investigate the consequences which

the velocity enhancement factor cause on the governing equations, in particular on the characteristic velocities of the system.

In chapter 3, conservation equations for both water and polymer were derived in a fractional flow formulation. Adding to this model a constant velocity enhancement factor $\alpha > 1$, the governing equations become

$$\phi \frac{\partial S_w}{\partial t} + u \frac{\partial f_w}{\partial x} = 0, \tag{4.3}$$

$$\phi \frac{\partial c S_w}{\partial t} + \alpha u \frac{\partial c f_w}{\partial x} = 0. \tag{4.4}$$

Here, we have omitted an adsorption term that is instead included in Bartelds governing equations. The adsorption term delays the polymer front, but plays no relevant role in the study of the IPV effect and its relation to well-posedness, so it will not be considered now. The fractional flow f_w is a function of water saturation and polymer concentration such that

$$\frac{\partial f_w}{\partial c} < 0, \qquad \frac{\partial f_w}{\partial S_w} \geq 0. \tag{4.5}$$

We aim to study how IPV/EPV affect the velocity of the polymer front. It will be shown below that the enhancement term does not simply increase the velocity of the polymer front, given by λ_p in (3.40) when $\alpha = 1$, but that the issue is more subtle. Expanding derivatives, equation (4.4) becomes

$$c\left(\phi \frac{\partial S_w}{\partial t} + \alpha u \frac{\partial f_w}{\partial x}\right) + \phi S_w \frac{\partial c}{\partial t} + \alpha u f_w \frac{\partial c}{\partial x} = 0.$$

Using equation (4.3), the expression above takes the form

$$u(\alpha - 1) c \frac{\partial f_w}{\partial x} + \phi S_w \frac{\partial c}{\partial t} + \alpha u f_w \frac{\partial c}{\partial x} = 0. \tag{4.6}$$

Note that if $\alpha = 1$ (no IPV/EPV), we recover (3.37) and, in particular, the first term where the concentration c appears explicitly cancels. This is the term in which the ill-posedness of the model is hidden. Lake [11] uses the approximation $c \approx 0$, so that the velocity of the polymer front results in

$$\lambda_p = \frac{u}{\phi} \frac{\alpha f_w}{S_w}. \tag{4.7}$$

Since $\alpha > 1$, the claim is that the factor accelerates the polymer front, and a solution can be found through the Buckley-Leverett construction presented in chapter 3, with (4.7) as the polymer characteristic velocity. However, this approach is not formally correct, because the equations rewritten in quasi-linear form with the assumption $c \approx 0$ are clearly not equivalent to (4.3)-(4.4). Even if (4.7) might be a good approximation for the polymer characteristic velocity, the manipulations used to obtain it ignore the fact that the nature of the mathematical model has changed. In fact, we are not even guaranteed that characteristic velocities are well-defined.

Before delving in the formal analysis of the system of PDEs with a constant enhancement model, we remark that the approximation $c \approx 0$ may be an acceptable physical assumption to understand the implications of IPV/EPV on the flow model, but it is a crucial fact for stability. Numerical schemes are developed based on the equations in conservation form, meaning that the term depending explicitly on c has not been neglected. The consequence is that the numerical algorithm is solving another set of equations and, due to the ill-posedness of the model that will be addressed below, simulations result in an uncontrolled peak in polymer concentration at the polymer front, as it is shown in figure 4.3. Furthermore, note that the polymer accumulates at the second water shock: a

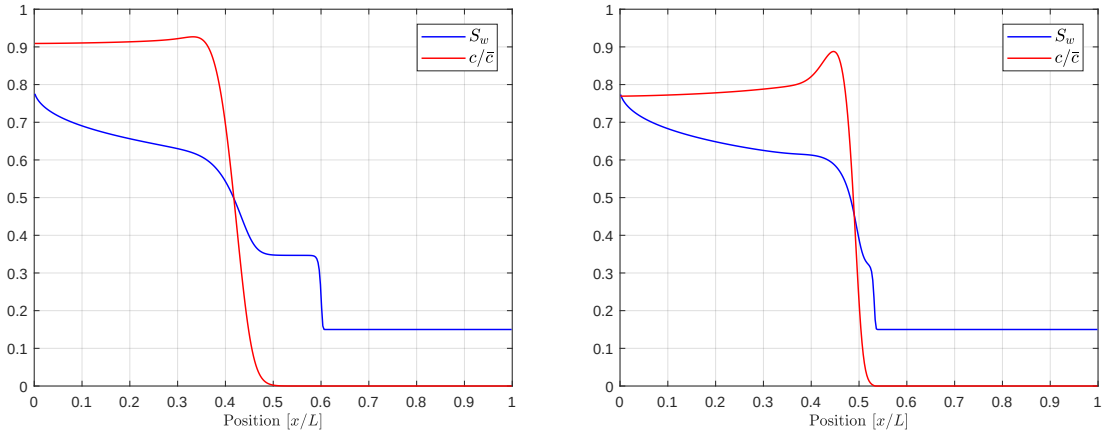

Figure 4.3: Saturation and concentration profiles obtained with implicit first order upwind schemes, 400 cells and timesteps, $\alpha = 1.1$ (left) and $\alpha = 1.3$ (right).

bulk of water free of polymer is flowing ahead of this front. We have not found a physical explanation that could justify why the polymer would not invade this water bank, so we classify this pile-up as unphysical. To summarize, introducing a (constant) velocity enhancement parameter has deeper consequences on the mathematical model and it does not simply accelerate the speed of the polymer front, as stated in the literature [11], [9].

A more precise mathematical analysis of the model has been carried out by Bartelds [4]. Bartelds shows that the model is not strictly hyperbolic, but there is an elliptic region that the solution must cross which leads to stability issues.

Since $f_w = f_w(S_w, c)$, we expand

$$\frac{\partial f_w}{\partial x} = \frac{\partial f_w}{\partial S_w}\frac{\partial S_w}{\partial x} + \frac{\partial f_w}{\partial c}\frac{\partial c}{\partial x}$$

and substitute in equations (4.3) and (4.6). Thus, the quasi-linear system rewritten in matrix form is

$$\frac{\partial}{\partial t}\begin{pmatrix} S_w \\ c \end{pmatrix} + A\frac{\partial}{\partial x}\begin{pmatrix} S_w \\ c \end{pmatrix} = \begin{pmatrix} 0 \\ 0 \end{pmatrix}, \tag{4.8}$$

where

$$A = \frac{u}{\phi}\begin{pmatrix} \dfrac{\partial f_w}{\partial S_w} & \dfrac{\partial f_w}{\partial c} \\ \dfrac{(\alpha-1)c\frac{\partial f_w}{\partial S_w}}{S_w} & \dfrac{\alpha f_w + (\alpha-1)c\frac{\partial f_w}{\partial c}}{S_w} \end{pmatrix}. \tag{4.9}$$

The nature of the system can be determined by computing the eigenvalues of A. In order to have a strictly hyperbolic system, the two eigenvalues must be real and distinct for all values of S_w and c. Note that, when no IPV/EPV effects are taken into account (i.e. $\alpha = 1$), the matrix of the system (4.9) is upper triangular. Using the approximation $c = 0$ would also result in an upper-triangular matrix, so that the eigenvalues lie on the diagonal and correspond to the characteristic velocities of water and polymer. In particular, they would be real (and positive), so that the problem would result well-posed. This is the reason why sometimes in the literature a Buckley-Leverett solution is computed even when considering the enhancement effect, but, as we remarked previously, the underlying equations are not equivalent to the conservation equations (4.3)-(4.4).

An additional remark could be helpful: in the literature, when computing the characteristic velocity for water saturation, sometimes the term $\partial f_w/\partial c$ is not considered because the polymer concentration is assumed to be constant before ($c = 0$) and after ($c = \bar{c}$) the shock. This simplification has no impact when $\alpha = 1$, since in this case the eigenvalues are the diagonal entries of the matrix. When $\alpha > 1$, the term $\partial f_w/\partial c$ has to be accounted for, since it will affect the eigenvalues of A. This means that the velocity enhancement has an impact not only on the speed of the polymer front, but it will affect also the characteristic velocity of water.

These remarks show how the velocity enhancement model changes deeply the nature and behaviour of the system. In particular, the eigenvalues of A are not always real, meaning that the system has an elliptic region. Fourier analysis shows that the system is unstable in these regions (see for instance [3]), so that the model is ill-posed. To show that the eigenvalues are complex for some values of (S_w, c), consider the discriminant of the quadratic equation

$$det(A - \lambda I) = 0, \tag{4.10}$$

as done by Bartelds. The discriminant is given by

$$D = \left(\frac{u}{\phi}\right)^2 \left[\left(\frac{\partial f_w}{\partial S_w} - \frac{\alpha f_w + (\alpha - 1)c\frac{\partial f_w}{\partial c}}{S_w}\right)^2 + 4\left(\frac{\partial f_w}{\partial c}\frac{(\alpha - 1)c\frac{\partial f_w}{\partial S_w}}{S_w}\right)\right]. \tag{4.11}$$

First, consider the case where $\alpha = 1$ (no velocity enhancement effect). As discussed above and within the fractional flow theory in chapter 3, at the polymer front the characteristic velocities of water and polymer are equal, giving

$$\frac{\partial f_w}{\partial S_w} = \frac{f_w}{S_w}. \tag{4.12}$$

Since it is reasonable to assume that ill-posedness of the model would cause problems close to the shock, we study expression (4.11) for the discriminant when (4.12) holds, showing that, in general, the eigenvalues are not real. Define then the region H to be the set of all pairs (S_w, c) where the two eigenvalues are equal for $\alpha = 1$, i.e. where (4.12) holds:

$$H = \left\{(S_w, c) \,\middle|\, \frac{\partial f_w}{\partial S_w} = \frac{f_w}{S_w}\right\}. \tag{4.13}$$

Setting $\alpha = 1 + \epsilon$, for $(S_w, c) \in H$ the expression for the discriminant is

$$D = \left(\frac{u}{\phi}\right)^2 \left[\frac{\epsilon}{S_w}\left(\frac{\epsilon}{S_w}\left(c\frac{\partial f_w}{\partial c} + f_w\right)^2 + 4c\frac{\partial f_w}{\partial c}\frac{\partial f_w}{\partial S_w}\right)\right]. \tag{4.14}$$

Since ϵ may be chosen arbitrarily small, the second term of (4.14) dominates and, due to (4.5), the discriminant is negative. This means that the eigenvalues are complex and there exists an elliptic region around the set H: the model is ill-posed. A plot of the discriminant for a fixed value of c and the elliptic region where $D < 0$ are shown in figures 4.4 and 4.5. We see that the discriminant is negative for a range of saturation values that correspond to the ones on the left of the water-polymer shock. Note that the two initial states $(S_{wir}, 0)$ and $(1 - S_{or}, \bar{c})$ of the Riemann problem lie on different sides of the elliptic region, so that the solution has to cross this region. Thus, numerical solutions result in uncontrolled and unphysical peaks at the polymer front. The velocity enhancement appears to have a double effect: it speeds up the polymer front, but at the same time the model is no more hyperbolic, so it cannot be treated as such by studying characteristic velocities. An alternative model for the velocity enhancement is needed to ensure a hyperbolic behavior.

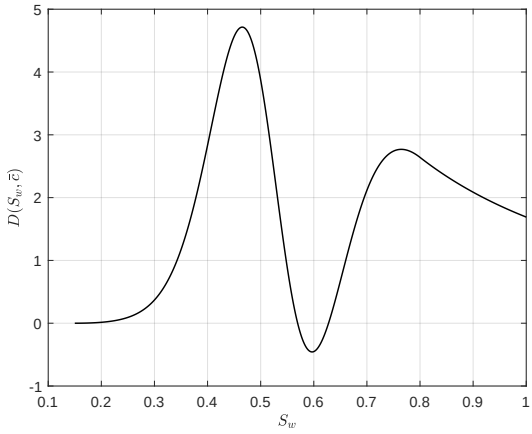

Figure 4.4: Discriminant (4.11) for a fixed value of concentration ($c = \bar{c}$) and $\alpha = 1.3$.

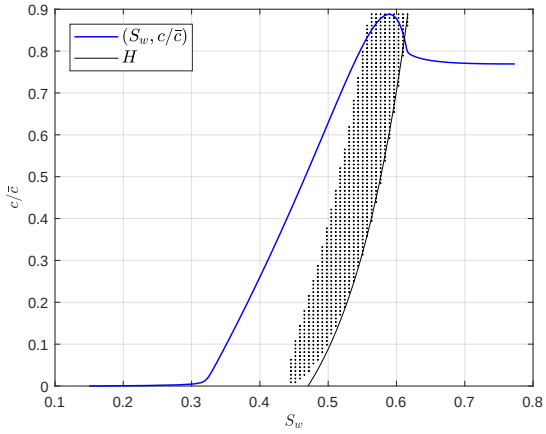

Figure 4.5: Solution in the phase plane (in blue) and elliptic region where $D < 0$ (dotted points), with $\alpha = 1.3$.

4.2.2. Percolation Model for IPV

In order to improve the model and get rid of instabilities, Bartelds [4] proposed a model of the velocity enhancement factor based on percolation theory. Percolation theory describes through statistical means the morphology of, and transport through, randomly disordered media. We restrict now the discussion exclusively to the IPV effect. Extension to EPV effect is studied by Bartelds in [2]; a brief discussion of this model will be carried out later in this chapter.

To use a percolation-type description, the polymer flood is seen as a three-phase flow. These phases are:

1. Water which cannot contain polymer, with saturation denoted by S_{w1}.
2. Water which may potentially contain polymer, with saturation denoted by S_{w2}.
3. Oil without polymer, with saturation S_o.

Polymer is restricted to water phase 2, while exchange of water molecules between phase 1 and 2 is allowed. It is assumed further that there is local equilibrium in the polymer concentration, meaning that there is instantaneous diffusion of polymer molecules between movable water and the part of connate water which is accessible to polymer.

Percolation theory is used to model networks that consist of branches and nodes. The basic idea used to apply a percolation approach is that the smallest pores do not contain polymer molecules (IPV), thus polymer is excluded from the pores with radius smaller than a threshold value r_{ipv}. The accessible pores for the polymer are then the ones with radius $r > r_{ipv}$. Figure 4.6 illustrates an example of a probability density function $P(r)$ describing the distribution of pores radii. This probability density function gives the fractional volume occupied by pores with radius belonging to a certain interval.

In a water-wet reservoir, water prefers to enter pores in a sequence of increasing radius. This means that all the pores with $r < r_{ipv}$ have to be filled with water before polymer is allowed to enter the porous medium. The threshold water saturation needed to fulfill this condition is denoted by S_{ipv} and it is assumed to be lower than the irreducible water saturation, i.e. $S_{ipv} < S_{wir}$[2]. The water

[2]The assumption of Bartelds is actually $S_{ipv} < S_{wc}$, but it is also assumed that the connate water is immobile. This fact was noticed by Hilden et al. [21], who then concluded that in Bartelds $S_{wc} = S_{wir}$. For the purpose of comparison, here we use the irreducible water saturation.

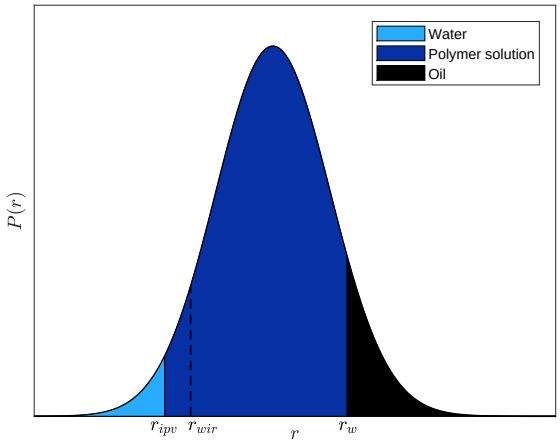

Figure 4.6: Illustrative example of a probability distribution showing the threshold radius and the three different phases.

phase 1 where polymer is not allowed corresponds then to the area of $P(r)$ with $r < r_{ipv}$. The associated saturation is $S_{w1} = S_{ipv}$. The water phase 2 correspond to the area where $r_{ipv} < r < r_w$, and its saturation is $S_{w2} = S_w - S_{ipv}$.

Model equations for the three phase flow read

$$\phi \frac{\partial S_{w1}}{\partial t} + \frac{\partial u_{w1}}{\partial x} = R, \tag{4.15}$$

$$\phi \frac{\partial S_{w2}}{\partial t} + \frac{\partial u_{w2}}{\partial x} = -R, \tag{4.16}$$

$$\phi \frac{\partial c_{w2} S_{w2}}{\partial t} + \frac{\partial c_{w2} u_{w2}}{\partial x} = 0, \tag{4.17}$$

where R denotes the net transfer rate of water molecules from phase 1 to phase 2. It is convenient to introduce the average polymer concentration c in the total water phase,

$$c = \frac{c_{w2} S_{w2}}{S_{w1} + S_{w2}}. \tag{4.18}$$

The velocity enhancement factor can be expressed as

$$\alpha = \frac{v_p}{v_w} = \frac{v_{w2}}{v_w} = \frac{u_{w2}}{S_{w2}} \frac{S_w}{u_w} = \frac{u_{w2}}{u_{w1} + u_{w2}} \frac{S_{w1} + S_{w2}}{S_{w2}}. \tag{4.19}$$

Since it assumed that $S_{w1} = S_{ipv} < S_{wir}$, $\partial S_{w1}/\partial t$ is zero and water phase 1 is unable to flow, giving $u_{w1} = 0$. It follows that the transfer rate R is zero: no water is exchanged between phase 1 and phase 2. Using $S_{w1} = S_{ipv}$ and $S_{w2} = S_w - S_{ipv}$ in (4.19), the velocity enhancement factor becomes

$$\alpha(S_w) = \frac{S_w}{S_w - S_{ipv}}. \tag{4.20}$$

Thus, in this model, the velocity enhancement factor is no longer constant, but it depends on the water saturation S_w. Near the irreducible water saturation the factor has higher values, and it decreases to an almost constant value as water saturation increases, see figure 4.7. This follows directly from the assumption that, in a water wet reservoir, water invades smallest pores first: at low water saturation values, the IPV will consist of a considerable fraction of the occupied volume, so

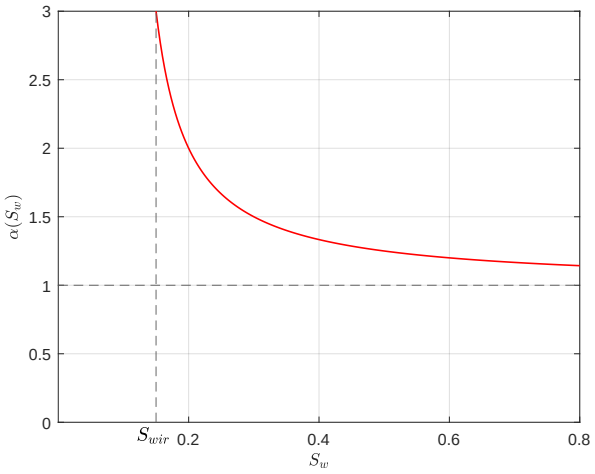

Figure 4.7: Velocity enhancement factor (4.20) proposed by Bartelds, for $S_{wir} = 0.15$ and $S_{ipv} = 0.1$.

that polymer has access to a small part of the occupied space and thus travels faster. It will be shown later that the decreasing property of this model is a key fact when proving well-posedness and monotonicity of the concentration profile.

Using (4.20), the average polymer concentration can be written as

$$c = \frac{c_{w2}}{\alpha}. \tag{4.21}$$

Rewriting the conservation equations in fractional flow formulation ($u_w = f_w u$) and using (4.21) and (4.20), the final governing system is

$$\phi \frac{\partial S_w}{\partial t} + u \frac{\partial f_w}{\partial x} = 0, \tag{4.22}$$

$$\phi \frac{\partial c S_w}{\partial t} + u \frac{\partial \alpha c f_w}{\partial x} = 0. \tag{4.23}$$

To study the well-posedness, the same approach as with the constant velocity enhancement factor is followed. Governing equations are rewritten in the quasi-linear matrix-vector form

$$\frac{\partial}{\partial t}\begin{pmatrix} S_w \\ c \end{pmatrix} + A \frac{\partial}{\partial x}\begin{pmatrix} S_w \\ c \end{pmatrix}, \tag{4.24}$$

where the matrix A is given by

$$A = \frac{u}{\phi}\begin{pmatrix} \frac{\partial f_w}{\partial S_w} & \frac{\partial f_w}{\partial c} \\ \frac{\frac{d\alpha}{dS_w} c f_w + (\alpha - 1) c \frac{\partial f_w}{\partial S_w}}{S_w} & \frac{\alpha f_w + (\alpha - 1) c \frac{\partial f_w}{\partial c}}{S_w} \end{pmatrix}. \tag{4.25}$$

Again, the purpose is to show that the eigenvalues of A are real by analyzing the discriminant of the characteristic equation. Note that in the lower-left entry there is now the term $d\alpha/dS_w \leq 0$. The discriminant D takes the form

$$D = \left(\frac{u}{\phi}\right)^2 \left[\left(\frac{\partial f_w}{\partial S_w} - \frac{\alpha f_w + (\alpha - 1) c \frac{\partial f_w}{\partial c}}{S_w} \right)^2 + 4 \left(\frac{\partial f_w}{\partial c} \frac{\frac{d\alpha}{dS_w} c f_w + (\alpha - 1) c \frac{\partial f_w}{\partial S_w}}{S_w} \right) \right]. \tag{4.26}$$

Here we see why the velocity enhancement factor must be decreasing (at least in the key interval where $D < 0$ in the constant α case) in order to achieve well-posedness: we must have $D \geq 0$ and, since $\partial f_w / \partial c \leq 0$, a positive term has now been added to the first order part of D. Using

$$\frac{d\alpha}{dS_w} = -\frac{\alpha(\alpha-1)}{S_w}, \tag{4.27}$$

after some tedious manipulations, the expression for the discriminant becomes

$$D = \left(\frac{u}{\phi}\right)^2 \left(\frac{\partial f_w}{\partial S_w} - \frac{\alpha f_w - (\alpha-1)c\frac{\partial f_w}{\partial c}}{S_w}\right)^2, \tag{4.28}$$

and it follows that the discriminant is nonnegative and there are no elliptic regions. Bartelds claims then that the model is strictly hyperbolic, but there is no guarantee that the discriminant (4.28) is always nonzero. Hence, we can only conclude that the model is hyperbolic. It must be remarked that this model is valid under the assumption $S_{ipv} < S_{wir}$. This restriction is though claimed to be acceptable since a commonly observed value for the enhancement is $\alpha \approx 1.1$, which corresponds, at the residual oil saturation $S_w = 1 - S_{or} = 0.8$, to a threshold saturation $S_{ipv} \approx 0.07$. Most reservoirs have a value of irreducible water saturation larger than 0.1, so that assuming $S_{ipv} < S_{wir}$ is reasonable. In addition, we remark that this restriction ensures also that division by zero in (4.20) does not occur. Caution must though be exercised when S_{ipv} is close to S_{wir}, since numerical difficulties may arise. In [10], this fact has been overlooked and it is stated that, in absence of adsorption, no restriction is needed on the value of S_{ipv}, but this is not the case.

Using the same test problem of the previous section, where a constant velocity enhancement factor caused a peak in the concentration at the polymer front, results of the new model are shown in figure 4.9. The peak now is absent and there is no polymer accumulation at the front. It is also interesting to observe that the (normalized) polymer concentration on the left boundary jumps immediately to a value lower than 1. Moreover, the concentration has now a decreasing profile.

Conclusions of Bartelds are that a constant velocity enhancement factor leads to an ill-posed model and causes an unlimited pile-up of the polymer at the polymer front. Retardation effects like adsorption play no role in the well-posedness of the model, as they result in a slowdown of the polymer front and do not affect the concentration profile's shape. The height of the peak for constant α is unbounded and depends on the grid spacing used in the simulation, highlighting the ill-posed behaviour of the model. Moreover, the constant velocity factor model does not have a clear physical counterpart and it is just a convenient mathematical model. The saturation-dependent model for the velocity enhancement factor presented by Bartelds is built on a clear physical concept and the resulting equations are shown to be well-posed (without elliptic regions). The model proposed takes into consideration only IPV effects. Other mechanisms, such as EPV, may be incorporated in the governing equations as well. As discussed previously, pile-up of the polymer is not necessarily unphysical, but it is unlikely to occur, especially when there is a water bank free of polymer ahead. Hence, we would be satisfied to have a stable model even if it does not allow polymer accumulation. However, no further analytical considerations have been carried out by Bartelds, so we have no guarantee that the concentration profile will always be monotone. This fact motivates us to investigate further the model of Bartelds, and possibly find an analytical solution.

Following the same ideas as for the simpler case when no IPV effects are taken into account, we compute now an analytical solution for the system of equations (4.22)-(4.23), employing the saturation dependent model (4.20) for $\alpha(S_w)$. Since it has been shown that the model is hyperbolic, we compute the eigenvalues, the respective eigenvectors and determine the nature of the water and polymer fields (linearly degenerate or genuinely nonlinear). Having already computed the discrim-

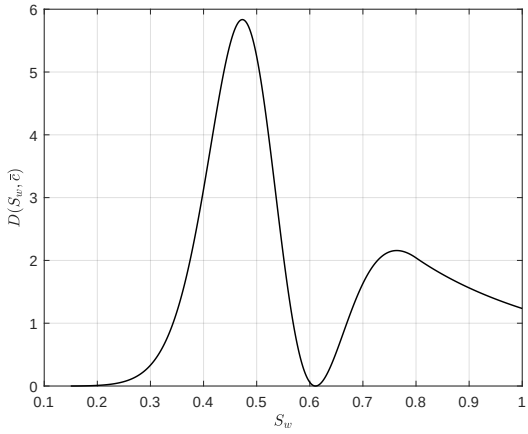

Figure 4.8: Discriminant (4.26) for a fixed value of concentration ($c = \bar{c}$) and $S_{ipv} = 0.1$.

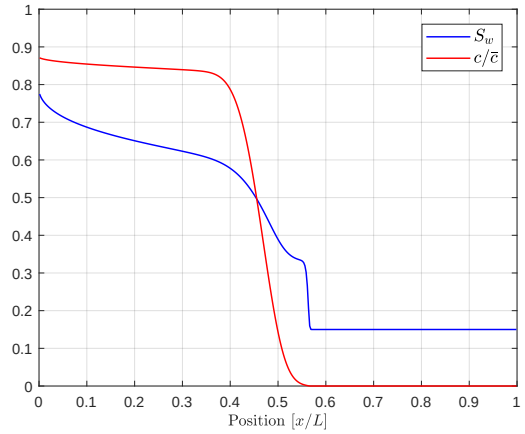

Figure 4.9: Saturation and concentration profiles obtained with implicit first order upwind schemes, 400 cells and timesteps, $S_{ipv} = 0.1$.

inant in (4.28), the eigenvalues are given by

$$\lambda_{w,p} = \frac{u}{2\phi}\left(\frac{\partial f_w}{\partial S_w} + \frac{\alpha f_w + (\alpha-1)c\frac{\partial f_w}{\partial c}}{S_w}\right) \pm \frac{1}{2}\sqrt{\left(\frac{u}{\phi}\right)^2\left(\frac{\partial f_w}{\partial S_w} - \frac{\alpha f_w - (\alpha-1)c\frac{\partial f_w}{\partial c}}{S_w}\right)^2}. \tag{4.29}$$

We select the sign in (4.29) that corresponds to water and polymer in such a way that we would recover the characteristic velocities (3.40) when $\alpha = 1$. Thus, the characteristic velocities are

$$\lambda_w = \frac{u}{\phi}\left(\frac{\partial f_w}{\partial S_w} + \frac{(\alpha-1)c}{S_w}\frac{\partial f_w}{\partial c}\right), \tag{4.30}$$

$$\lambda_p = \frac{u}{\phi}\frac{\alpha f_w}{S_w}. \tag{4.31}$$

Note that, since $\alpha(S_w) > 1$ and $\partial f_w/\partial c \leq 0$, the characteristic velocity of polymer is larger than the case without IPV effects, while the characteristic velocity of water is lower. This fact agrees with the interpretation that, if polymer travels faster and invades more water ahead, then the invaded water will suffer from an increase in viscosity and, consequently, a mobility drop.

The eigenvectors of the system are

$$r_w = \begin{bmatrix} 1 \\ \dfrac{(\alpha-1)c}{S_w} \end{bmatrix}, \qquad r_p = \begin{bmatrix} \dfrac{\partial f_w}{\partial c} \\ \dfrac{\alpha f_w}{S_w} - \dfrac{\partial f_w}{\partial S_w} \end{bmatrix}. \tag{4.32}$$

The main difference with the respect to the eigenvectors (3.41) where $\alpha(S_w) = 1$, is that the second component of r_w is nonzero. The gradients of the eigenvalues are

$$\nabla\lambda_w = \frac{u}{\phi}\begin{bmatrix} \dfrac{\partial^2 f_w}{\partial S_w^2} + \dfrac{(\alpha-1)c}{S}\dfrac{\partial^2 f_w}{\partial S_w \partial c} + \dfrac{d\alpha}{dS_w}\dfrac{c}{S_w}\dfrac{\partial f_w}{\partial c} - \dfrac{(\alpha-1)c}{S_w^2}\dfrac{\partial f_w}{\partial c} \\ \dfrac{\partial^2 f_w}{\partial S_w \partial c} + \dfrac{(\alpha-1)}{S_w}\dfrac{\partial f_w}{\partial c} + \dfrac{(\alpha-1)c}{S_w}\dfrac{\partial^2 f_w}{\partial c^2} \end{bmatrix}, \tag{4.33}$$

$$\nabla\lambda_p = \frac{u}{\phi}\begin{bmatrix} \dfrac{d\alpha}{dS_w}\dfrac{f_w}{S_w} + \dfrac{\alpha}{S_w}\dfrac{\partial f_w}{\partial S_w} - \dfrac{\alpha f_w}{S_w^2} \\ \dfrac{\alpha}{S_w}\dfrac{\partial f_w}{\partial c} \end{bmatrix}. \tag{4.34}$$

Computing the inner products, for the polymer field we obtain

$$\nabla\lambda_p \cdot r_p = 0, \tag{4.35}$$

meaning that the field behaves as a contact discontinuity, as for the $\alpha = 1$ case. It has been remarked that in figure 4.9 the profile of polymer concentration is decreasing. This feature must then be a consequence of the water continuity equation. For the water field,

$$\nabla\lambda_w \cdot r_w = \frac{u}{\phi}\left(\frac{\partial^2 f_w}{\partial S_w^2} + 2\frac{(\alpha-1)c}{S_w}\frac{\partial^2 f_w}{\partial S_w \partial c} - 2\frac{(\alpha-1)c}{S_w^2}\frac{\partial f_w}{\partial c} + \frac{(\alpha-1)^2 c^2}{S_w^2}\frac{\partial^2 f_w}{\partial c^2}\right). \tag{4.36}$$

Given the complicated analytical expression of (4.36), it is hard to prove that there is no physical admissible couple (S_w, c) for which the inner product is zero. We expect a situation similar to the case without velocity enhancement: there might be a couple for which (4.36) is zero, but this state is not reached by the solution. Therefore, we assume that the water field is genuinely nonlinear. Therefore, the rarefaction waves are defined by the system of ODEs

$$\tilde{S}_w'(x/t) = \frac{1}{\nabla\lambda_w \cdot r_w}, \qquad \lambda_w(S_b, c_b) < x/t < \lambda_w(S_l, c_l), \tag{4.37}$$

$$\tilde{c}'(x/t) = \frac{(\alpha-1)c}{S_w}\frac{1}{\nabla\lambda_w \cdot r_w}, \qquad \lambda_w(S_b, c_b) < x/t < \lambda_w(S_l, c_l), \tag{4.38}$$

where the couple (S_l, c_l) are the values of saturation and concentration immediately left of the water-polymer front, while (S_b, c_b) are the values on the left boundary (which may now be different from the injected values $(1 - S_{or}, \bar{c})$). In order to solve (4.37)-(4.38), we need to determine the initial condition $(\tilde{S}_w(0), \tilde{c}(0)) = (S_b, c_b)$. The reason why the values on the left boundary change, is that the water with polymer is injected at rate u, but the polymer will immediately start to flow at a higher velocity, hence its concentration will decrease. We model this situation by setting a Riemann problem with discontinuous flux function for the polymer continuity equation:

$$\begin{cases} \dfrac{\partial(cS_w)}{\partial t} + u\dfrac{\partial(cf_w)}{\partial x} = 0 & \text{for} \quad x < 0, \\ \dfrac{\partial(cS_w)}{\partial t} + u\dfrac{\partial(\alpha c f_w)}{\partial x} = 0 & \text{for} \quad x > 0. \end{cases} \tag{4.39}$$

The problem (4.39) is completed by the initial data

$$S_w(x,0) = \begin{cases} 1 - S_{or} & \text{for} \quad x < 0, \\ S_{wir} & \text{for} \quad x > 0, \end{cases} \tag{4.40}$$

$$c(x,0) = \begin{cases} \bar{c} & \text{for} \quad x < 0, \\ 0 & \text{for} \quad x > 0. \end{cases} \tag{4.41}$$

A jump in the concentration implies that also the fractional flow function $f_w = f_w(S_w, c)$ might be discontinuous, but this will not be the case here. Indeed, a material balance around $x = 0$ for water and polymer gives, respectively,

$$\begin{cases} f_w(1 - S_{or}, \bar{c}) = f_w(S_b, c_b), \\ f_w(1 - S_{or}, \bar{c})\bar{c} = \alpha(S_b) f_w(S_b, c_b) c_b. \end{cases} \tag{4.42}$$

Since $f_w(1 - S_{or}, \bar{c}) = 1$ for any value of $\bar{c}$, then the first equation of (4.42) yields $S_b = 1 - S_{or}$ (recall that the fractional flow function reaches value 1 only for $S_w = 1 - S_{or}$). The second equation results in

$$c_b = \frac{\bar{c}}{\alpha(1 - S_{or})}. \tag{4.43}$$

Now that we have computed the initial condition for the ODEs, the next step is to determine the values of (S_l, c_l) at which the ODEs must be stopped. These values are precisely the ones for which the characteristic velocities (4.30) and (4.31) are equal, because the polymer field is still a contact discontinuity as in the case $\alpha = 1$. Therefore, the ODEs are solved numerically through a MATLAB solver, setting an event ($\lambda_w = \lambda_p$) at which the solver must stop. At the front (S_l, c_l), the polymer concentration jumps to zero, so we expect a shock in water saturation as well. The same procedure as in the case disregarding IPV can be adopted to compute the value S_r on the right of the polymer front and the velocity of the first shock. Rankine-Hugoniot relation at the polymer front gives the shock velocity

$$\sigma_2 = \frac{u}{\phi}\frac{f_w(S_l, c_l) - f_w(S_r, 0)}{S_l - S_r}. \tag{4.44}$$

The value of S_r is given by imposing the equality $\sigma_2 = \lambda_w(S_l, c_l)$. If S_r is smaller than the saturation value S^* (i.e. the saturation value at the front of a waterflooding), then the velocity of the first pure water front is

$$\sigma_1 = \frac{u}{\phi}\frac{f_w(S_r, 0) - f_w(S_{wir}, 0)}{S_r - S_{wir}}. \tag{4.45}$$

To summarize, assuming $S_r < S^*$, the solution to the Riemann problem defined by (4.22), (4.39), (4.40) and (4.41) is given by

$$S_w(x,t) = \begin{cases} 1 - S_{or} & \text{for} \quad x/t < 0, \\ \tilde{S}_w(x/t) & \text{for} \quad 0 < x/t < \lambda_w(S_l, c_l), \\ S_r & \text{for} \quad \lambda_w(S_l, c_l) < x/t < \sigma_1, \\ S_{wir} & \text{for} \quad x/t > \sigma_1, \end{cases} \tag{4.46}$$

$$c(x,t) = \begin{cases} \bar{c} & \text{for} \quad x/t < 0, \\ \tilde{c}(x/t) & \text{for} \quad 0 < x/t < \lambda_w(S_l, c_l), \\ 0 & \text{for} \quad x/t > \lambda_w(S_l, c_l). \end{cases} \tag{4.47}$$

In figure 4.10, we depict the graphical method typically used to build the solution for waterflooding and polymer flooding. Few differences must be remarked when $\alpha(S_w)$ is incorporated in the governing equations. First, the rarefaction wave does not follow one specific fractional flow curve, but will touch all the curves in between the two limiting values of concentration c_b, c_l. In particular, the starting point of the rarefaction wave will be on the curve $f_w(S_w, c_b)$ (red line) at saturation value $S_w = 1 - S_{or}$. The end point will be on the curve $f_w(S_w, c_l)$ (green line) at saturation value $S_w = S_l$. Hence, the straight line that connects the two points $f_w(S_l, c_l)$ and $f_w(S_r, 0)$ is not tangent to the curve $f_w(S_w, c_l)$, but rather intersects it in two points. Another interesting observation is that this line intersect the x-axis at $S_w = S_{ipv}$, while without velocity enhancement we have seen that the straight line passes through the origin. This is a consequence of the acceleration provoked in the polymer front. We can verify analytically: this line is defined by the relations $\lambda_p = \lambda_w = \sigma_2$, from which we have seen the triplet (c_l, S_l, S_r) is computed. Therefore, the equation of the line $y = y(S_w)$ is

$$y(S_w) = f_w(S_l, c_l) + \underbrace{\frac{f_w(S_l, c_l) - f_w(S_r, 0)}{S_l - S_r}}_{=\sigma_2 = \lambda_p(S_l, c_l)}(S_w - S_l). \tag{4.48}$$

Since $\lambda_p(S_l, c_l)$ has the form (4.31), it is easy to compute the value of S_w for which $y(S_w) = 0$:

$$\begin{aligned} -f_w(S_l, c_l) &= \frac{\alpha(S_l) f_w(S_l, c_l)}{S_l}(S_w - S_l) \\ \iff \qquad -S_l &= \frac{S_l}{S_l - S_{ipv}}(S_w - S_l) \\ \iff \qquad S_w &= S_{ipv}. \end{aligned}$$

Solutions for different values of S_{ipv} and different numerical schemes are shown in figures 4.11 and 4.12. The fact that the concentration profile is decreasing as a function of x can be explained, from a physical point of view, in the following way: since $\alpha(S_w)$ is a decreasing function of the saturation, and the saturation itself has a decreasing profile, the polymer acceleration keeps increasing through the reservoir. As a consequence, the polymer molecules keep getting more distant between each other, and the concentration decreases. This consideration does not mean that every decreasing enhancement factor will result in a monotone profile, because hyperbolicity of the model is needed in order to study analytical solutions. The value of S_{ipv} strongly affects the velocity of the fronts: when $S_{ipv} \to S_{wir}$, the two shocks almost coincide. Hence, the model of Bartelds allows to speed up the polymer front until the limit case, where there is no more water flowing ahead, is reached, see figure 4.12. In this sense, the model is quite powerful: being $\alpha(S_w)$ a continuous function, all the intermediate states between $\alpha = 1$ (no enhancement) and the limit case just discussed can be reached.

While an analytical proof ensuring monotonicity for the concentration seems hard to be found due to the complicated expressions, the matter will be addressed from a numerical point of view in chapter 5, working with the discretized equations. It will turn out that monotonicity is strictly related to well-posedness, and the insights that we will get suggest that the accumulation of polymer at the front is merely a result of a mathematical ill-posedness, while a well-posed model, related in turn to a decreasing $\alpha(S_w)$, results in a decreasing concentration profile. Note that in the case of figure 4.12, there is a slight non-monotonous profile for the concentration computed with semi-implicit scheme. This issue is numerical, and restrictions on the time step for the semi-implicit scheme will be addressed in the following chapter.

Since the aim of polymer flooding is to improve oil recovery, in figure 4.13 we depict the oil production in two cases: one without including IPV effects, and one using Bartelds IPV model. Because the water-polymer front is accelerated when including IPV, the water breakthrough at the production well is seen sooner and, initially, the oil recovery is improved. However, the height of the saturation front (i.e. the value of S_l) is lower than the case without IPV, so that, once both the water breakthroughs have reached the production well, the predicted oil recovery becomes lower. This is, in turn, a consequence of the mass balance principle: the water front travels with the polymer front and is accelerated as well, hence the value of S_l is lower.

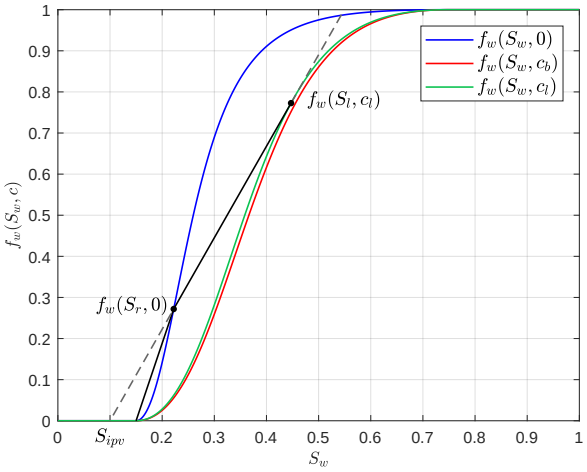

Figure 4.10: Illustration of the construction of the solution with enhancement factor modeled by (4.20).

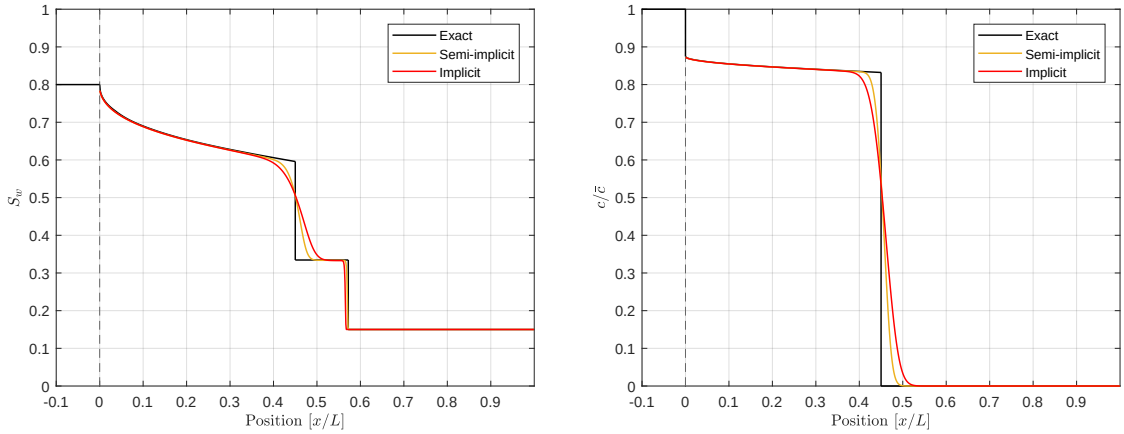

Figure 4.11: Saturation (left) and concentration (right) profiles obtained with implicit and semi-implicit first order upwind schemes, 1000 cells and timesteps, $S_{ipv} = 0.1$.

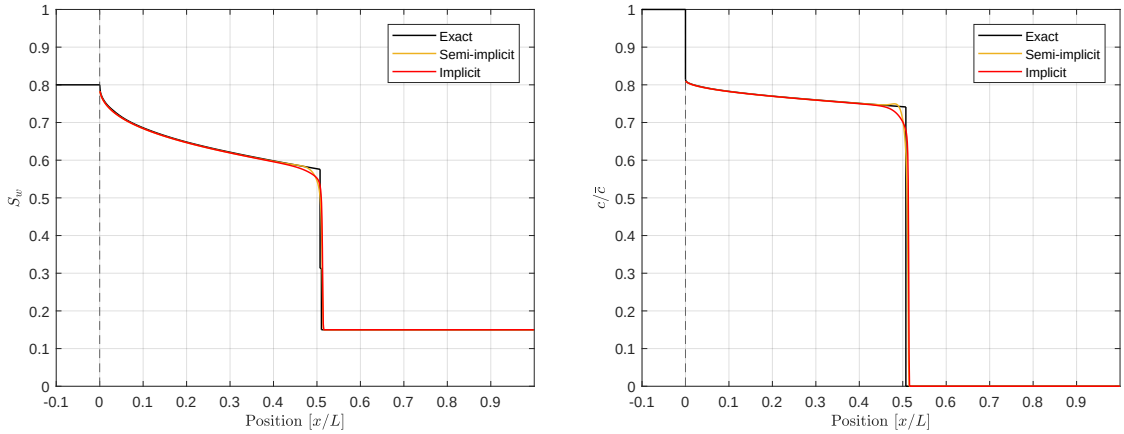

Figure 4.12: Saturation (left) and concentration (right) profiles obtained with implicit and semi-implicit first order upwind schemes, 1000 cells and timesteps, $S_{ipv} = 0.149$. The two shocks in water saturation are barely distinguishable.

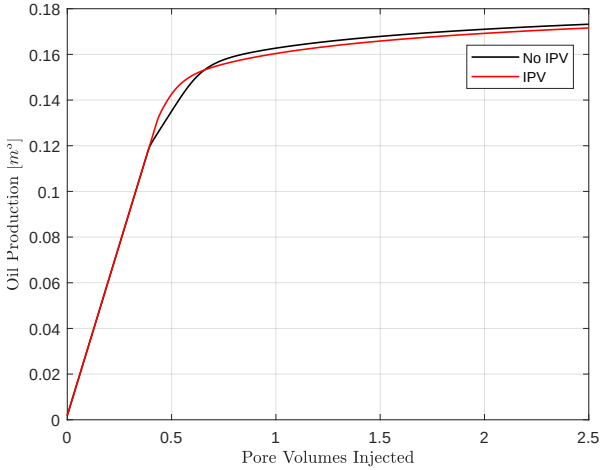

Figure 4.13: Oil production for a case without velocity enhancement (black line) and with velocity enhancement modeled by Bartelds factor (4.20) and $S_{ipv} = 0.1$ (red line).

The percolation model has been extended by Bartelds in [2] to consider the EPV effect as the major cause of velocity enhancement. The conservation equations are still (4.22) and (4.23), while the velocity enhancement factor is expressed as

$$\alpha(S_w) = \frac{S_w k_{r,w2}}{S_{w2} k_{r,w}}, \tag{4.49}$$

where $S_w = S_{w1} + S_{w2}$ and the subscripts refer to the three phase model discussed before. The relative permeabilities $k_{r,w}$ and $k_{r,w2}$ are determined using a percolation approach. Since this approach results in a more complex model for the relative permeabilities, which do not have a closed form but are computed numerically, it is not feasible to determine the well-posedness of the model through the eigenvalues of the system matrix, as done previously. It must be remarked that the enhancement factor in this alternative models depends also on the polymer concentration, i.e. $\alpha = \alpha(S_w, c)$. Numerical plots of $\alpha(S_w, c)$ presented in [2] show that it decreases with both concentration and water saturation. The curve for $\alpha(S_w, c)$ is though really steep for low saturation values, warning that a division for a value close to 0 may occur. This fact may cause serious numerical issues that would further lead to instabilities and unphysical results. Even if it is not possible to compute explicitly $\alpha(S_w, c)$ and its derivatives, it is still interesting to see how the matrix A of the system, and hence the discriminant, change when considering a concentration dependent factor. The matrix A reads

$$A = \frac{u}{\phi} \begin{pmatrix} \dfrac{\partial f_w}{\partial S_w} & \dfrac{\partial f_w}{\partial c} \\ \dfrac{\frac{\partial \alpha}{\partial S_w} c f_w + (\alpha - 1) c \frac{\partial f_w}{\partial S_w}}{S_w} & \dfrac{\alpha f_w + (\alpha - 1) c \frac{\partial f_w}{\partial c} + c f_w \frac{\partial \alpha}{\partial c}}{S_w} \end{pmatrix}. \tag{4.50}$$

In the lower-right entry, there is now the partial derivative of $\alpha(S_w, c)$ with respect to the concentration. The expression for the discriminant then changes to

$$D = \left(\frac{u}{\phi}\right)^2 \left[\left(\frac{\partial f_w}{\partial S_w} - \frac{\alpha f_w + (\alpha - 1) c \frac{\partial f_w}{\partial c} + c f_w \frac{\partial \alpha}{\partial c}}{S_w} \right)^2 + 4 \left(\frac{\partial f_w}{\partial c} \frac{\frac{\partial \alpha}{\partial S_w} c f_w + (\alpha - 1) c \frac{\partial f_w}{\partial S_w}}{S_w} \right) \right]. \tag{4.51}$$

Since $\partial\alpha/\partial c$ appears in the quadratic term of the discriminant (4.51), it is hard to conclude whether it will help to achieve well-posedness: the term inside brackets can be either positive or negative, depending on the values of (S_w, c). If this term is positive, the $\partial\alpha/\partial c \leq 0$ will contribute to get a larger quadratic term, contrasting ill-posedness. Viceversa, $\partial\alpha/\partial c$ will contribute to ill-posedness when the sum of the other terms is negative. Since here the eigenvalues cannot be computed as in the case focusing solely on IPV, the system is not guaranteed to be strictly hyperbolic.

For a detailed discussion of the percolation model, the reader is referred to [2]. A result that must be outlined is that smooth accumulation of polymer at the front is observed in the numerical simulations of this model. Given the above discussion, the peak is probably the result of an ill-posed behaviour of the model rather than a realistic physical state. In addition, a diffusive term has been added to the governing system of equations to avoid numerical instabilities. This operation seems more a mathematical artifact to overcome numerical issues and reinforces our idea that the extended model is not well-posed, although we stress that no formal analysis has been carried out.

Technically, the numerical solutions obtained were qualitatively in good agreement with the physical experiments, that measured a pile-up of the polymer in [2]. However, it has been discussed at the beginning of the chapter that experimental measurement of [2] are not entirely reliable. Considering the experimental unreliability, the complexity of the model for the relative permeabilities which requires the use of numerical algorithms, the shape of $\alpha(S_w, c)$, the impossibility to prove well-posedness and the ambiguous simulations result, we will not adopt this model that includes EPV, but rather focus on IPV effects only.

4.2.3. Hilden-Nilsen-Raynaud Model for IPV

The models proposed by Bartelds for IPV seeks and succeeds in solving stability issues related to the velocity enhancement factor modeling. An analytical solution can be computed, and no peaks in polymer concentration appears to grow unbounded in the numerical simulations. The model is though subject to the restriction $S_{ipv} < S_{wir}$, where we recall S_{ipv} is some threshold saturation that must be reached by water before polymer is allowed to be transported through the porous medium. Since it is not guaranteed that this condition holds for every reservoir, Hilden et al. [21] proposed an extended model to relax this assumption. Based on an heuristic physical understanding of the relative permeabilities, an alternative saturation dependent enhancement factor is derived. This model reduces to the one proposed by Bartelds when $S_{ipv} < S_{wir}$. To verify well-posedness, a necessary condition is proposed by considering shock solutions and hyperbolic laws with discontinuous flux function (for an introduction to such theory, refer to [5]).

The underlying flow equations adopted by Hilden et al. are again (4.22)-(4.23), but the necessary condition is derived under some further assumptions. Indeed, the water flow is assumed to be not affected by the presence of polymer (i.e. $f_w = f_w(S_w)$ does not depend on polymer concentration). In this way, the governing equations become

$$\frac{\partial S_w}{\partial t} + \frac{u}{\phi}\frac{\partial f_w(S_w)}{\partial x} = 0, \tag{4.52}$$

$$\frac{\partial (S_w c)}{\partial t} + \frac{u}{\phi}\frac{\partial}{\partial x}\left(c\alpha(S_w) f_w(S_w)\right) = 0, \tag{4.53}$$

where it is clear that water continuity equation is uncoupled from the polymer one, and hence the flow can be solved independently. We stress that this assumption is used only to derive the necessary condition for well-posedness and it is not applied to the governing equations. Defining $z = S_w c$, a Riemann problem with values (S_l, z_l) and (S_r, z_r) on, respectively, the right hand side and the left hand side, is considered. Moreover, the solution to (4.52) is assumed to be a pure shock (which is of course not true in general, but, since the equation is uncoupled, the value on the left of the water shock can be computed through the procedure discussed in chapter 3. The focus can then be devoted to the polymer equation and, in particular, to the behaviour at the water shock). Since the water saturation solution is discontinuous, the flux function of (4.53) is discontinuous as well. Polymer continuity equation is then reformulated in a frame moving with the shock velocity given by the usual Rankine-Hugoniot condition applied to (4.52). In this way, a Riemann problem with discontinuous flux function centered in the origin is obtained. Through the theory elaborated in the work of Holden and Risebro [5], several requirements are derived in order to build a solution to such problem. These requirements lead to the following restriction on the enhancement factor:

$$\alpha(S_w) \leq \frac{S_w}{S_w - S_{wir}}. \tag{4.54}$$

Inequality (4.54) is a necessary condition for well-posedness of the Riemann problem. Note that, in the model derived by Bartelds, the velocity enhancement factor is

$$\alpha(S_w) = \frac{S_w}{S_w - S_{ipv}}. \tag{4.55}$$

In the case $S_{ipv} < S_{wir}$ (which is the restriction imposed by Bartelds model), the necessary condition for the factor (4.55) is satisfied. On the other hand, if $S_{ipv} \geq S_{wir}$, (4.54) does not hold and the resulting model is ill-posed. Hilden et al. have shown that, under mild assumptions on the fractional flow function, condition (4.54) is also sufficient.

Condition (4.54) is adopted to classify the velocity enhancement models as well-posed or ill-posed. Although the approach followed to derive it is appealing because (4.54) can be verified and

applied to any model of enhancement (as far as the governing equations are (4.22)-(4.23)), quite strict assumptions have been made in the problem formulation. We will show that the model of $\alpha(S_w)$ proposed by Hilden et al. and reported below, despite fulfilling condition (4.54), will not result in a well-posed model (in the sense of a strictly hyperbolic model). This fact was overlooked by the authors probably because the behaviour of numerical simulations is much more stable than the constant factor model, but concentration profile can still result in a peak at the polymer front when $S_{ipv} > S_{wir}$ is chosen.

We present now the main ideas behind the model of $\alpha(S_w)$ proposed by Hilden et al. [21]. For a thorough and detailed discussion, the reader is referred to the original paper. The assumption that will guide the model derivation is that, in a water wet system, water invades smallest pores first. In these smallest pores, permeability is lower and water travels slower.

Similarly to the percolation model, a distribution function $\chi(\hat{r})$ is defined, where $\hat{r}$ denotes the radius of a pore. Since permeability is assumed to depend on the pore size, for each $\hat{r}$ there corresponds a permeability $\hat{k}(\hat{r})$ and the total permeability is given by

$$k = n\int_0^\infty \hat{\phi}(\hat{r})\hat{k}(\hat{r})\chi(\hat{r})d\hat{r}, \tag{4.56}$$

where n is the number of pores in a cross section and the function $\hat{\phi}$ contains the geometric information on the structure of this section.

Due to the assumption that pores are filled successively in increasing size, for a given global saturation S_w there exists a threshold value for the pore size, denoted by r, for which

$$\hat{S}_w(\hat{r}) = \begin{cases} 1 & \text{if } \hat{r} \le r, \\ 0 & \text{if } \hat{r} > r. \end{cases} \tag{4.57}$$

The global water saturation is then defined similarly to (4.56) as

$$S_w = \frac{n}{\phi}\int_0^r \hat{\phi}(\hat{r})\chi(\hat{r})d\hat{r}, \tag{4.58}$$

Polymer is then included in the model. The inaccessible pore volume effect is modeled by defining a threshold value r_{ipv} such that polymer cannot enter pores with $\hat{r} < r_{ipv}$. Polymer concentration can then be expressed as

$$\hat{c}(\hat{r}) = \begin{cases} 0 & \text{if } \hat{r} \le r_{ipv}, \\ \bar{c} & \text{if } \hat{r} > r_{ipv}, \end{cases} \tag{4.59}$$

where it is assumed that in the region $\hat{r} > r_{ipv}$ the polymer diffuses uniformly and reaches a constant concentration $\bar{c}$. An expression for the total polymer concentration is then given by

$$S_w c = \frac{n}{\phi}\bar{c}\int_{r_{ipv}}^r \hat{\phi}(\hat{r})\chi(\hat{r})d\hat{r}. \tag{4.60}$$

These expressions for permeability, saturation and concentration are inserted into the governing equations. An analytical expression for the velocity enhancement factor is found manipulating the system of equations, but the necessary condition (4.54) is still not fulfilled. Hence, the model has to be slightly modified.

The idea is then to introduce a weighting function $\hat{w}(\hat{r})$ and relax the definition of inaccessible pore volume by allowing a small quantity of polymer to enter the smallest pores as well. The polymer concentration (4.59) becomes

$$\hat{c}(\hat{r}) = \hat{w}(\hat{r})\bar{c}, \tag{4.61}$$

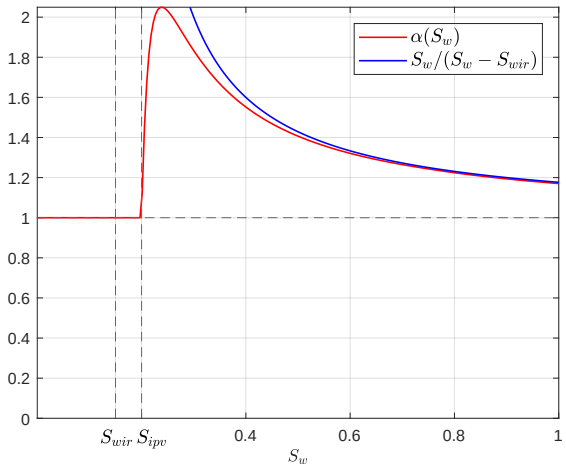

Figure 4.14: Velocity enhancement factor (4.63) proposed by Hilden et al. (red line) and necessary condition (4.54) (blue line), for $S_{wir} = 0.15$ and $S_{ipv} = 0.2$.

where

$$\hat{w}(\hat{r}) = \begin{cases} \epsilon / S_{ipv} & \text{if } \hat{r} \le r_{ipv}, \\ 1 & \text{if } \hat{r} > r_{ipv}. \end{cases} \tag{4.62}$$

It is shown by Hilden et al. that an optimal[3] value for ϵ can be found, and the resulting model of the velocity enhancement factor, namely

$$\alpha(S_w) = \begin{cases} \left(1 - \dfrac{S_{wir}}{S_{ipv}} \dfrac{k_{r,w}(S_{ipv})}{k_{r,w}(S_w)}\right) \dfrac{S_w}{S_w - S_{wir}} & \text{if } S_{ipv} \ge S_{wir} \text{ and } S_w > S_{ipv}, \\ \dfrac{S_w}{S_w - S_{ipv}} & \text{if } S_{ipv} < S_{wir} \text{ and } S_w > S_{ipv}, \\ 1 & \text{if } S_w \le S_{ipv}, \end{cases} \tag{4.63}$$

fulfills the necessary condition (4.54). Note that, when Bartelds restriction $S_{ipv} < S_{wir}$ is complied, $\alpha(S_w)$ reduces indeed to Bartelds model. Caution must be used when $S_{ipv} \approx S_{wir}$, because a division for a quantity close to zero may lead to numerical issues. Therefore, in the implementation of these models in MATLAB, we make sure to define a tolerance value $\delta > 0$ such that

$$|S_{ipv} - S_{wir}| \ge \delta.$$

A plot of the enhancement factor defined by (4.63), along with the necessary condition (4.54), is shown in figure 4.14. Note that there is an initial region where $\alpha(S_w)$ is increasing. In figure 4.15, illlustrating the discriminant D for this model, we see that $D < 0$ for certain S_w, showing that the model is not hyperbolic for all S_w. It turns out, though, that the loss of hyperbolicity is not due only to the region where $\alpha(S_w)$ is increasing. The discriminant is negative for a range of values of S_w that are not necessarily associated to the region where $\alpha(S_w)$ is increasing.

Due to the loss of hyperbolicity, characteristic velocities are not well-defined, and the theory presented in chapter 2 for the solution of hyperbolic equations cannot be applied here. Hence, we do not have an analytical solution for the enhancement model proposed by Hilden.

All the numerical solutions presented in [21], obtained with the MRST simulator and an explicit two-points upwind scheme, result in a decreasing concentration profile for the proposed model

[3] optimal in the sense that for every smaller value there is a Corey coefficient n_w (recall that n_w is used in the model of relative permeabilities (3.2)) such that the necessary condition (4.54) is not fulfilled, and every greater value will allow more polymer to enter the inaccessible pore volume

n_w	n_o	$k^0_{r,w}$	$k^0_{r,o}$	μ_w	μ_o	S_{wir}	S_{or}
2	2	0.6	0.9	1cP	30cP	0.15	0.25

Table 4.1: Alternative case for the problem parameters, highlighting the instability of numerical solutions.

(4.63). However, we show now numerical simulations where a non-monotonous concentration profile is obtained. The reference models for relative permeabilities and viscosity are used, but we change the numerical values of some parameters, because they were seen to emphasize the ill-posed behaviour of this model. The choice for these values is illustrated in table 4.1. We vary the value of the inaccessible pore volume saturation S_{ipv} in order to monitor the solution profile when only the enhancement model is modified. We use implicit first order upwind schemes, so that any non-monotonous result is most likely due to the analytical model. Results of the simulations are depicted in figures below.

An interesting fact that must be remarked, is that accumulation of polymer is observed as the grid is refined. This means that the numerical diffusion introduced by the adopted schemes might smear the concentration front, disguising the non-monotonicity property and giving misleading results. Moreover, the solution was observed to be generally more stable than the one where a constant velocity enhancement is employed, and the accumulation phenomenon is much more limited. For these reasons, the authors might have overlooked the non-monotonous profile of the polymer concentration that can arise by implementing the proposed model. It must be remarked that in the conclusions of [21], the authors state clearly that there is no guarantee that the polymer concentration will always be monotone, and that a pile-up of polymer was observed in the unphysical case where the connate water saturation is less than the irreducible water saturation.

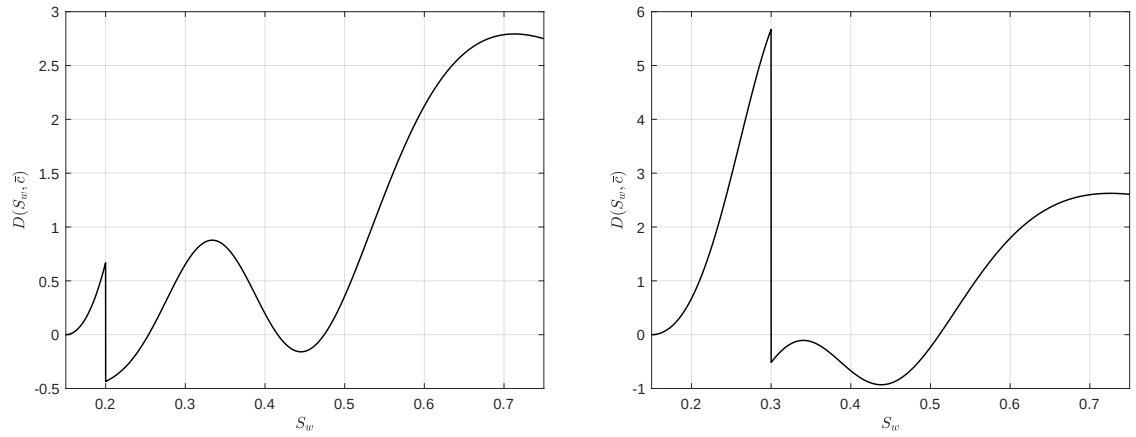

Figure 4.15: Discriminant (4.26) for a fixed value of concentration $c = \bar{c}$, $S_{ipv} = 0.2$ (left) and $S_{ipv} = 0.3$ (right).

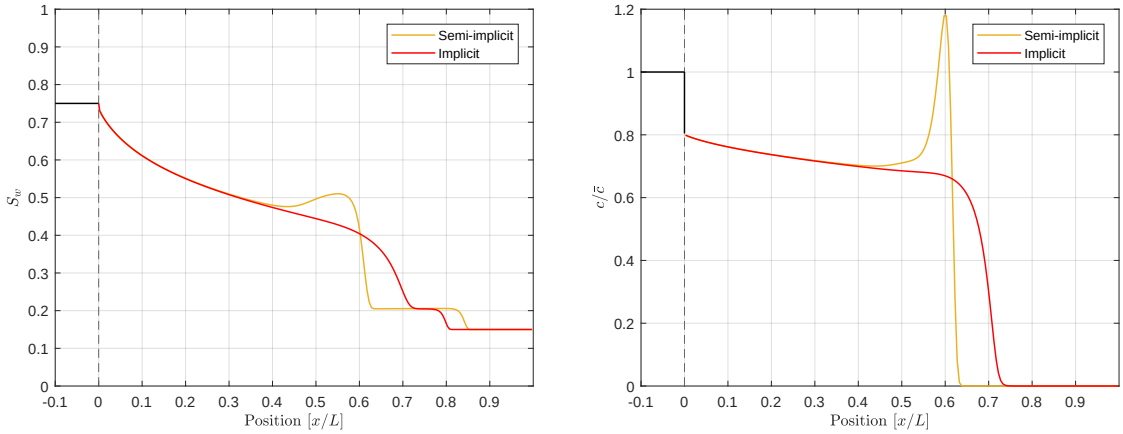

Figure 4.16: Saturation (left) and concentration (right) profiles obtained with implicit and semi-implicit first order upwind schemes, 200 cells and timesteps, $S_{ipv} = 0.2$.

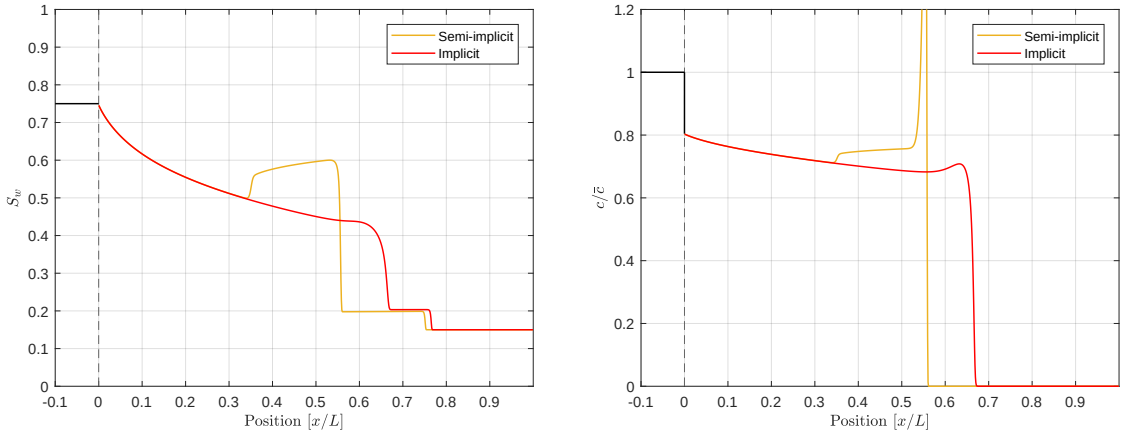

Figure 4.17: Saturation (left) and concentration (right) profiles obtained with implicit and semi-implicit first order upwind schemes, 1000 cells and timesteps, $S_{ipv} = 0.2$.

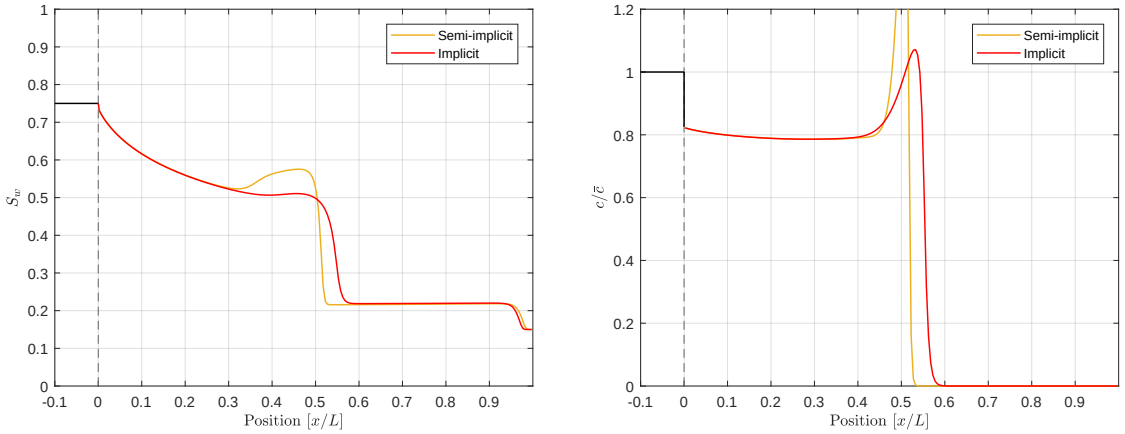

Figure 4.18: Saturation (left) and concentration (right) profiles obtained with implicit and semi-implicit first order upwind schemes, 200 cells and timesteps, $S_{ipv} = 0.3$.

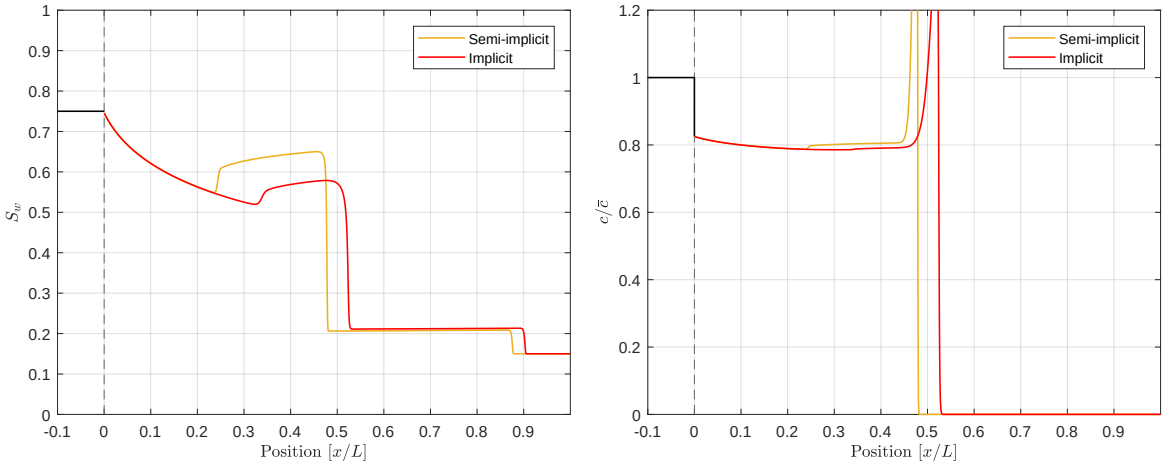

Figure 4.19: Saturation (left) and concentration (right) profiles obtained with implicit and semi-implicit first order upwind schemes, 1000 cells and timesteps, $S_{ipv} = 0.3$.

4.2.4. Further Remarks on Enhancement Modeling and Conclusions

Several models for the velocity enhancement factor have been proposed. It was shown that a constant factor leads to an ill-posed model and numerical simulations show a peak in polymer concentration at the polymer front, therefore this approach should be avoided. This peak grows uncontrolled depending on the grid size adopted for the numerical method. These facts motivate us to consider more accurate models that can prevent stability issues. A model based on a percolation approach to predict IPV effects was first derived by Bartelds et al. [4], introducing a saturation dependent enhancement factor. Such model is shown to be well-posed[4] and, moreover, we could compute the analytical solution. However, this model is subject to the restriction that the inaccessible pore volume saturation must be smaller than the irreducible water saturation. In practical situations, we are not guaranteed that this will always be the case. Therefore, Hilden et al. [21] proposed a model that relaxes this restriction. In this model, a small fraction of polymer is allowed to enter the inaccessible pores. Despite the conclusions reported in the paper were positive that this enhancement factor would lead to a well-posed problem, we have shown that this is not the case, so we will discard this choice of $\alpha(S_w)$. Hence, we suggest to adopt the model proposed by Bartelds, even if it does not seem to allow for any accumulation of polymer (monotonicity of the concentration profile will be further addressed in the next chapter). In fact, accumulation seems to be strictly related to ill-posed models, and if the desired output of the model should allow for accumulation, the overall modelling approach might need to be reviewed. Even if there are no experimental data that can support the results of Bartelds model, neither we have found clear measurement of an accumulation of polymer caused by IPV effects. In the PhD. Thesis [2], Bartelds reported several physical experiments where a higher polymer concentration right after the water breakthrough was observed at the effluent, but the measurement methods adopted may have caused severe experimental errors, so we classify these data as unreliable. In this thesis, Bartelds tries to model EPV (excluded pore volume) effects as well, so a saturation and concentration dependent factor $\alpha = \alpha(S_w, c)$ was introduced. The model has been briefly discussed previously and we concluded that it will be discarded in this research.

Introducing a dependency on the concentration could be an interesting idea. A concentration dependent model could offer an alternative way to prevent (or allow) accumulation of polymer. A driving idea could be that, if concentration locally grows, it may originate counter forces which will contrast polymer accumulation. For instance, we would expect viscosity to grow locally with concentration. The effect of a local raise in viscosity needs to be understood better. Indeed, viscosity as a function of polymer concentration is already accounted for in Darcy velocity, and a raise in viscosity will alter the properties of the flow. It is unclear if an increased viscosity would affect directly the velocity enhancement, raising the question whether it makes sense or not to insert a viscosity dependency in the enhancement factor. This approach has been undertaken in [12] to model the enhancement effect in the case of colloids, which have though different chemical properties compared to polymers. Moreover, the equation for the colloid transport is the usual linear advection equation, so viscosity is not modeled through a Darcy velocity. In addition, we discussed that a decreasing concentration dependent factor mat not have a beneficial effect on the sign of the discriminant.

Given these uncertainties, we prefer to work with an enhancement factor depending only on saturation and focusing on IPV effect. The EPV effect is much harder to model: on a macro scale, this phenomenon appears hard to be captured. Moreover, if we use the assumption of water invading pores in increasing size, we would imagine that EPV effects increases with water saturation. This fact would contradict the previous analysis, where it was shown that an enhancement factor decreasing with saturation is needed to achieve well-posedness.

The model for IPV developed by Bartelds is more suited for porous medium with low permeabil-

[4] here well-posedness is intended in the sense that the resulting system of governing equations is strictly hyperbolic.

ity, since we recall that in this case IPV dominates over EPV. Since these models result in monotone concentration profile, they are also more addressed to model flows in which synthetic polymers are injected, as a pile-up would be very unlikely to occur. Although the model is subject to the aforementioned restriction, we can think of a way to overcome this limitation. We have seen that the model proposed by Bartelds allows to reach the limit case where the two shocks in water saturation basically coincide. The polymer cannot travel any faster, because the water ahead is immobile. As Hilden et al. tried to overcome this limitation, the model lost the hyperbolicity property. Hence, we can employ the model of Bartelds transcending the underlying physical motivation and using it in a bit more abstract way. In fact, the value of S_{ipv} can be adjusted in order to accelerate the polymer front as much as desired, keeping in mind the restriction $S_{ipv} < S_{wir}$. If experimental data concerning the enhancement effect are available for a specific reservoir, the value of S_{ipv} can be selected in order to properly fit these data. With this interpretation, we can even go beyond the distinction between IPV and EPV, since both effects are supposed to cause an acceleration of the polymer front. The chemical composition of the polymer may also affect the enhancement magnitude, so again the value of S_{ipv} can be chosen consequently. To sum up, the model of Bartelds may be employed to capture any kind of acceleration effect, independently of the origin of such phenomenon. The speed of the polymer front can be varied using different quantitative values for S_{ipv}. In particular, as S_{ipv} increases, the velocity of the front increases as well.

We mention one last mechanism that affects polymer flow through a porous medium and is usually observed in experimental measurements. The molecules of the injected polymers do not have all the same size, but are rather distributed within a certain interval. The consequence is that the bigger molecules are trapped and retained in the porous medium, so that the polymer profile at the effluent will be more smeared than the tracer's one when approaching injected concentration, see for instance results from [16]. This phenomenon is commonly referred to as filtration. However, filtration is usually treated as a retention term, independent from IPV/EPV effects. Since there is no clear evidence of how filtration is correlated to hydrodynamic acceleration, we will not include it in the model.

5

Monotonicity Analysis

As it has been remarked in the previous chapter, the crucial point of the velocity enhancement modeling is to understand whether the peak observed in the polymer concentration right after the second shock is a physical prediction that the model aims to capture, or rather the result of a mathematically ill-posed problem. It has been shown that the model proposed by Bartelds is the only one resulting in a hyperbolic system of equations, while the constant factor and the Hilden et al. models result in a system with elliptic regions, causing a pile-up of polymer at the front. However, we could not prove analytically how monotonicity is affected by these regions, nor we could actually guarantee that Bartelds model always gives a monotone solution (although we are quite confident that this is the case).

The aim of this chapter is to study thoroughly the monotonicity of the numerical solution given the different models of the enhancement. In particular, we will derive a monotonicity condition for the discretized equations and relate it to the analytical properties of the models. This approach will show that monotonicity is not guaranteed for the constant factor and the factor proposed by Hilden et al., while we will gain insights that support our idea of a monotone solution in the case of Bartelds factor and, more in general, in the case of a hyperbolic model. Furthermore, restrictions on the time step will be derived for the semi-implicit scheme, and high-resolution methods will be discussed as well.

5.1. Monotonicity Analysis for a Constant Factor

We start by studying the monotonicity of the discretized equations using the constant velocity enhancement factor model. The sequential approach used to solve for the flow and transport of polymer results in the following scheme:

1. Compute S_w^{n+1} using c^n and the fully implicit solver

$$\begin{cases} S_{o,j}^{n+1} = S_{o,j}^n - \frac{\Delta t}{\phi \Delta x}\left(u_o(S_{o,j}^{n+1}, c_j^n) - u_o(S_{o,j-1}^{n+1}, c_{j-1}^n)\right) \\ S_{w,j}^{n+1} = S_{w,j}^n - \frac{\Delta t}{\phi \Delta x}\left(u_w(S_{w,j}^{n+1}, c_j^n) - u_w(S_{w,j-1}^{n+1}, c_{j-1}^n)\right). \end{cases}$$

2. Compute c^{n+1} using S_w^{n+1}

$$(cS_w)_j^{n+1} = (cS_w)_j^n - \frac{\Delta t}{\phi \Delta x}\left(F_{j+1/2}(S_w^{n+1}, c^n, c^{n+1}) - F_{j-1/2}(S_w^{n+1}, c^n, c^{n+1})\right).$$

Since we address now the problem of monotonicity, we consider first order upwind schemes for the fluxes to avoid dealing with complicate expressions. To use a lighter notation, the subscript w in S_w will be omitted in the subsequent. The expressions for the fluxes become

- Semi-implicit:
$$F_{j+1/2} = \alpha u_w(S_j^{n+1}, c_j^n) c_j^n = \alpha u_{w,j}^{n+1} c_j^n,$$
- Implicit:
$$F_{j+1/2} = \alpha u_w(S_j^{n+1}, c_j^n) c_j^{n+1} = \alpha u_{w,j}^{n+1} c_j^{n+1}.$$

Note that the implicit flux is not fully implicit, since the velocity is evaluated for the concentration at time level n.

5.1.1. Semi-implicit Fluxes

In order to perform a local monotonicity analysis, we freeze the concentration at time level n. On the left of the second shock, it holds $c_{j-1}^n = c_j^n = \bar{c}$. The discretized equation for polymer becomes

$$c_j^{n+1} S_j^{n+1} = \left(S_j^n - \frac{\Delta t \alpha}{\phi \Delta x} (u_{w,j}^{n+1} - u_{w,j-1}^{n+1}) \right) \bar{c}.$$

Rearranging the equation and substituting the implicit scheme for S_j^{n+1} gives

$$c_j^{n+1} = \frac{S_j^n - \frac{\Delta t \alpha}{\phi \Delta x} (u_{w,j}^{n+1} - u_{w,j-1}^{n+1})}{S_j^n - \frac{\Delta t}{\phi \Delta x} (u_{w,j}^{n+1} - u_{w,j-1}^{n+1})} \bar{c}.$$

To have a decreasing concentration profile, the denominator must be greater than the numerator, hence

$$\begin{aligned} & S_j^n - \frac{\Delta t}{\phi \Delta x} (u_{w,j}^{n+1} - u_{w,j-1}^{n+1}) \geq S_j^n - \frac{\Delta t \alpha}{\phi \Delta x} (u_{w,j}^{n+1} - u_{w,j-1}^{n+1}) \\ \iff \quad & \alpha (u_{w,j}^{n+1} - u_{w,j-1}^{n+1}) \geq (u_{w,j}^{n+1} - u_{w,j-1}^{n+1}). \end{aligned} \tag{5.1}$$

Since the saturation decreases in space, it holds $S_{j-1}^{n+1} \geq S_j^{n+1} \; \forall j, \; \forall n$. Rewriting u_w with the fractional flow function as $u_w = u f_w$, we see that it holds $u_{w,j-1}^{n+1} \geq u_{w,j}^{n+1}$ because the fractional flow is an increasing function of the saturation. Hence, the condition (5.1) results in the requirement

$$\alpha \leq 1,$$

which is in contrast with the physical modeling assumption $\alpha > 1$. Therefore, semi-implicit fluxes for the constant enhancement factor will give a non monotone profile for the concentration.

5.1.2. Implicit Fluxes

The discretized equation employing implicit fluxes becomes

$$(cS)_j^{n+1} = (cS)_j^n - \frac{\Delta t \alpha}{\phi \Delta x} \left(u_{w,j}^{n+1} c_j^{n+1} - u_{w,j-1}^{n+1} c_{j-1}^{n+1}) \right).$$

Since the peak in the concentration is observed to occur close to the shock, assume that $c_{j-1}^{n+1} = \bar{c} = c_j^n$, so that we can focus on the local behavior of the concentration at cell j and time $n+1$. Rearranging the equation in the following form

$$\left(S_j^{n+1} + \frac{\Delta t \alpha}{\phi \Delta x} u_{w,j}^{n+1} \right) c_j^{n+1} = \left(S_j^n + \frac{\Delta t \alpha}{\phi \Delta x} u_{w,j-1}^{n+1} \right) \bar{c},$$

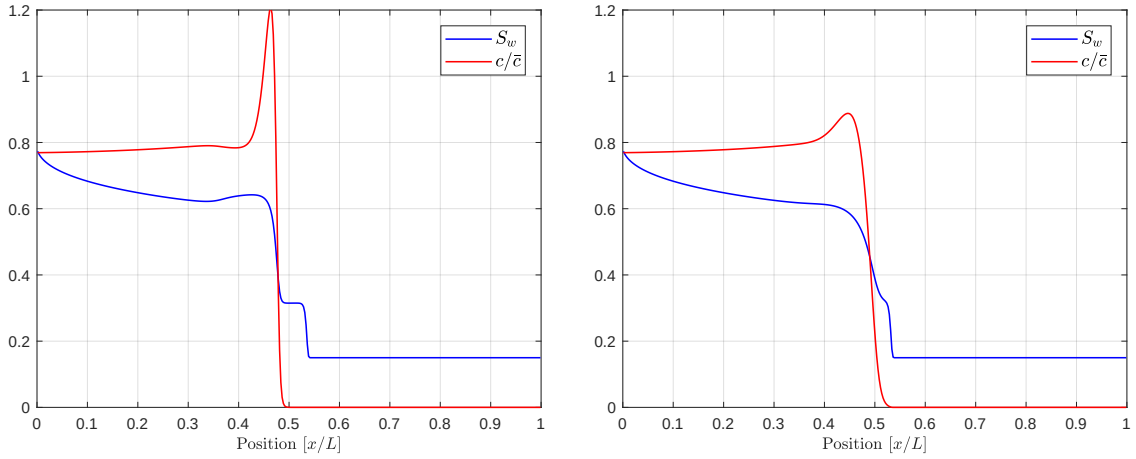

Figure 5.1: Saturation and concentration profiles obtained with semi-implicit (left) and implicit (right) first order upwind schemes, 400 cells and timesteps, $\alpha = 1.3$.

the study of the monotonicity can be carried out as in the previous section. Substituting the implicit scheme for S_j^{n+1}, the condition for monotonicity reads

$$\begin{aligned} S_j^n - \frac{\Delta t}{\phi \Delta x}(u_{w,j}^{n+1} - u_{w,j-1}^{n+1}) + \frac{\Delta t \alpha}{\phi \Delta x} u_{w,j}^{n+1} &\geq S_j^n + \frac{\Delta t \alpha}{\phi \Delta x} u_{w,j-1}^{n+1}, \\ \iff \quad u_{w,j-1}^{n+1} - u_{w,j}^{n+1} &\geq \alpha (u_{w,j-1}^{n+1} - u_{w,j}^{n+1}), \\ \iff \quad 1 &\geq \alpha, \end{aligned}$$

where we used that $u_{w,j-1}^{n+1} \geq u_{w,j}^{n+1}$. The condition derived to achieve a monotone profile is again in contrast with the physical meaning of the hydrodynamic acceleration.

Hence, the conclusion is that a constant enhancement factor leads to a non-monotonous numerical solution for both schemes adopted for the fluxes. This result confirms the analytical considerations discussed in the previous chapter and the output of the numerical simulation in figure 5.1. Note that the peak in the concentration becomes more evident with the semi-implicit scheme.

The approach used by Braconnier et al. [1] to study the effect of inaccessible pore volume on the monotonicity of the numerical solution, where the flow and the transport of polymer are solved explicitly, leads to similar results.

The MRST simulator uses a constant factor to model the velocity enhancement effect, and it introduces a numerical control parameter $c_{\max}$ to impose a limit on the values of the concentration. In particular, if $c_{\max} = \bar{c}$, then no peak will appear in the polymer concentration profile. This sort of dangerous approach is not recommendable, since it forces the numerical solution to a solution which is not the one of the governing equation, but rather an artificial one. Moreover, the ill-posed model is sometimes observed to affect also the water saturation profile, giving an unphysical solution. Thus, the control parameter $c_{\max}$ might hide the origin of these unphysical results.

5.2. Monotonicity Analysis for a Saturation Dependent Factor

Having proved that using a constant factor will not give a monotone solution, we analyze now how introducing a dependency on the saturation affects the monotonicity issue. As shown in the previous chapter, numerical simulations with Bartelds model give smooth and decreasing concentration profiles, while accumulation of polymer was still observed for Hilden model. We expect to find conditions on the problem parameters and restrictions on the time step that can be fulfilled in order

to achieve monotonicity. We do not focus now on Bartelds or Hilden model, but rather keep a general saturation dependent factor $\alpha = \alpha(S)$. As before, both the semi-implicit and the implicit first order upwind schemes are studied. Since the sequential approach is used, the enhancement factor is evaluated at $\alpha_j^{n+1} = \alpha(S_j^{n+1})$.

5.2.1. Semi-implicit Fluxes

Using a semi-implicit scheme and assuming $c_j^n = c_{j-1}^n = \bar{c}$ on the left of the shock, the discrete equation for polymer becomes

$$c_j^{n+1} S_j^{n+1} = \left(S_j^n - \frac{\Delta t}{\phi \Delta x} (\alpha_j^{n+1} u_{w,j}^{n+1} - \alpha_{j-1}^{n+1} u_{w,j-1}^{n+1}) \right) \bar{c}.$$

Substituting once again the implicit scheme for S_j^{n+1}, the discrete equation can be rewritten in the form

$$c_j^{n+1} = \frac{S_j^n - \frac{\Delta t}{\phi \Delta x} (\alpha_j^{n+1} u_{w,j}^{n+1} - \alpha_{j-1}^{n+1} u_{w,j-1}^{n+1})}{S_j^n - \frac{\Delta t}{\phi \Delta x} (u_{w,j}^{n+1} - u_{w,j-1}^{n+1})} \bar{c}.$$

For monotonicity, we impose that the denominator must be greater than the numerator and, after rearrangements and simplifications, the condition becomes

$$\begin{aligned} & \alpha_j^{n+1} u_{w,j}^{n+1} - \alpha_{j-1}^{n+1} u_{w,j-1}^{n+1} \geq u_{w,j}^{n+1} - u_{w,j-1}^{n+1}, \\ \iff \quad & \frac{\alpha_j^{n+1} - 1}{\alpha_{j-1}^{n+1} - 1} \geq \frac{u_{w,j-1}^{n+1}}{u_{w,j}^{n+1}}. \end{aligned}$$

Rewriting using the fractional flow function, the condition for monotonicity is

$$\frac{\alpha_j^{n+1} - 1}{\alpha_{j-1}^{n+1} - 1} \geq \frac{f_{w,j-1}^{n+1}}{f_{w,j}^{n+1}}. \tag{5.2}$$

Since it holds that $S_{j-1}^{n+1} \geq S_j^{n+1}$ and, consequently, $f_{w,j-1}^{n+1} \geq f_j^{w,n+1}$, for the condition (5.2) we have that

$$\frac{\alpha_j^{n+1} - 1}{\alpha_{j-1}^{n+1} - 1} \geq \frac{f_{w,j-1}^{n+1}}{f_{w,j}^{n+1}} \geq 1. \tag{5.3}$$

Here it becomes more evident why the shape of $\alpha(S)$ is a crucial feature in order to have a decreasing solution for c: in regions where $\alpha(S)$ is an increasing function of S, inequality (5.3) will never be satisfied since, on the left of the second shock, strict inequality $S_{j-1}^{n+1} > S_j^{n+1}$ holds. Hence, in order to guarantee monotonicity, the enhancement factor must be a decreasing function of the water saturation S. This remark is a discrete counterpart of what we observed when studying analytically the sign of the eigenvalues of the system of equations: the fact that $d\alpha/dS \leq 0$ was a key feature to ensure that the eigenvalues would always be real. Note that condition (5.2) does not lead to any restriction on the grid size or time step. Since the concentration is fixed, inequality (5.2) results in a condition only on the saturation value. For this reason, we claim that (5.2) arises from the analytical model rather than from the numerical scheme employed, as we will see that the same inequality is found for the implicit scheme. We will investigate further the monotonicity condition (5.2) later on in this chapter.

To ensure monotonicity, it is not enough to study the solution only on the left of the shock. A specific analysis must be carried out for the cell J where the concentration is jumping to zero. Assuming then $c_J^n = 0$, the discrete equation for cell J is

$$c_J^{n+1} S_J^{n+1} = \frac{\Delta t}{\phi \Delta x} \alpha_{J-1}^{n+1} u_{w,J-1}^{n+1} c_{J-1}^n.$$

As done previously, we require

$$\frac{\frac{\Delta t}{\phi \Delta x}\alpha_{J-1}^{n+1}u_{w,J-1}^{n+1}}{S_J^{n+1}} \leq 1.$$

This is a CFL type condition, which can be restated as

$$\frac{\Delta t}{\phi \Delta x} \leq \frac{S_J^{n+1}}{\alpha_{J-1}^{n+1}u_{w,J-1}^{n+1}} \quad \forall J, \forall n. \tag{5.4}$$

Thus, the time step can be chosen sufficiently small in order to avoid stability issues.

5.2.2. Implicit Fluxes

The discretized equation using an implicit scheme is

$$c_j^{n+1}S_j^{n+1} = c_j^n S_j^n - \frac{\Delta t}{\phi \Delta x}(\alpha_j^{n+1}u_{w,j}^{n+1}c_j^{n+1} - \alpha_{j-1}^{n+1}u_{w,j-1}^{n+1}c_{j-1}^{n+1}).$$

As done when studying the implicit scheme for a constant enhancement factor, we focus on local monotonicity for cell j at time $n+1$, thus assuming $c_{j-1}^{n+1} = c_j^n = \bar{c}$. The equation is rewritten in the form

$$\left(S_j^{n+1} + \frac{\Delta t}{\phi \Delta x}\alpha_j^{n+1}u_{w,j}^{n+1}\right)c_j^{n+1} = \left(S_j^n + \frac{\Delta t}{\phi \Delta x}\alpha_{j-1}^{n+1}u_{w,j-1}^{n+1}\right)\bar{c}.$$

Substituting the implicit scheme for the saturation S_j^{n+1} leads to

$$c_j^{n+1} = \frac{S_j^n + \frac{\Delta t}{\phi \Delta x}\alpha_{j-1}^{n+1}u_{w,j-1}^{n+1}}{S_j^n - \frac{\Delta t}{\phi \Delta x}(u_{w,j}^{n+1} - u_{w,j-1}^{n+1}) + \frac{\Delta t}{\phi \Delta x}\alpha_j^{n+1}u_{w,j}^{n+1}}\bar{c}.$$

Therefore, we find the same monotonicity condition as for the explicit scheme:

$$\begin{aligned} & u_{w,j}^{n+1}(\alpha_j^{n+1} - 1) \geq u_{w,j-1}^{n+1}(\alpha_{j-1}^{n+1} - 1) \\ \iff \quad & \frac{\alpha_j^{n+1} - 1}{\alpha_{j-1}^{n+1} - 1} \geq \frac{f_{w,j-1}^{n+1}}{f_{w,j}^{n+1}}. \end{aligned} \tag{5.5}$$

Finding the same monotonicity result for the two different discretization confirm our previous hint: this monotonicity condition derives from the analytical modeling of $\alpha(S)$, not by the numerical scheme adopted. Moreover, implicit schemes do not usually require any restriction on the time step in order to ensure stability of the results. Indeed, studying monotonicity for the cell J where the concentration jump to zero, meaning $c_J^n = 0$, the discrete equation becomes

$$c_J^{n+1}S_J^{n+1} = -\frac{\Delta t}{\phi \Delta x}(\alpha_J^{n+1}u_{w,J}^{n+1}c_J^{n+1} - \alpha_{J-1}^{n+1}u_{w,J-1}^{n+1}c_{J-1}^{n+1}).$$

Use the implicit scheme for S_J^{n+1} and rewrite in the ratio form:

$$c_J^{n+1} = \frac{\frac{\Delta t}{\phi \Delta x}\alpha_{J-1}^{n+1}u_{w,J-1}}{S_J^n - \frac{\Delta t}{\phi \Delta x}(u_{w,J}^{n+1} - u_{w,J-1}^{n+1}) + \frac{\Delta t}{\phi \Delta x}\alpha_J^{n+1}u_{w,J}^{n+1}}c_{J-1}^{n+1}.$$

Thus, the requirement for monotonicity is

$$S_J^n + \frac{\Delta t}{\phi \Delta x}u_{w,J}^{n+1}(\alpha_J^{n+1} - 1) \geq \frac{\Delta t}{\phi \Delta x}u_{w,J-1}^{n+1}(\alpha_{J-1}^{n+1} - 1). \tag{5.6}$$

Since $S_J^n \geq 0$, condition (5.6) is less restrictive than condition (5.5). Hence, if (5.5) is satisfied also for cell J, the implicit scheme will result in a monotone profile. In particular, there is no restriction on the time step as for the explicit scheme.

5.2.3. Monotonicity Condition and Well-Posedness

The purpose of this section is to investigate the meaning and implications of the monotonicity condition (5.2), and relate it to the well-posedness of the models. We have already remarked that a necessary condition to fulfill (5.2) is the decreasing property of $\alpha(S)$. While the model of Bartelds proposes a decreasing hydrodynamic acceleration factor, in the extended model proposed by Hilden et al. there is a region where $\alpha(S)$ is increasing with the saturation. Thus, the latter model will not fulfill (5.2) for all the physical values of S. However, requirement (5.2) is more restrictive than simply asking that $\alpha(S)$ is decreasing, and in most of the cases this region where $\alpha(S)$ is increasing is not the one causing a peak in the polymer concentration. Indeed, the plots presented in chapter 4 showed that the range of saturation values for which the discriminant is negative is quite wide, and it does not correspond only with the increasing part of the enhancement factor curve. Unfortunately, due to the functional form of $\alpha(S)$ and $f_w(S)$, it is hard to derive a closed form for the restriction on the saturation from the monotonicity condition. To gain insights on the actual values that S can take in order to accomplish monotonicity, we plotted numerically the ratios of the velocity enhancement and of the fractional flow functions, using a set of equidistant points in the interval $[S_{wir}, 1 - S_{or}]$ for S_j^{n+1}. Results for both Bartelds and Hilden models are shown in figure 5.2 and 5.3, respectively. Note that condition (5.2) is fulfilled for all values of saturation greater than a threshold value, which will be denoted by S_{mon}. Since the monotonicity condition has been derived for cells on the left of the shock, if we assume the saturation to be decreasing, then S_l is the minimum value and (5.2) is fulfilled when $S_l \geq S_{\text{mon}}$.

In the case of Bartelds with $S_{ipv} = 0.1$, the approximated value of S_{mon} is very close to $S_l = 0.596$, which is computed through the analytical solution. It appears clear that there must be a relation between the monotonicity condition and the value of water saturation at the polymer front. Also for Hilden, when the reference case defined in table 3.1 is used, the value of S_{mon} seems close to the value of saturation at the polymer front, and the accumulation effect is slightly noticeable.

The value computed numerically of S_{mon} is not enough accurate to derive further conclusions, but the insights gained in this paragraph suggest that there is more to be discovered about the monotonicity condition.

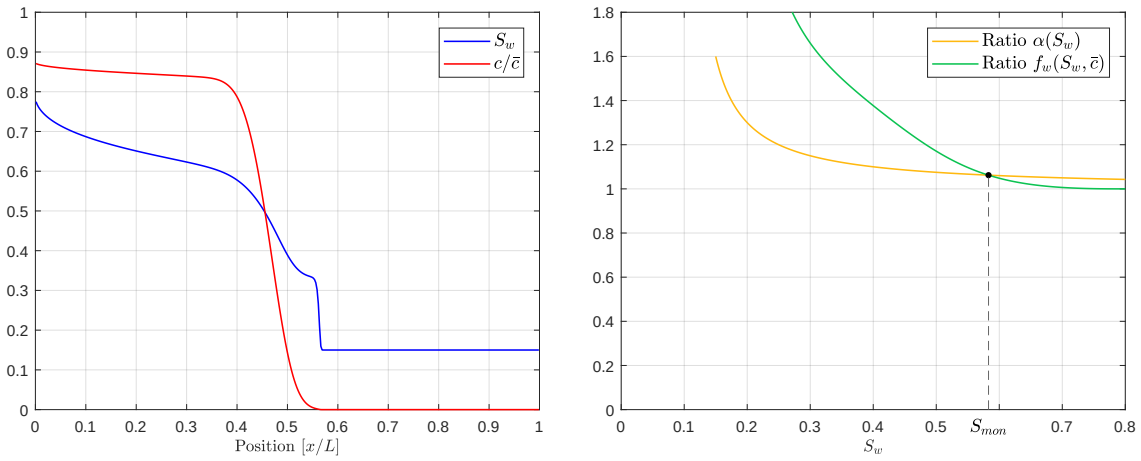

Figure 5.2: Numerical solution (left) and monotonicity condition (right) for Bartelds model, with $S_{ipv} = 0.1$, 400 cells and time steps, settings defined in table 3.1.

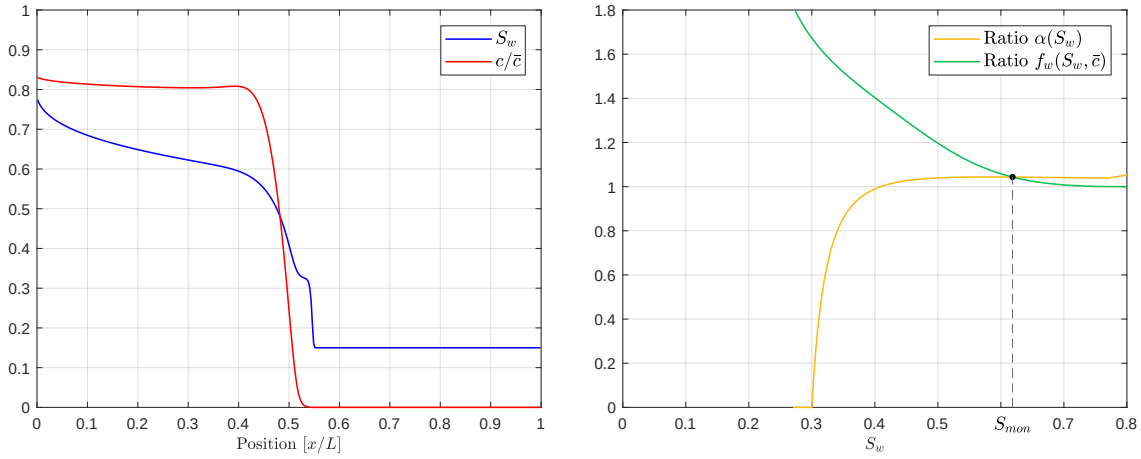

Figure 5.3: Numerical solution (left) and monotonicity condition (right) for Hilden model, with $S_{ipv} = 0.3$, 400 cells and time steps, settings defined in table 3.1.

Consider the Rankine-Hugoniot relations applied to both the water and polymer conservation equations (4.22)-(4.23) at the polymer front. We know that the polymer concentration jumps to $c = 0$ and that the shock velocity $\sigma_{2,p}$ is equal to the characteristic velocity λ_p because of the linearly degenerate nature of polymer transport equation. However, suppose that the value of the concentration on the right of the shock is unknown. In this case, the shock velocities of water and polymer are

$$\sigma_{2,w} = \frac{u}{\phi}\frac{f_w(S_l,c_l) - f_w(S_r,c_r)}{S_l - S_r}, \tag{5.7}$$

$$\sigma_{2,p} = \frac{u}{\phi}\frac{\alpha(S_l)f_w(S_l,c_l)c_l - \alpha(S_r)f_w(S_r,c_r)c_r}{S_l c_l - S_r c_r}, \tag{5.8}$$

where c_r denotes the value of the concentration on the right of the shock. At the shock, it holds $\sigma_{2,p} = \sigma_{2,w}$. Adopt now the same point of view of the monotonicity analysis for the discrete equations: right on the left of the shock, the concentration is constant and equal to c_l, while, for an $h > 0$, the saturation jumps from the value S_h to the value $S_h - h$ (interpreting as the values of S in cells $j-1, j$). Therefore, we consider the states

- $c_l = c_r$,
- $S_r = S_h - h$,
- $S_l = S_h$.

Since we claim to be really close to the shock, we impose the equality $\sigma_{2,w} = \sigma_{2,p}$ for the states above, giving

$$\frac{f_w(S_h,c_l) - f_w(S_h-h,c_l)}{S_h - S_h + h} = \frac{\alpha(S_h)f_w(S_h,c_l)c_l - \alpha(S_h-h)f_w(S_h-h,c_l)c_l}{S_h c_l - (S_h-h)c_l}.$$

The expression can be simplified to the form

$$f_w(S_h,c_l) - f_w(S_h-h,c_l) = \alpha(S_h)f_w(S_h,c_l) - \alpha(S_h-h)f_w(S_h-h,c_l). \tag{5.9}$$

Rename now the variables as

- $f_{w,j}^{n+1} = f_w(S_h - h, c_l), \quad f_{w,j-1}^{n+1} = f_w(S_h, c_l),$
- $\alpha_j^{n+1} = \alpha(S_h - h), \qquad \alpha_{j-1}^{n+1} = \alpha(S_h).$

Relation (5.9) is thus rewritten as

$$\begin{aligned} & f_{w,j-1}^{n+1} - f_{w,j}^{n+1} = \alpha_{j-1}^{n+1} f_{w,j-1}^{n+1} - \alpha_j^{n+1} f_{w,j}^{n+1} \\ \iff \quad & \frac{\alpha_j^{n+1} - 1}{\alpha_{j-1}^{n+1} - 1} = \frac{f_{w,j-1}^{n+1}}{f_{w,j}^{n+1}}, \end{aligned} \tag{5.10}$$

which is the same expression as the monotonicity condition (5.2), except that we have an equality. Therefore, we have found an analytical counterpart of (5.2): the value of saturation S_{mon}, for which the monotonicity condition is satisfied when $S \geq S_{mon}$, corresponds to the value S_l on the left of the shock. In order to have a monotone profile for the polymer concentration, the values of saturation must be greater than the value S_l of saturation at the shock. This requirement is equivalent to stating that the rarefaction wave must be decreasing. Therefore, we conclude that the monotonicity condition (5.2) is indeed a consequence of the analytical solution, and does not depend on the numerical scheme employed.

Note that, in the case of Bartelds, the value S_l is well-defined and computed through the procedure illustrated in the previous chapter. If the water rarefaction wave is decreasing, then the monotonicity condition is naturally fulfilled and, using adequate restrictions on the time step for the semi-implicit scheme, the numerical concentration profile will be monotone as well. This fact is, in turn, a consequence of the expression of the ODEs that define the rarefaction waves for water and polymer: monotonicity of the rarefaction waves depends only on the sign of the inner product $\nabla\lambda_w \cdot r_w$ which appears in both the ODEs, see previous chapter and expressions (4.37)-(4.38). Hence, the monotonicity of saturation and concentration is correlated: if the rarefaction wave of S is decreasing, then the rarefaction wave of c will be decreasing as well.

On the other hand, the model proposed by Hilden et al. leads to an ill-posed problem, and no analytical solution is available. Therefore, there is no guarantee that the values of saturation on the left of the shock are greater than S_l. If this is the case, the monotonicity condition is not fulfilled and the concentration results in a non-monotone profile. One may claim then that a non-monotone numerical solution should then be observed for both S and c. Water saturation appears though to be more subject to numerical diffusion that may mask a non-monotone behaviour.

Although the discussion above may not be completely formal, it gives valuable insights on the origin of the polymer accumulation effect and on the expected results of the selected model for the enhancement. The hyperbolic model proposed by Bartelds is the only one that does not lead to numerical instabilities. Although we could not prove analytically that saturation and concentration profiles will always be monotone, we are quite confident that this will be the case, given also the discussion of chapter 4. The accumulation effect for the constant and Hilden enhancement factor is due to mathematical ill-posedness, as confirmed from the monotonicity analysis carried out in this chapter.

There is one last aspect that we would like to remark. When Bartelds model is adopted and $S_{ipv} \to S_{wir}$, the CFL-type restriction on the time step (5.4) for the semi-implicit scheme becomes much more expensive. This happens because $\alpha(S_{wir})$ can take very high values (recall $\alpha(S) = S/(S - S_{ipv})$) and, concurrently, the two shocks in water saturation almost coincide. As a consequence, the saturation basically jumps from S_l to S_{wir} and the enhancement factor will be evaluated at values close to the irreducible water saturation. When the two shocks in water are more separated, the numerical method manages to catch the constant plateau where $S = S_r$, and the enhancement

factor is evaluated for values of S greater than S_r. In figures 5.4 and 5.5, we show that, for $S_{ipv} \to S_{wir}$, as the selected number of time steps increases, the peak in the concentration disappears.

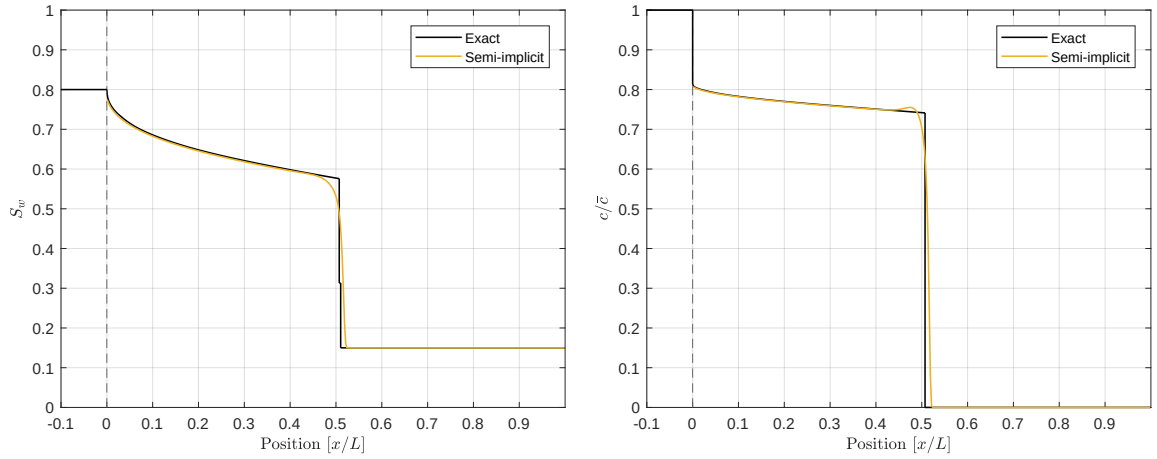

Figure 5.4: Saturation (left) and concentration (right) profiles obtained with semi-implicit first order upwind schemes, 400 cells and time steps, $S_{ipv} = 0.149$, $S_{wir} = 0.15$, condition (5.4) not fulfilled.

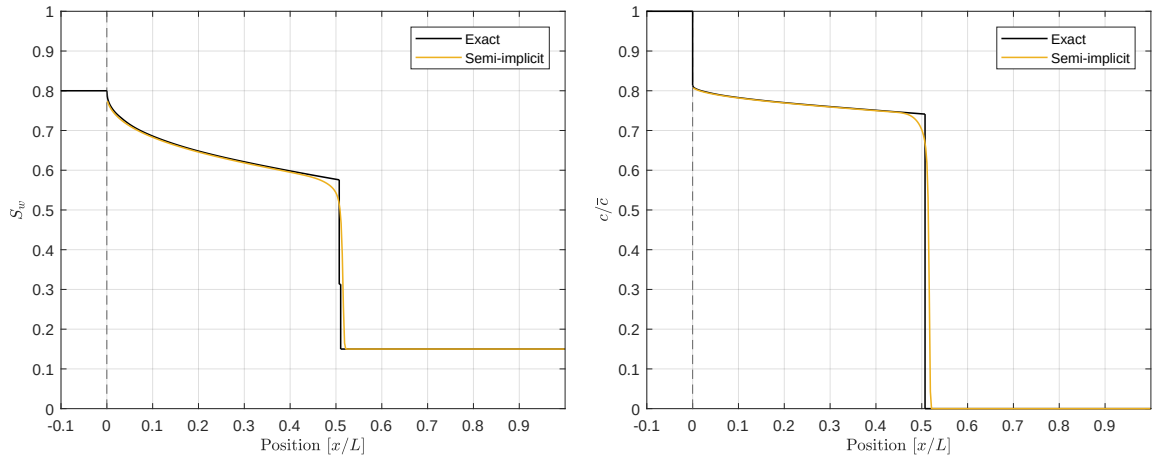

Figure 5.5: Saturation (left) and concentration (right) profiles obtained with semi-implicit first order upwind schemes, 400 cells, 800 timesteps, $S_{ipv} = 0.149$, $S_{wir} = 0.15$, condition (5.4) fulfilled.

5.3. High-Resolution Methods

In this section, we restrict our interest to the model proposed by Bartelds, as it is the only one well-posed. First order methods introduce a severe numerical diffusion, resulting in smeared profiles for saturation and concentration. This effect is clearly noticeable for instance in figure 4.11, where even on a grid with 1000 cells the numerical methods have difficulties in capturing a sharp front. As it is well-known, implicit schemes have the advantage of being unconditionally stable, but they result in a poor approximation as numerical diffusion is much stronger than for explicit (or semi-implicit) methods. On the other hand, explicit schemes are subject to a time step constraint in order to guarantee stability. Unless $S_{ipv} \to S_{wir}$, this time step restriction is not exceptionally strict, but the numerical solution is still smeared out at the shock, even on fine grids. For these reasons, we consider now high-resolution methods to solve the polymer conservation equation, while for the water flow

the fully-implicit solver implemented in MRST is still used. It has been remarked in chapter 3 that the implicit high-resolution method does not bring relevant improvement to the accuracy of the solution, despite being the most expensive scheme. Given the computational inefficiency and the raise in complexity, this kind of schemes are generally not adopted in the industry. However, since some issues raise when the polymer transport equation is solved through higher order methods, we will compare the semi-implicit and the implicit high-resolution schemes proposed in chapter 3. Adding a saturation dependent velocity enhancement factor, the numerical fluxes $F_{j+1/2}$ take the form

- Semi-implicit

$$F^n_{j+1/2} = \alpha^{n+1}_j c^n_j u^{n+1}_{w,j} + \Phi(\theta^n_{j+1/2}) \frac{1}{2} \alpha^{n+1}_j u^{n+1}_{w,j} \left(1 - \frac{\Delta t}{\Delta x} \alpha^{n+1}_j u^{n+1}_{w,j}\right) (c^n_{j+1} - c^n_j), \tag{5.11}$$

- Implicit

$$F^{n+1}_{j+1/2} = \alpha^{n+1}_j c^{n+1}_j u^{n+1}_{w,j} + \Phi(\theta^{n+1}_{j+1/2}) \frac{1}{2} \alpha^{n+1}_j u^{n+1}_{w,j} \left(1 - \frac{\Delta t}{\Delta x} \alpha^{n+1}_j u^{n+1}_{w,j}\right) (c^{n+1}_{j+1} - c^{n+1}_j). \tag{5.12}$$

Simulations are shown in the figures below. For the semi-implicit flux, a peak in polymer concentration is observed even when the CFL condition (5.4) is complied. We have set $S_{wir} = 0.15$ and $S_{ipv} = 0.14$, since we have seen that when $S_{ipv} \to S_{wir}$ instabilities become more evident. A slight peak in polymer concentration has though been observed even for lower values of S_{ipv}. Although the height of the peak becomes lower as the time step is refined, it does not disappear completely. Simulations were run with very fine time steps, but the non-monotonous behaviour seems to characterize the high-resolution semi-implicit scheme. Unfortunately, we cannot analyze the monotonicity of the scheme as for first order methods, because the assumption $c^n_j = c^n_{j-1} (= c^n_{j+1})$ would cancel the higher order contribute in (5.11). Using different flux limiters does not help either to fix the monotonicity issue.

These issues motivate us to solve the water-polymer flow with the implicit high-resolution method to understand if the non-monotonicity is due to a very strict time step constraint, or is rather a problem caused, more in general, by higher order fluxes. Simulations are shown in figures 5.9, 5.10 and 5.11. At first glance, it seems that the concentration profile is monotone. However, when grid size and time step are proportionally refined in order to get rid of numerical diffusion, a slight peak appears at the polymer front. Since implicit schemes are known for being unconditionally stable, this feature suggests that the high-resolution fluxes (5.11)-(5.12) proposed to improve the accuracy of the polymer flow solver are not appropriate.

Slight variations on the high-resolution schemes (different flux limiters or, alternatively, use of slope limiters) have been tested as well, but no significant changes have been observed: a non-monotonous concentration profile seems to characterize high-resolution methods for this specific problem. A question that naturally arises, is if we could find a reason explaining why the high-resolution methods, which work for polymer flooding without hydrodynamic acceleration, do not result in monotone solutions for a model including such effect. An aspect that might be worth to investigate, is the impact that using a (fully implicit) first order upwind scheme to solve the water flow can have on the high order scheme for the concentration. In fact, a saturation dependent enhancement factor $\alpha(S)$ introduces a stronger coupling between the governing equations. The inaccuracy of the water flow solver at the shock may cause the higher order methods to fail. Thus, we use a high-resolution method for both the water and polymer conservation equations, with an explicit time discretization to avoid difficulties due to the solution of a non-linear system that would arise

from an implicit discretization. The scheme becomes

$$S_j^{n+1} = S_j^n - \frac{\Delta t}{\phi \Delta x}\left(F^s_{j+1/2} - F^s_{j-1/2}\right), \tag{5.13}$$

$$(cS)_j^{n+1} = (cS)_j^n - \frac{\Delta t}{\phi \Delta x}\left(F^c_{j+1/2} - F^c_{j-1/2}\right). \tag{5.14}$$

The numerical fluxes $F^s_{j+1/2}$, $F^c_{j+1/2}$ are given by

$$F^s_{j+1/2} = u^n_{w,j} + \Phi\left(\theta^{s,n}_{j+1/2}\right)\frac{1}{2}\left(1 - \frac{\Delta t}{\Delta x}u^n_{w,j}\right)\left(u^n_{w,j+1} - u^n_{w,j}\right), \tag{5.15}$$

$$F^c_{j+1/2} = \alpha^n_j c^n_j u^n_{w,j} + \Phi\left(\theta^{c,n}_{j+1/2}\right)\frac{1}{2}\alpha^n_j u^n_{w,j}\left(1 - \frac{\Delta t}{\Delta x}\alpha^n_j u^n_{w,j}\right)(c^n_{j+1} - c^n_j), \tag{5.16}$$

where

$$\theta^s_{j+1/2} = \frac{u_j - u_{j-1}}{u_{j+1} - u_j}, \qquad \theta^c_{j+1/2} = \frac{c_j - c_{j-1}}{c_{j+1} - c_j}.$$

In figure 5.12, a numerical solution computed with this method and same settings as in figure 5.7 is shown. The concentration profile is now monotone. However, there is no evident gain in the accuracy of the solution, and the time step must be much smaller than the grid size to avoid stability issues.

A similar monotone solution has been observed for different settings, when proper restrictions on the time step are fulfilled. These results suggest that the problems encountered using a high-resolution scheme for the polymer transport equation and a first order solver for the underlying flow, are indeed due to an incompatibility between the two different schemes. The hydrodynamic acceleration factor introduces a stronger coupling between the equations that leads to the failure of this sequential solver. This conclusion raises a warning: commercial simulators are used to simulate much more complicated models, and usually adopt first order implicit schemes. Hence, modifying the whole flow solver to tailor it to the high-resolution scheme for the polymer transport may not be a feasible option. This fact might preclude the chance of implementing a high-resolution methods for transport equations of active chemicals as polymers. However, further research may lead to the development of a high-resolution scheme that works when coupled with the first order flow solver. Designing a well-suited scheme is though an hard task, since the performance of a method could be strongly affected by the non-linearity of the equations. A thorough analysis of high-resolution methods is beyond the scope of this thesis, and can be the subject of future research.

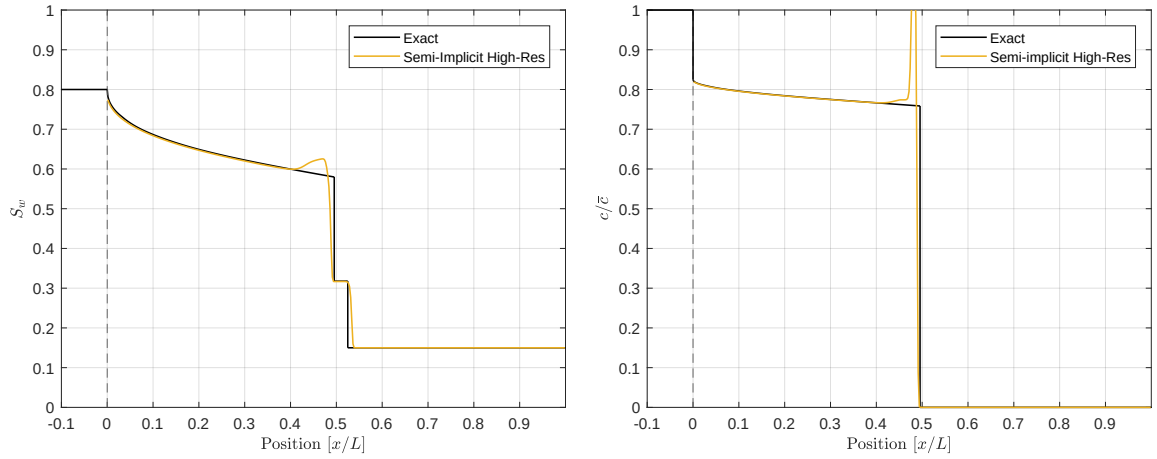

Figure 5.6: Solution for saturation (left) and concentration (right) using the semi-implicit high-resolution scheme, 400 cells and 800 time steps.

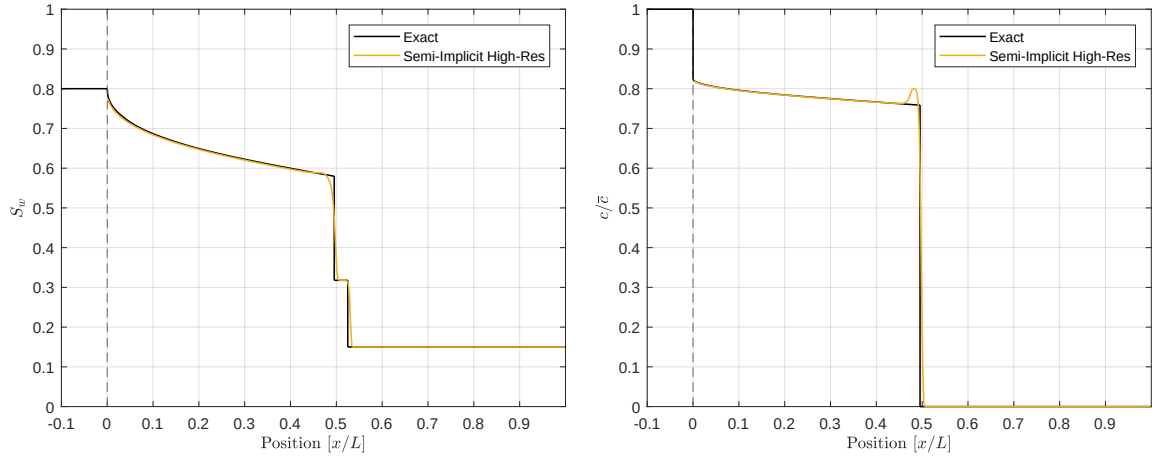

Figure 5.7: Solution for saturation (left) and concentration (right) using the semi-implicit high-resolution scheme, 400 cells and 3200 time steps.

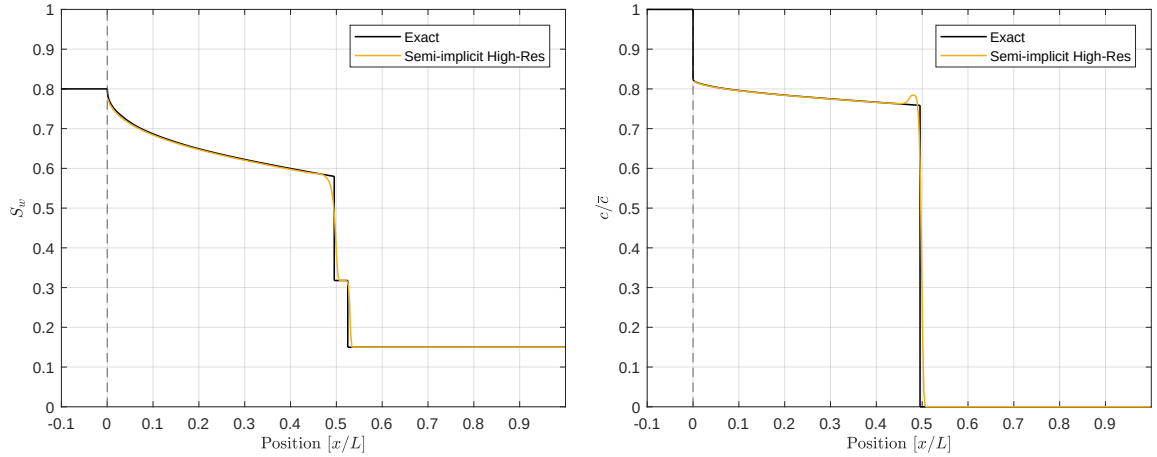

Figure 5.8: Solution for saturation (left) and concentration (right) using the semi-implicit high-resolution scheme, 400 cells and 6400 time steps.

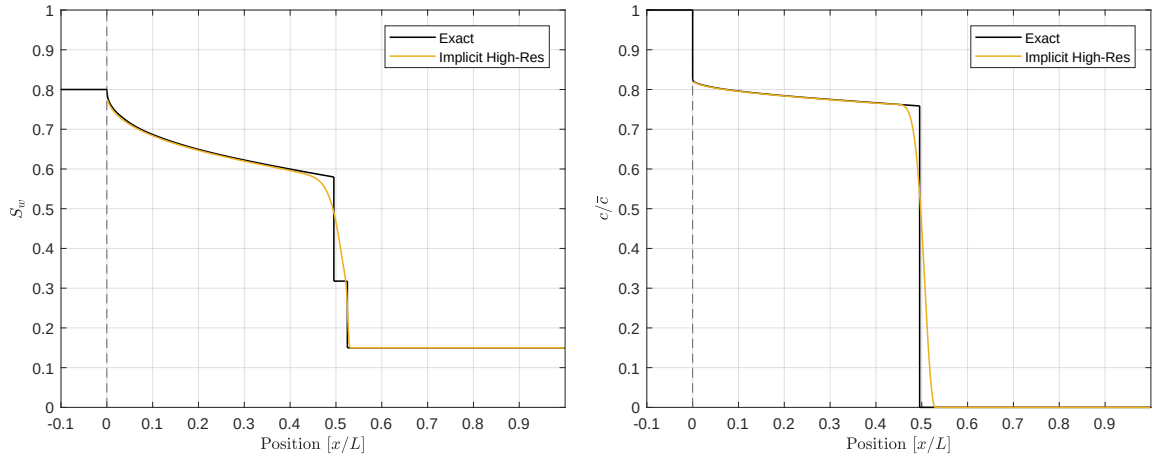

Figure 5.9: Solution for saturation (left) and concentration (right) using the implicit high-resolution scheme, 400 cells and 800 time steps.

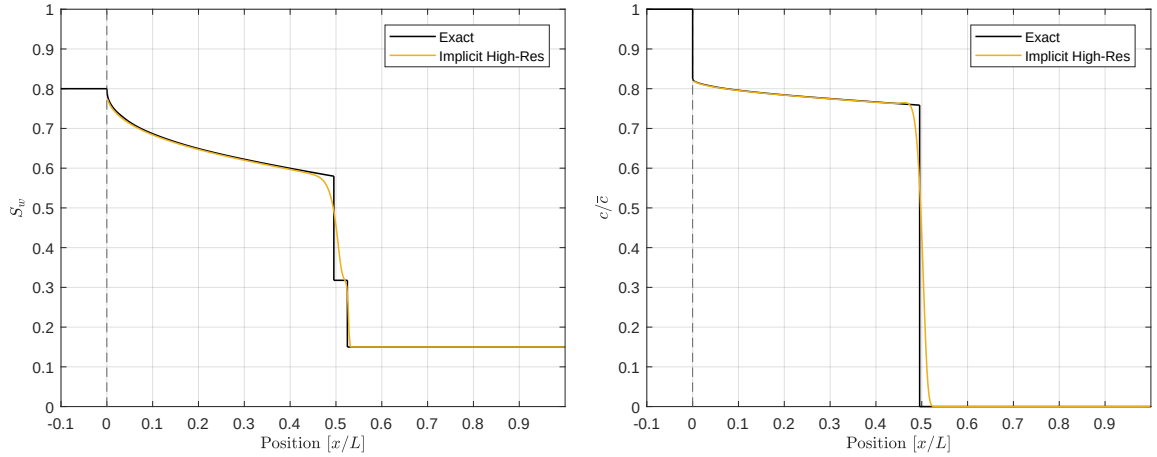

Figure 5.10: Solution for saturation (left) and concentration (right) using the implicit high-resolution scheme, 400 cells and 1600 time steps.

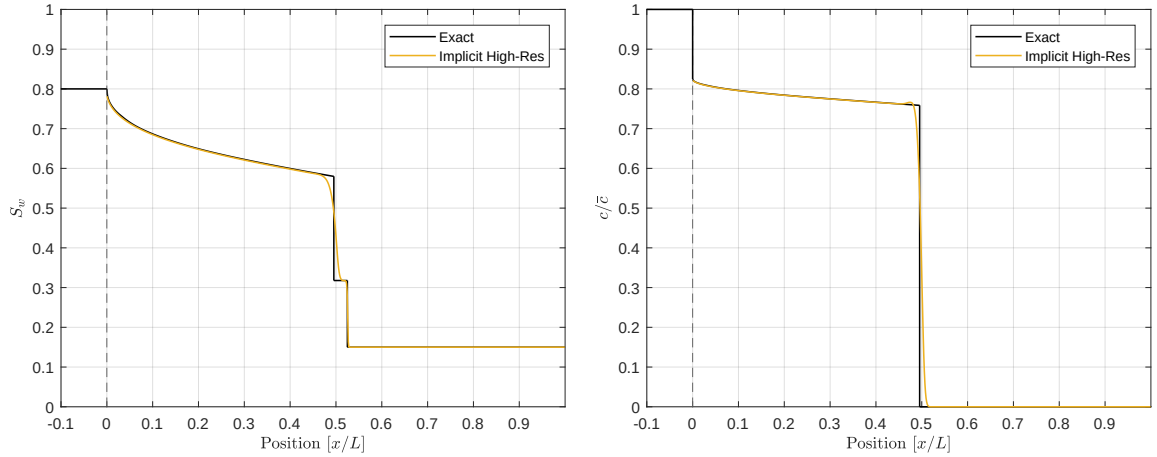

Figure 5.11: Solution for saturation (left) and concentration (right) using the implicit high-resolution scheme, 800 cells and 3200 time steps.

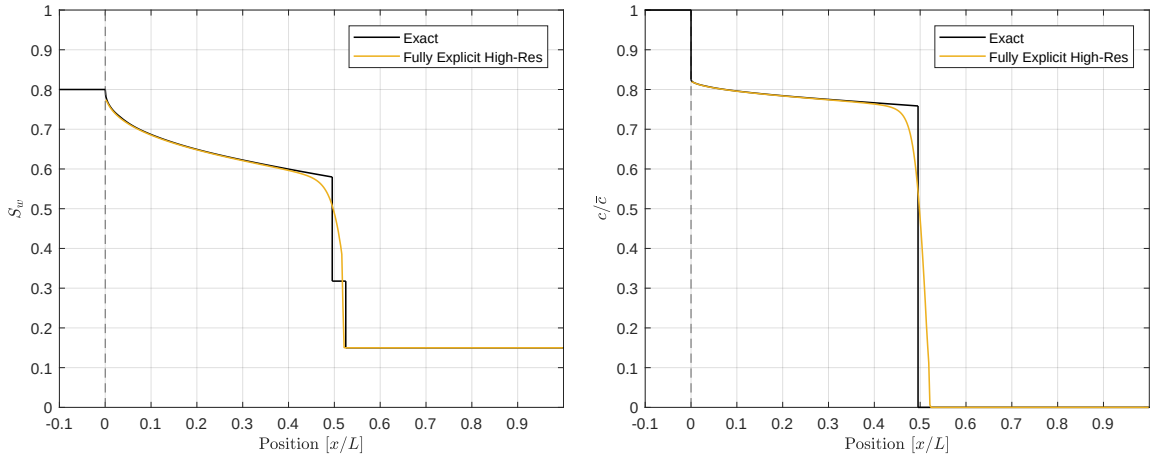

Figure 5.12: Solution for saturation (left) and concentration (right) using the fully explicit high-resolution scheme, 400 cells and 3200 time steps.

6

Adsorption and Extension to 2D

In this chapter, we incorporate in the governing equations an adsorption term and we apply the presented models of IPV to the two-dimensional case. Because of adsorption, the water bank will be gradually denuded of polymer, resulting in a delay of the polymer front [11]. We expect then the concentration profile to maintain the same shape as in the case where only IPV effects are accounted for, and to observe a slow down of the polymer front. While the numerical solutions comply with this hint, an analytical study shows that the system of equations is affected by additional complexity, and computing an analytical solution becomes much harder. However, the well-posedness of the model is maintained, so that stability of numerical methods can be ensured by fulfilling the adequate restrictions on the time step.

The extension to two dimensions does not arise any particular new issue. Equations are properly reformulated for the multi-dimensional case, and the finite volume discretization is briefly discussed. Numerical results reflect what has been observed in the one-dimensional case: the constant and Hilden factors lead to accumulation of polymer at the front, while Bartelds factor results in a monotone concentration profile

6.1. Adsorption

Depending on the reservoir and on the chemical species employed, adsorption of polymer onto the rock will play a key role in the front propagation. Experimental results [15],[22] show that adsorption effects slow down the polymer front. This phenomenon ultimately affects the predicted oil recovery, so it should be included in any realistic model. In the following, we investigate analytical and numerical solutions of the flow when an adsorption term is added to the governing equations. Given the discussion on the well-posedness of IPV models, the enhancement factor proposed by Bartelds will be adopted throughout this section.

6.1.1. Adsorption Model and Analysis of the Equations

The conservation equations in fractional flow formulation and with an adsorption term are

$$\phi \frac{\partial S_w}{\partial t} + u \frac{\partial f_w}{\partial x} = 0, \tag{6.1}$$

$$\phi \frac{\partial c S_w}{\partial t} + \phi \frac{\partial a}{\partial t} + u \frac{\partial a c f_w}{\partial x} = 0, \tag{6.2}$$

where $a(c)$ is a function depending on c such that

$$\frac{da}{dc} \geq 0. \tag{6.3}$$

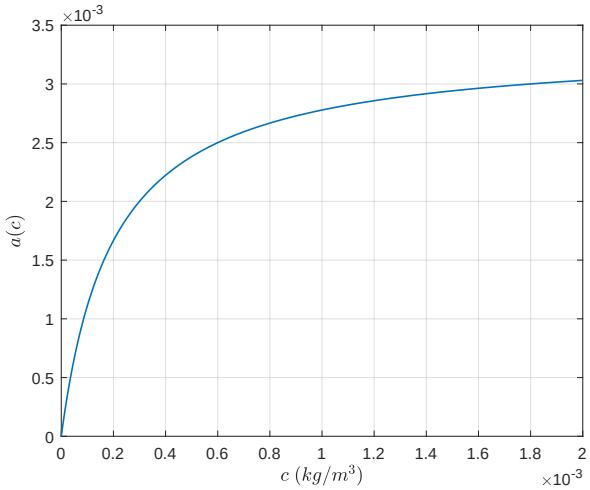

Figure 6.1: Langmuir adsorption isotherm for $b = 10$, $a_{max} = 0.5\bar{c}$, $\bar{c} = 0.002$ is the usual injected polymer concentration.

Note that, because of the adsorption term, polymer is being subtracted by the system and mass is not conserved. In order to have an analytical expression of $a(c)$, we adopt a Langmuir adsorption isotherm model (see [16]):

$$a(c) = \frac{a_{max}}{\phi}\frac{bc}{1+bc}, \tag{6.4}$$

where a_{max} represents the maximum adsorbed polymer concentration and b is a parameter representing the non-linearity of the isotherm. A typical curve for the model (6.4) is shown in figure 6.1.

To study analytically equations (6.1)-(6.2), we proceed as in the previous section, rewriting the system in quasi-linear form and computing the characteristic velocities. The equations in matrix-vector form are

$$\frac{\partial}{\partial t}\begin{pmatrix} S_w \\ c \end{pmatrix} + A\frac{\partial}{\partial x}\begin{pmatrix} S_w \\ c \end{pmatrix} = 0, \tag{6.5}$$

where the matrix A is given by

$$A = \frac{u}{\phi}\begin{pmatrix} \frac{\partial f_w}{\partial S_w} & \frac{\partial f_w}{\partial c} \\ \frac{\frac{d\alpha}{dS_w}cf_w + (\alpha-1)c\frac{\partial f_w}{\partial S_w}}{S_w + \frac{da}{dc}} & \frac{\alpha f_w + (\alpha-1)c\frac{\partial f_w}{\partial c}}{S_w + \frac{da}{dc}} \end{pmatrix}. \tag{6.6}$$

Bartelds had already considered an adsorption term in the study of well-posedness, so we report here the computed discriminant which becomes

$$D = \left(\frac{u}{\phi}\right)^2\left[\left(\frac{\partial f_w}{\partial S_w} - \frac{\alpha f_w - (\alpha-1)c\frac{\partial f_w}{\partial c}}{S_w + \frac{da}{dc}}\right)^2 - 4\frac{\alpha(\alpha-1)}{S_w\left(S_w + \frac{da}{dc}\right)^2}cf_w\frac{\partial f_w}{\partial c}\frac{da}{dc}\right]. \tag{6.7}$$

Since $\alpha > 1$, $\partial f_w/\partial c \le 0$ and $da/dc \ge 0$, the discriminant (6.7) is nonnegative. In particular, it is positive for non trivial values of (S_w, c). This fact has a significant impact on the nature of the system: the governing equations are now classified as *strictly* hyperbolic, meaning that the characteristic velocities λ_w, λ_p are distinct. Thus, the polymer equation does not behave as a contact discontinuity, and the procedure used in chapter 4 to compute the analytical solution must be reviewed.

Unfortunately, the expressions of the characteristic velocities are much more complicated in this case:

$$\lambda_{w,p} = \frac{u}{2\phi}\left(\frac{\partial f_w}{\partial S_w} + \frac{\alpha f_w + (\alpha - 1)c\frac{\partial f_w}{\partial c}}{S_w + \frac{da}{dc}} \pm \sqrt{D}\right), \tag{6.8}$$

where D is given by (6.7). Given the complexity of expression (6.8), we have not verified if the water and polymer fields are genuinely nonlinear or linearly degenerate. Since the system of ODEs that defines the rarefaction waves requires the computation of the eigenvectors and of the gradients of λ_w, λ_p, we rely on numerical solutions. Despite the raise in complexity, the system of equations conserves the well-posedness property ensured by the strict hyperbolicity, so we do not expect instabilities in the numerical solutions.

6.1.2. Numerical Solutions with Adsorption

The finite volume discretization presented in chapter 3 is extended to the equations including the adsorption term. Such term must be discretized only in time, so the first order backward scheme is employed. The discretized equation results in

$$\frac{(cS_w)_j^{n+1} - (cS_w)_j^n}{\Delta t} + \frac{a_j^{n+1} - a_j^n}{\Delta t} = -\frac{1}{\phi \Delta x}\left(F_{j+1/2}(S_w^{n+1}, c^n, c^{n+1}) - F_{j-1/2}(S_w^{n+1}, c^n, c^{n+1})\right), \tag{6.9}$$

where for the flux $F_{j+1/2}$ we use the semi-implicit discretization

$$F_{j+1/2} = \alpha_j^{n+1} u_{w,j}^{n+1} c_j^n,$$

since it ensures a more accurate solution without severe time step constraints (as long as we are not in the case of $S_{ipv} \to S_{wir}$). Hence, the discretized equation (6.9) can be rewritten as

$$(cS_w)_j^{n+1} + a_j^{n+1} = (cS_w)_j^n + a_j^n - \frac{\Delta t}{\phi \Delta x}\left(\alpha_j^{n+1} u_{w,j}^{n+1} c_j^n - \alpha_{j-1}^{n+1} u_{w,j-1}^{n+1} c_{j-1}^n\right). \tag{6.10}$$

Equation (6.10) is nonlinear in c_j^{n+1}, so a nonlinear solver must be called at every iteration. The default `fsolve` Matlab solver is used. Note that, given N control volumes, N independent equations must be solved, so no numerical difficulties due to a coupling of the discrete equations arise. An implicit choice of the flux $F_{j+1/2}$ would have coupled these non-linear discrete equations into a system, so we have another good reason to discard that approach.

In the following, some numerical simulations are shown, along with a plot of the discriminant. The polymer front (figures 6.3-6.4) is clearly delayed with respect to the case without adsorption. It is interesting to observe that the rarefaction waves for both saturation and concentration seem to coincide with the (exact) solution computed in chapter 4, at least until the point where the earlier shock of the IPV-adsorption case occurs. However, there is no guarantee that these waves are the same: the change in polymer concentration magnitude might be too small to be noticed with numerical solutions. A second rarefaction wave for water saturation occurs in both configurations of figures 6.3 and 6.4, even if in the latter case it is only slightly visible. The formation of this wave depends, as discussed in chapter 3, by the saturation value of the constant plateau ahead of the polymer front. In the case of adsorption, the constant plateau value is higher, so that a second rarefaction wave has more chances to occur. In figure 6.2, a plot of the discriminant is depicted. Although it goes very close to zero for saturation values around 0.6, we have verified that it stays positive. Note that the saturation value on the left of the polymer front is greater than the saturation for which the discriminant reaches its minimum, while in the case without adsorption these two values coincide. This fact reinforces our argument that the polymer front is no more a contact discontinuity, because the shock occurs at a saturation value for which the characteristic velocities are considerably different.

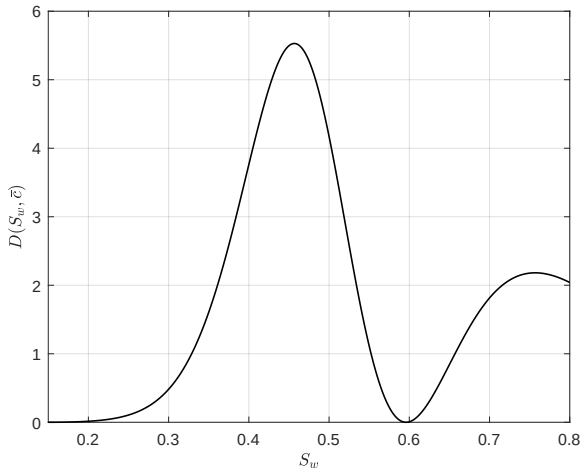

Figure 6.2: Discriminant (6.7) for a fixed value of c and $S_{ipv} = 0.1$, $b = 10$, $a_{max} = 0.5\bar{c}$, $\bar{c} = 0.002$ injected concentration.

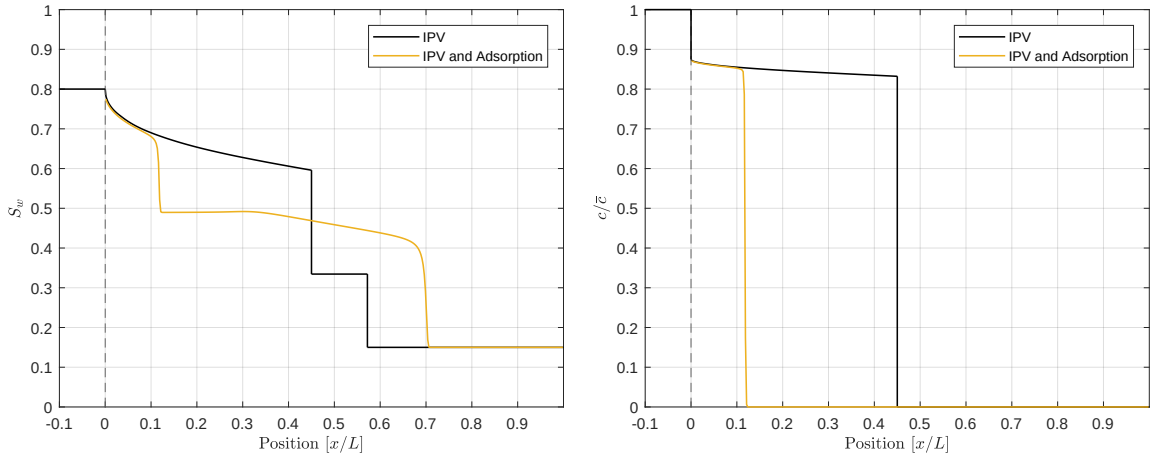

Figure 6.3: Saturation (left) and concentration (right) profiles obtained with semi-implicit first order upwind schemes, 400 cells and timesteps, $S_{ipv} = 0.1$, $b = 10$, $a_{max} = 0.5\bar{c}$.

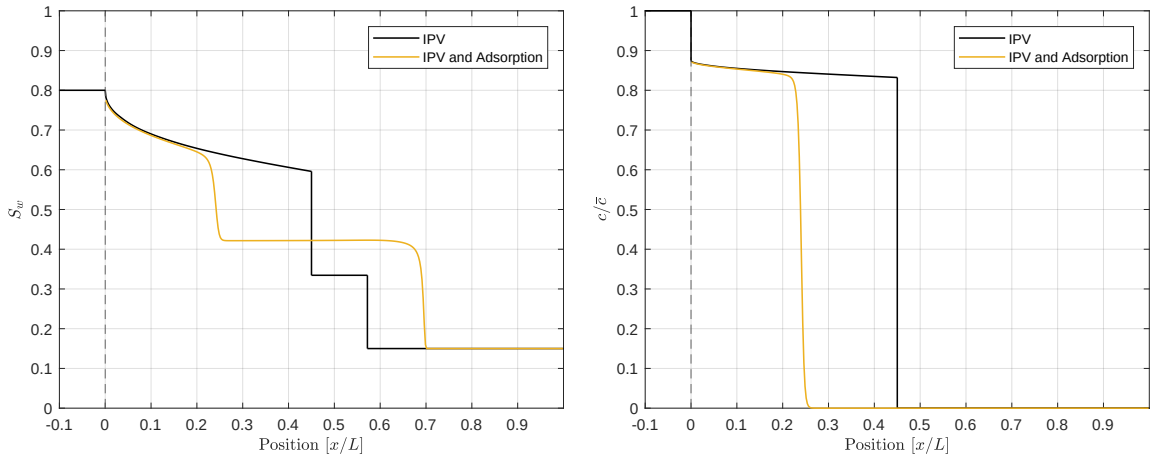

Figure 6.4: Saturation (left) and concentration (right) profiles obtained with semi-implicit first order upwind schemes, 400 cells and timesteps, $S_{ipv} = 0.1$, $b = 1$, $a_{max} = 0.3\bar{c}$.

6.2. Extension to 2D

We are now interested in applying the velocity enhancement factor models to the two-dimensional case and see if we get similar results. Given the complexity that inevitably raises by considering a multi-dimensional system, we prefer to focus on the numerical solutions and their stability. Since we have seen that adsorption does not influence the well-posedness of the problem, it will be disregarded in this section.

The governing equations in conservation form reformulated in a two-dimensional framework, with the incompressibility assumption, are

$$\phi \frac{\partial S_w}{\partial t} + \nabla \cdot \mathbf{u}_w = 0, \tag{6.11}$$

$$\phi \frac{\partial (cS_w)}{\partial t} + \nabla \cdot (\alpha c \mathbf{u}_w) = 0, \tag{6.12}$$

where we do not select now a particular model for the enhancement factor. Gravity effects and capillary pressure are neglected as well, so that Darcy velocity takes the form

$$\mathbf{u}_w = \frac{\mathbf{k} k_{r,w}}{\mu_w} \nabla p, \tag{6.13}$$

where $\mathbf{k}$ is the permeability tensor. Assuming the porous medium to be isotropic with constant permeability, the tensor $\mathbf{k}$ becomes a diagonal matrix:

$$\mathbf{k} = \begin{bmatrix} k & \\ & k \end{bmatrix}.$$

The cell-centered finite volume discretization is used in the two-dimensional case as well. The domain consists of a square $D = [0, L] \times [0, L]$, uniformly subdivided in $N \times N$ cells. The unknowns are denoted by $\{(S_{i,j}, c_{i,j})\}_{i,j=1}^{N}$. The injection well is placed at the lower-left vertex and the production well at the upper-right vertex, as shown in figure 6.5. Integration over a control volume

$$V_{ij} = [i - 1/2, i + 1/2] \times [j - 1/2, j + 1/2]$$

of equation (6.11) gives

$$\phi \int_{V_{ij}} \frac{\partial S_w}{\partial t} dV + \int_{V_{ij}} (\nabla \cdot \mathbf{u}_w) dV = 0. \tag{6.14}$$

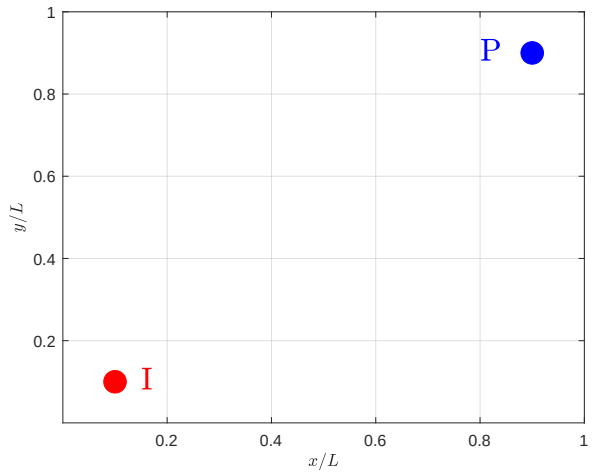

Figure 6.5: Two-dimensional domain and illustration of the injection (I) and production (P) wells.

Applying the divergence theorem results in

$$\phi \int_{V_{ij}} \frac{\partial S_w}{\partial t} dV + \int_{\partial V_{ij}} (\mathbf{u}_w \cdot \mathbf{n}) d\partial V = 0, \tag{6.15}$$

where $\mathbf{n}$ is the outward normal to cell V_{ij}. The boundary integral is approximated by

$$\int_{\partial V_{ij}} (\mathbf{u}_w \cdot \mathbf{n}) d\partial V = \Delta y \, u_x \Big|_{i-1/2,j}^{i+1/2,j} + \Delta x \, u_y \Big|_{i,j-1/2}^{i,j+1/2}, \tag{6.16}$$

where

$$u_x = -\frac{k k_{r,w}}{\mu_w} \frac{\partial p}{\partial x}.$$

Using a first order upwind approximation for the relative permeability and the viscosity and a central differentiation scheme for the pressure gradient, gives

$$u_x \Big|_{i+1/2,j} = -\frac{k k_{r,w}}{\mu_w} \Big|_{i,j} \frac{p_{i+1,j} - p_{i,j}}{\Delta x}. \tag{6.17}$$

Hence, the discretized water conservation equation is

$$\phi \Delta x \Delta y \frac{S_{i,j}^{n+1} - S_{i,j}^{n}}{\Delta t} = -\Delta y \, u_x \Big|_{i-1/2,j}^{i+1/2,j} - \Delta x \, u_y \Big|_{i,j-1/2}^{i,j+1/2}. \tag{6.18}$$

A similar procedure leads to the discretized polymer conservation equation

$$\phi \Delta x \Delta y \frac{(cS)_{i,j}^{n+1} - (cS)_{i,j}^{n}}{\Delta t} = -\Delta y \left[\alpha u_x c \right]_{i-1/2,j}^{i+1/2,j} - \Delta x \left[\alpha u_y c \right]_{i,j-1/2}^{i,j+1/2}. \tag{6.19}$$

As for the one-dimensional case, we use a sequential approach to solve the system of equations. The flow is solved through the fully implicit discretization implemented in MRST, except that the old value for the concentration is used. The polymer transport equations is then solved with the current value of saturation and either a semi-implicit or an implicit time discretization for the fluxes:

- Semi-implicit
$$\alpha u_x c \Big|_{i+1/2,j} = \alpha_{i,j}^{n+1} u_x(S_{i,j}^{n+1}, c_{i,j}^{n}) c_{i,j}^{n},$$
- Implicit
$$\alpha u_x c \Big|_{i+1/2,j} = \alpha_{i,j}^{n+1} u_x(S_{i,j}^{n+1}, c_{i,j}^{n}) c_{i,j}^{n+1}.$$

As the number of cells increases, the implicit method becomes very expensive, and the semi-implicit scheme is subject to severe time step restrictions [10]. Hence, alternative methods have been proposed, for instance in [10]. However, the scope of this section is to study how the enhancement factor affects the two-dimensional problem, with particular regard to the accumulation phenomenon that has been observed in some of the one-dimensional simulations. Therefore, the methods presented above are implemented for the polymer equation and coupled to the MRST solver in order to use the sequential approach just discussed. The high-resolution methods showed unclear results even in the one-dimensional case, so they will not be considered here.

Below, we show the results of the simulations. On the boundary, a no-flow condition is set by MRST as default. At the injector and producer wells, a constant injection rate and a constant pressure conditions are assumed, respectively. Settings of table 4.1 are used in order to emphasize the pile-up effect of the ill-posed models. In figures 6.6 and 6.7, the solution computed through the

semi-implicit and implicit schemes with $\alpha = 1$ is shown. With appropriate choice of the time step, both schemes result in the expected profiles for saturation and concentration. Due to the rough grids, a great deal of numerical diffusion is introduced in the simulations, causing a severe smearing of the fronts. The semi-implicit scheme is particularly expensive, since 3000 time steps had to be used to avoid numerical issues.

In figure 6.8, a constant enhancement factor α is selected. An accumulation effect occurs for the polymer: the height of the peak is bounded to low values of c because of the large amount of numerical diffusion introduced by the implicit scheme and the rough grid. To test Hilden model, we set $S_{ipv} = 0.3$ and we choose again an implicit scheme to avoid stability issues. Similarly to the constant factor model, the concentration profile shown in figure 6.9 is not monotone, and numerical diffusion helps to keep the pile-up limited. Last, the model of Bartelds is tested with $S_{ipv} = 0.05$. Since graphically we did not observe a huge difference between the semi-implicit and implicit methods when $\alpha = 1$, we employ again the implicit scheme to avoid expensive restrictions on the time step. Results in figure 6.10 show a monotone profile for the polymer concentration.

The key facts observed and remarked for the one-dimensional case seem to apply to the two-dimensional case as well. In particular, the enhancement factor proposed by Bartelds is the only one leading to a well-posed problem, while for the constant and Hilden factor a peak in the concentration is obtained. No significant changes were observed when using Bartelds model with different values of S_{ipv}, as long as the condition $S_{ipv} < S_{wir}$ was fulfilled, beside the stricter time step constraint for the semi-implicit method. This restriction on the time step becomes much more severe for the two-dimensional case. Also the computational cost of the implicit scheme raises consistently as the grid is refined. Moreover, the shocks, especially the one in the saturation, are severely smeared. Therefore, alternative numerical methods have been proposed in the literature, see for instance [10] and references therein.

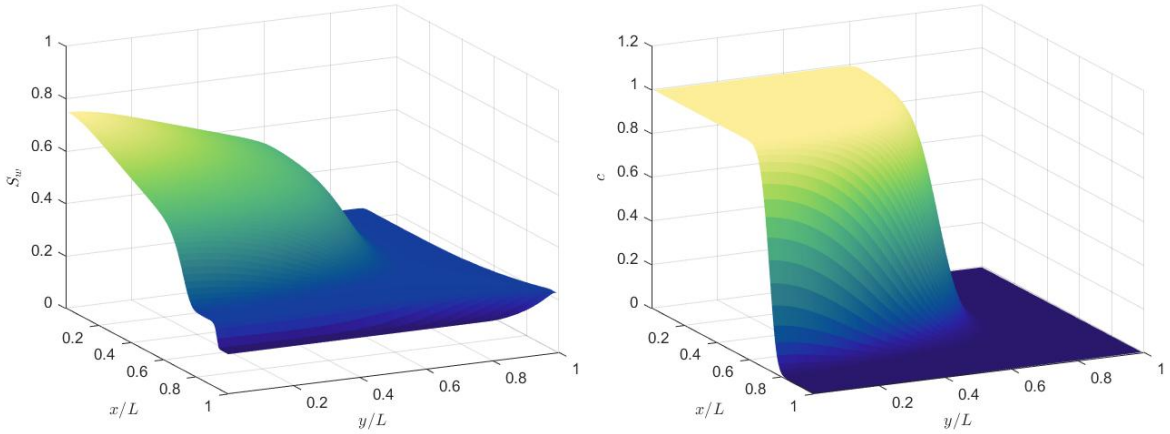

Figure 6.6: Solution using $\alpha = 1$, semi-implicit scheme, 100×100 cells, 3000 time steps.

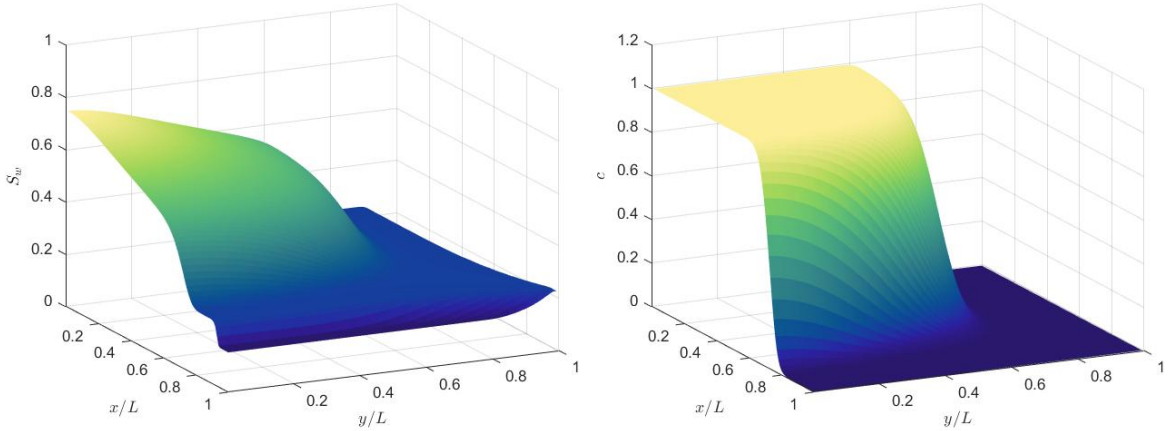

Figure 6.7: Solution using $\alpha = 1$, implicit scheme, 100×100 cells, 500 time steps.

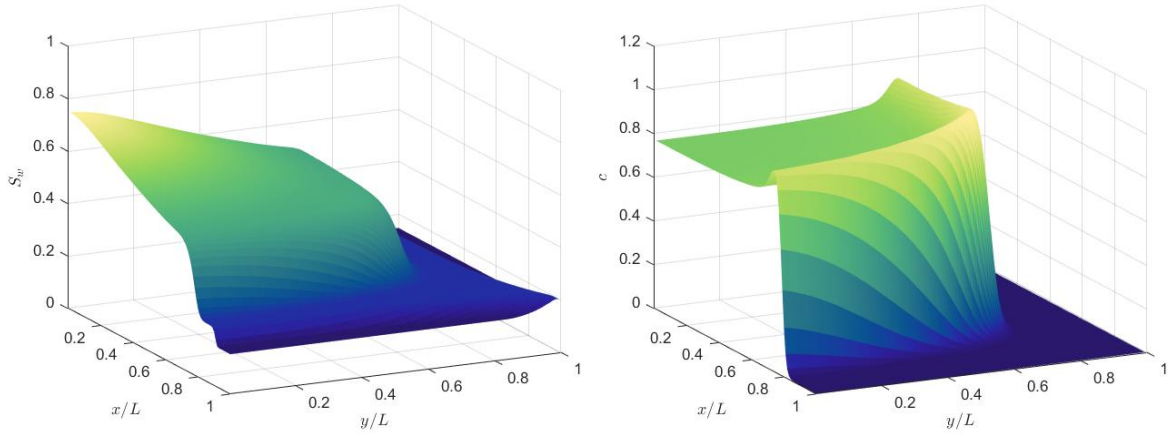

Figure 6.8: Solution using $\alpha = 1.3$, implicit scheme, 100×100 cells, 500 time steps.

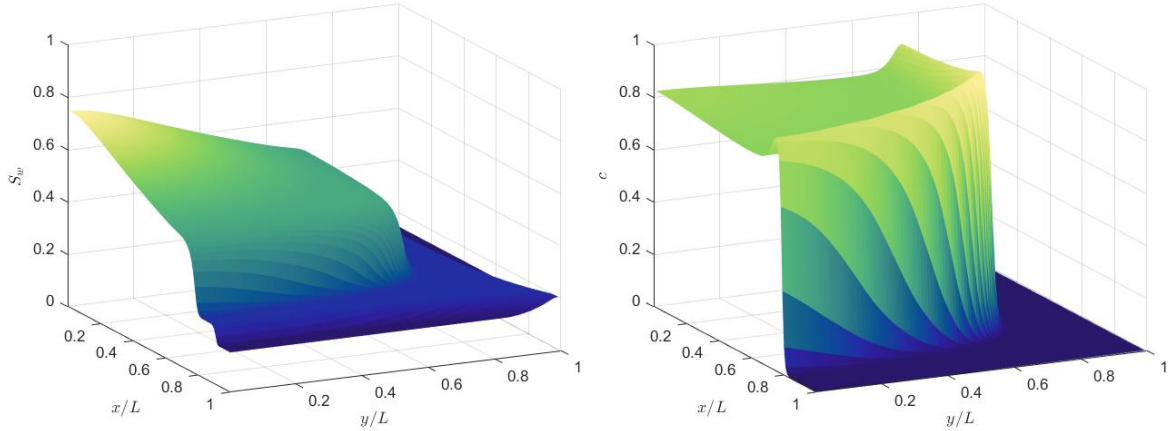

Figure 6.9: Solution adopting Hilden model, implicit scheme, 100×100 cells, 500 time steps, $S_{ipv} = 0.3$.

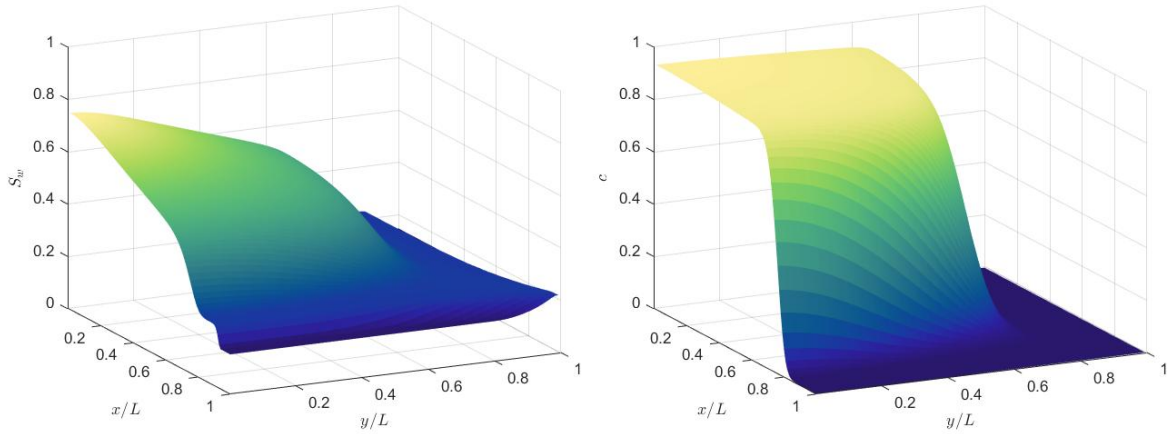

Figure 6.10: Solution adopting Bartelds model, implicit scheme, 100×100 cells, 500 time steps, $S_{ipv} = 0.05$.

7

Conclusions

The goal of this thesis was to investigate the velocity enhancement (or hydrodynamic acceleration) effect that occurs when injecting a solution of water and polymer into a reservoir. The polymer molecules, due to inaccessible and excluded pore volume, are observed to travel faster than inert chemical species. The modeling of this phenomenon leads to analytical and numerical difficulties, which have been addressed throughout the report. In this chapter, we present the main conclusions of this research, along with recommendations for future work.

In chapter 2, a review of the theory on hyperbolic laws has been carried out. This formal theory allowed us to analyze properly the different models proposed, and to compute solutions where possible. Often, the polymer flooding problem is approached in a more intuitive but less formal way. Although this approach works for simpler cases, it leads to wrong conclusions when the velocity enhancement is incorporated in the governing equations.

In chapter 3, we introduced the physics of the reservoir and the conservation equations that govern the flow of water and polymer through the reservoir. Analytical solutions are computed using the tools presented in chapter 2, resulting in the typical Buckley-Leverett profile well-known in the literature. The various numerical methods adopted to solve the flow were also introduced here. In particular, a sequential solver is discussed: at each time step, the water conservation equation is solved through an implicit discretization and, then, the computed value of saturation is used to solve the polymer transport equation through different schemes, that are briefly compared (for a thorough analysis of these schemes, refer to [10]).

Next, we addressed the main target of this research: the velocity enhancement effect. Experimentally, the polymer is observed to travel faster than a passive tracer. This phenomenon is explained physically through the inaccessible and excluded pore volume theory: due to their larger size, the polymer molecules do not enter the smallest pores (IPV) and tend to travel at the center of the pore channels (EPV). A simple model employed in most of the commercial simulator consist in inserting into the polymer continuity equation a constant factor α to increase the polymer front velocity. It was shown by Bartelds [4] that this model leads to an ill-posed problem. In particular, numerical simulations result in a sharp peak in the polymer concentration at the front. Although a pile-up of polymer at the front is not necessarily unphysical, this peak arises because of the loss of hyperbolicity of the system that the factor α causes. Hence, it is the result of a mathematical ill-posedness rather than a physical outcome predicted by the model. Therefore, alternative models have been proposed. Bartelds [4] derived a saturation dependent factor $\alpha(S_w)$ suited to model only IPV effects. In this research, we have computed the analytical solution for this model, which is shown to be hyperbolic and hence well-posed. Analytical considerations on this model allowed us to conclude also that the monotonicity of saturation and concentration profiles are related: if the

saturation profile is decreasing (which is a very plausible feature for the problem considered), concentration profile will be decreasing as well. The pile-up of polymer seems to be strictly related with the loss of hyperbolicity that the enhancement factor may cause. In [2], Bartelds derived a saturation and concentration dependent factor $\alpha(S_w, c)$ in order to model both IPV and EPV effects. This model results in a pile-up of polymer at the front, and the experimental data presented to validate the model have reliability issues. Hence, we have discarded it from the discussion, and the modeling of EPV remains an open question. Since the IPV model of Bartelds is subject to the restriction $S_{ipv} < S_{wir}$, Hilden et al. [21] tried to extend the model in order to overcome any kind of constraints on the physical parameters. Using an alternative definition of well-posedness, a new enhancement factor is proposed, and numerical simulations shown in their work result in a decreasing profile of the polymer concentration. However, we showed that this model leads to the loss of hyperbolicity and simulations are subject to stability issues as in the constant factor case.

In chapter 5, we studied the monotonicity of the first order numerical methods. We showed that, when using a constant enhancement factor, monotonicity cannot be achieved, as expected from the ill-posedness of the model. For a saturation dependent factor, we obtained a usual CFL-type restriction on the time step when using the semi-implicit method, and an additional condition more related to the analytical model. This condition defines a saturation value S_{mon} such that monotonicity is achieved as long as, on the left of the shock, $S_w > S_{mon}$. We related the monotonicity condition to the Rankine-Hugoniot relation at the shock, claiming then that $S_{mon} = S_l$. Since for Bartelds model the Rankine-Hugoniot relation is one of the ingredients used to build the solution and contributes to determine formally the value S_l of saturation at the polymer front, we claimed that the monotonicity condition can be fulfilled (although we could not prove that this will always be the case). For Hilden model, instead, the value S_l is not well-defined, so there is no guarantee that the monotonicity condition can be satisfied.

A section has been dedicated to the study of high-resolution methods. When these schemes are adopted to solve the polymer transport equation, the resulting concentration profile is not monotone even when using the well-posed model of Bartelds. In particular, we highlighted an incompatibility between the water flow and polymer transport solvers: if a first order implicit scheme is used to compute the saturation profile, then the proposed high-resolution schemes for the polymer do not maintain a monotone profile. When a fully explicit high-resolution method was applied to both water and polymer conservation equations, we achieved again a monotone profile for the concentration. However, the solution did not show any relevant gain in accuracy and, furthermore, it is desirable to have a scheme that works when coupled to the existing solver. Therefore, the derivation of a high-resolution method suited to accurately solve the transport of polymer subject to hydrodynamic acceleration remains an open question.

In chapter 6, we incorporated in the governing equations the adsorption of polymer onto the rock. Adsorption is known for causing a delay in the polymer front. This retardation effect is indeed observed in the numerical results. Unfortunately, the analysis of the equation becomes much more complicated and we did not compute the analytical solution. The system with adsorption becomes strictly hyperbolic, meaning that it maintains the stability property, but the characteristic velocities are different for every point, so the polymer equation is no more a contact discontinuity. The enhancement models were then applied to the two-dimensional case. Essentially, the same conclusion as in the one-dimensional case can be drawn. The numerical methods become though much more expensive, so alternative schemes may be considered in order to improve accuracy and efficiency of the solution.

In this research, we have focused on the origin of the ill-posedness for velocity enhancement models and carried out a thorough analysis showing that Bartelds model is the only one leading to a well-posed problem. An experimental validation of this model is still missing and can be addressed

in future work. This work will hopefully provide useful tools to study analytically polymer flooding equations, and give important insights for the derivation of alternative models of the hydrodynamic acceleration in case the one of Bartelds is seen to predict unphysical fronts acceleration. Although we could not prove that the saturation dependent factor proposed by Bartelds will always result in a monotone solution, the knowledge gained throughout this work makes us think that this will be the case.

Diffusion or dispersion effects have been left out of this research. Often, these terms help to overcome stability issues by smoothening the sharp fronts. However, when these effects are inserted just as mathematical artifacts to avoid instabilities, they may lead to unphysical solutions.

Excluded pore volume modeling are also still an open question. We proposed to adopt Bartelds factor to model a general acceleration of the polymer front, disregarding its physical origin. The enhancement of the polymer front is determined by the magnitude of S_{ipv} and as $S_{ipv} \rightarrow S_{wir}$, the front will reach its maximum enhancement achievable (no more pure water is flowing ahead). Hence, the value of S_{ipv} can be used to adjust the magnitude of the front acceleration and to match the experimental data available for a certain reservoir, independently of the cause of the velocity enhancement.

Future research can be dedicated to investigate why high-resolution methods failed to result in the correct solution and if alternative solvers, that improve the accuracy of the solution, can be proposed.

Bibliography

[1] Braconnier B., Preux C., Flauraud É, Tran Q.H., and Berton C. An analysis of physical models and numerical schemes for polymer flooding simulations. *Computational Geoscience*, 21: 1267–1279, 2017.

[2] Gepke Alies Bartelds. *The influence of inaccessible and excluded pore volume in polymer flooding*. PhD thesis, Delft University of Technlogy, 1998.

[3] J. B. Bell, J. A. Trangenstein, and G. R. Shubin. Conservation laws of mixed type describing three-phase flow in porous media. *SIAM Journal of Applied Mathematics*, 46:1000–1018, 1986.

[4] Bartelds G.A., Bruining J., and Molenaar J. The modeling of velocity enhancement in polymer flooding. *Transport in porous media*, 26(1):75–88, 1997.

[5] Holden H. and Risebro N.H. *Front tracking for hyperbolic conservation laws*. 2nd edn. Springer, Heidelberg, 2015.

[6] Aziz K. and Settari A. *Petroleum Reservoir Simulations*. Elsevier Applied Science, London, 1979.

[7] Bao K., Lie K.A., Møyner O., and Liu M. Fully implicit simulation of polymer flooding with mrst. *Computational Geoscience*, 21:1219–1244, 2017.

[8] Lie K.A. *An introduction to reservoir simulation using MATLAB: user guide for the Matlab Reservoir Simulation Toolbox (MRST). SINTEF ICT*. 2016.

[9] Sorbie K.S. *Polymer-Improved Oil Recovery*. Blackie, Glasgow, 1991.

[10] Wiegman L. Numerical aspects of transport modelling in enhanced oil recovery. Master's thesis, Delft University of Technlogy, 2017.

[11] Lake L.W., Johns R.T., Rossen W.R., and Pope G. *Fundamentals of Enhanced Oil Recovery*. Society of Petroleum Engineers, 2014.

[12] Panfilov M., Panfilova I., and Stepanyants Y. Mechanism of particle transport acceleration in porous media. *Transport Porous Medium*, 74:49–71, 2008.

[13] Todd M.R. and Longstaff W.J. The development, testing, and application of a numerical simulator for predicting miscible flood performance. *Journal of Petroleum Engineering*, 24(7):874–882, 1972.

[14] Gary A. Pope. The application of fractional flow theory to enhanced oil recovery. *Society of Petroleum Engineers journal*, 20:191–205, 1980.

[15] Dawson R., Lantz R.B., and Aime M. Inaccessible pore volume in polymer flooding. *Society of Petroleum Engineers journal*, 12(5):448–452, 1972.

[16] Farajzadeh R., Bedrikovetsky P., Lotfollahi M., and Lake L. W. Simultaneous sorption and mechanical entrapment during polymer flow through porous media. *Water Resources Research*, 52(3):2279–2298, 2016.

[17] Leveque R.J. *Finite Volume Methods for Hyperbolic Problems*. Cambridge university press, 2002.

[18] Krogstad S., Lie K.A., Møyner O., Nilsen H.M., Raynaud X., and Skaflestad B. Mrst-ad-an open-source framework for rapid prototyping and evaluation of reservoir simulation problems. *In: SPE reservoir simulation symposium. Society of Petroleum Engineers*, 2015.

[19] Salsa S. *Partial Differential Equations in Action. From Modelling to Theory.* Springer, 2008.

[20] Buckley S.E. and Leverett M.C. Mechanism of fluid displacement in sands. *Trans AIME*, 146(1): 107–116, 1942.

[21] Hilden S.T., Nilsen H.M., and Raynaud X. Study of the well-posedness of models for the inaccessible pore volume in polymer flooding. *Transport in porous media*, 114(1):65–86, 2016.

[22] E. Unsal, A.B.G.M. ten Berge, and D.A.Z. Wever. Low salinity polymer flooding: Lower polymer retention and improved injectivity. *Journal of Petroleum Science and Engineering*, 163:671–682, 2018.

[23] Chen Z. *Reservoir Simulation-Mathematical Techniques in Oil Recovery*. SIAM, Philadelphia, 2007.